BIOMECHANICS OF BLUNT LIVER INJURY: RELATING INTERNAL PRESSURE TO INJURY SEVERITY AND DEVELOPING A CONSTITUTIVE MODEL OF STRESS-STRAIN BEHAVIOR

DISSERTATION

Presented in Partial Fulfillment of the Requirements for

the Degree Doctor of Philosophy in the Graduate

School of The Ohio State University

By

Jessica L. Sparks, M.S.

* * * * *

The Ohio State University
2007

Dissertation Committee:

Professor Alan Litsky, Adviser

Professor Kenneth Jones

Professor Rebecca Dupaix

Approved by

_____

Adviser
Biomedical Engineering Graduate Program

ABSTRACT

Research suggests that in certain types of blunt liver trauma the mechanism of injury is linked to rapid increases in internal pressure within the liver. The objectives of this study were (1) to characterize the relationship between impact-induced pressures and blunt liver injury in an *ex vivo* organ experimental model; (2) to compare human liver intra-parenchymal pressure and vascular pressure with other biomechanical variables as predictors of liver injury risk; (3) to investigate the feasibility of measuring liver vascular pressure in impacts to pressurized full body post-mortem human subjects (PMHS); and (4) to develop a constitutive model of the mechanical behavior of human liver tissue in blunt impact loading.

Test specimens included 19 *ex vivo* porcine livers, 14 *ex vivo* human livers, and 2 full body PMHS. Specimens were perfused with normal saline solution at physiological pressures, and a drop tower applied blunt impact at varying energies. Impact-induced pressures were measured by transducers in the hepatic veins and parenchyma (caudate lobe) of *ex vivo* specimens. Binary logistic regression demonstrated that tissue pressure measured in the parenchyma was the best indicator of serious liver injury risk ($p = .002$, Pseudo-$R^2 = .78$). A peak tissue pressure of 48 kPa was correlated to 50% risk of serious (AIS ≥ 3) liver injury. A burst injury mechanism directly related to hydrostatic pressure is

postulated for the *ex vivo* liver loaded dynamically in a drop test experiment. A constitutive model previously developed for finite strain behavior of amorphous polymers was adapted to model liver stress-strain behavior observed in the *ex vivo* human liver impacts. The model includes six material properties and captures three features of liver stress-strain behavior in impact loading: (1) a relatively stiff initial modulus; (2) a rate-dependent yield or rollover to viscous "flow" behavior; and (3) strain hardening at large strains.

Results of this research could be applied to improve the abdominal injury assessment capabilities of both anthropomorphic crash dummies and finite element human body models used in vehicle safety research.

Dedicated to my husband, David Sparks,

and to my parents, Tim and Karen Smatlak

ACKNOWLEDGMENTS

I wish to thank my adviser, Alan Litsky, for his support and guidance and for always finding the humor in any situation. I am indebted to Ken Jones for his patience and support, and I am grateful to Rebecca Dupaix for encouraging me and advising me on the application of mechanics principles to my experimental work.

I would like to thank John Bolte for his advice and assistance with the experimental aspects of this project. I also wish to thank Steven Steinberg for sharing his surgical expertise and Johannes Heverhagen, Regina Koch, and Steffen Sammet for their assistance with computed tomography scanning. I am grateful to Mark Whitmer and the Body Donor Program of the Ohio State University Division of Anatomy for their assistance with subject procurement.

This research was reviewed and approved by The Ohio State University Biomedical Sciences Human Subjects Review Committee and otherwise conducted in compliance with applicable NHTSA requirements. This research was sponsored by Contract No. DTNH22-03-D-08000 from the National Highway Traffic Safety Administration. I would like to thank Rod Herriott, Jason Stammen, and Bruce Donnelly for their assistance with this project.

VITA

November 10, 1976 .....Born – Pittsburgh, Pennsylvania

1999 .....B.S. Science Pre-Professional Studies and Philosophy, University of Notre Dame

2002-2003 .....Graduate Fellow, The Ohio State University

2003-2006 .....Graduate Research Associate, The Ohio State University

2006-2007 .....Engineering Research Assistant, The Ohio State University

2007 .....Graduate Fellow, The Ohio State University

2007 .....M.S. Anatomy, The Ohio State University

FIELDS OF STUDY

Major Field: Biomedical Engineering

TABLE OF CONTENTS

LIST OF TABLES

LIST OF FIGURES

CHAPTER 1

INTRODUCTION

1.1 BACKGROUND AND SIGNIFICANCE

Blunt Liver Injury Incidence and Mortality Rates

Several studies have investigated the incidence of abdominal injuries in motor vehicle crashes (Ricci 1980; Bondy 1980; Rouhana and Foster 1985; Elhagediab and Rouhana 1998; Augenstein et al. 2000). Results from these studies indicate that abdominal injuries comprise only 3-5% of the total number of injuries due to automotive crashes. However, abdominal injuries account for increasingly higher proportions of serious injuries. For example, Elhagediab and Rouhana (1998) reported that abdominal injuries constituted 8% of AIS ≥ 3 injuries, 16.5% of AIS ≥ 4 injuries, and 20.5% of AIS ≥ 5 injuries in a review of frontal impacts in the NASS database for the years 1988 through 1994. A similar pattern was observed in studies by Ricci (1980), Rouhana and Foster (1985), and Augenstein et al. (2000). The vehicle contact points associated with abdominal injury include the steering wheel, lap-shoulder belt, airbag, armrest, side interior, and instrument panel.

Solid organs such as the liver, spleen, and kidney are the most frequently injured abdominal organs in both frontal and side impact collisions (Rouhana and Foster 1985; Elhagediab and Rouhana 1998). According to clinical studies, the reported mortality rate for blunt liver injury ranges from 9-17% overall and increases to 30% if operative intervention is required (Christmas et al. 2005; Hurtuk et al. 2006). For liver injuries involving the inferior vena cava or hepatic veins, the mortality rate is as high as 67% (John et al. 1992). These statistics indicate that blunt liver injury is a significant problem in motor vehicle crashes. To date, no existing crash dummy is equipped to represent solid abdominal organs located asymmetrically in the human abdomen (Tamura et al. 2002). All existing instrumented abdominal components in crash dummies assume homogeneity in their response. A need exists for thorough investigations of the injury mechanisms and mechanical response of the individual solid abdominal organs in blunt impact loading.

The present study provides a detailed investigation of the biomechanics of blunt liver injury. A technique was developed to simulate blunt liver injury in a laboratory setting, and a series of impact experiments were conducted to evaluate whether any of a number of biomechanical variables were significantly associated with injury severity. Several physical parameters such as force, velocity, and compression have been examined in previous studies as potential indicators of liver injury severity, with conflicting results (Lau and Viano 1981, Rouhana et al. 1985, Rouhana et al. 1986). The proposed injury indicator that is novel to the current study is internal fluid pressure (i.e.

hydrostatic pressure) within the liver vasculature and parenchyma. Since the liver is a fluid-filled solid organ, it is postulated that impact-induced changes in internal fluid pressure play a role in the injury mechanism in burst and compressive liver injury outcomes. Consequently, it is reasonable to expect that internal fluid pressure would be a statistically significant predictor of blunt liver injury severity. The present study is designed to investigate this hypothesis. Knowledge of a significant relationship between internal fluid pressure and liver injury severity could be used to enhance the injury prediction capabilities of anthropomorphic dummies used in vehicle safety testing.

In addition to examining the relationship between internal fluid pressure and liver injury, the current work provides an evaluation of the mechanical response of the liver in blunt impact loading. Measurements of applied stress and nominal compressive strain were obtained in the series of impact experiments, and these measurements were used to develop a constitutive mathematical model of liver stress-strain behavior. The constitutive model could be applied to develop finite element representations of the human abdomen to simulate injury-producing impact events.

The following discussion summarizes relevant background information from a variety of sources to place the current research in the context of previous work. Background information from a biological perspective includes liver anatomy and clinically observed injury patterns in blunt hepatic trauma. Literature from the field of injury biomechanics is also addressed. Finally, previously developed liver constitutive

models are summarized. The discussion concludes with a statement of the purpose and objectives of the current research.

Overview of Liver Anatomy

The liver is the largest gland in the body. It is situated below the diaphragm in the upper right quadrant of the abdomen. It is a solid, blood-filled organ with a mass of approximately 1.5 kg, or 2% of the normal adult body weight (Burdi 1970).

Two schemes are used to divide the liver into lobes. In one scheme, anatomic landmarks serve to divide the liver into four lobes: the larger right lobe and smaller left lobe, visible from the anterior surface (see Figure 1.1), and the quadrate lobe and caudate lobe, visible from the visceral surface (see Figure 1.2). The right and left lobes are separated by the falciform ligament anteriorly. Structures surrounding the quadrate lobe include the gallbladder, the round ligament (ligamentum teres) of the liver, and the porta hepatis (entrance point of portal vein and proper hepatic artery, exit point of hepatic bile ducts). Structures surrounding the caudate lobe are the porta hepatis, the groove for the inferior vena cava, and the fissure for the ligamentum venosum.

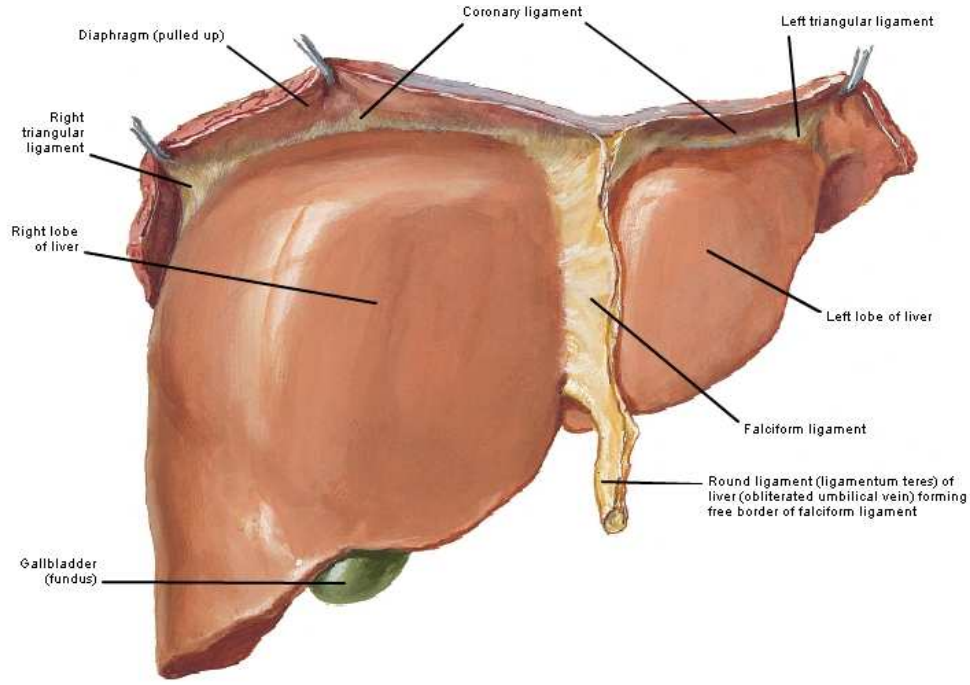

Figure 1.1: Anterior surface of liver (Netter 1997)

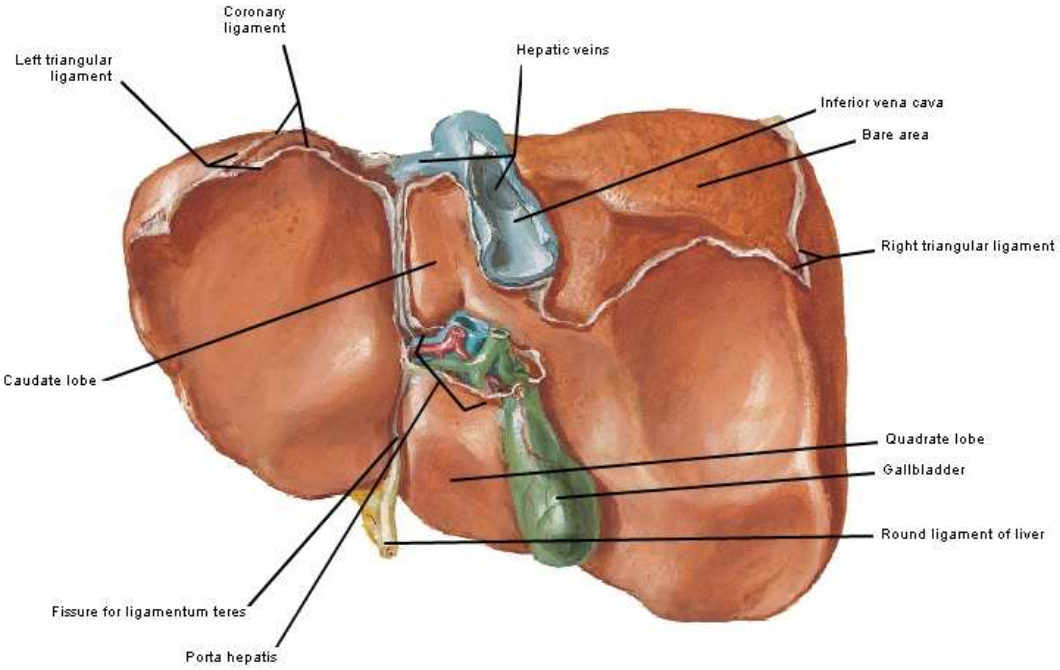

Figure 1.2: Visceral (inferior/posterior) surface of liver (Netter 1997)

The second scheme divides the liver functionally into two lobes, left and right, based on the major division of the hepatic artery, portal vein, and hepatic bile ducts into left and right branches. As a rough approximation, this two-lobe scheme includes the caudate and quadrate lobes as part of the right lobe, while the left lobe remains as it was in the previous classification. The relatively systematic branching of the intra-hepatic vessels and bile ducts enables the right and left lobes to be divided into smaller functional segments for potential surgical purposes, as shown in Figure 1.3.

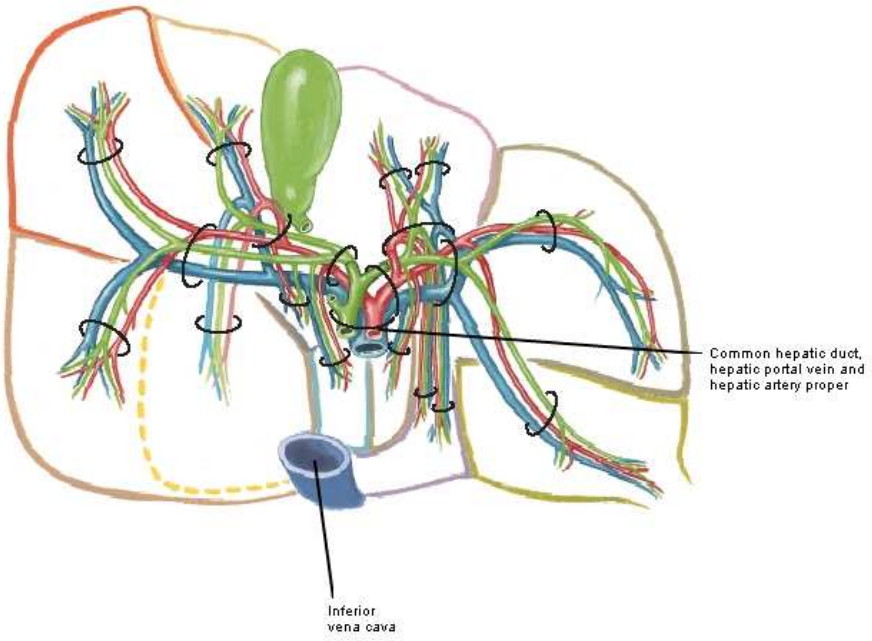

Figure 1.3: Liver functional segmentation and vascular anatomy (Netter 1997)

The liver receives a dual blood supply from both venous and arterial sources. The arterial blood supply to the liver exits the abdominal aorta through the celiac trunk,

traverses the common hepatic artery, and finally enters the proper hepatic artery, which divides into left and right branches as it enters the liver at the porta hepatis. Venous blood enters the liver through the hepatic portal vein, which is formed from the junction of the superior mesenteric vein and the splenic vein. The veins draining many gastrointestinal organs including the stomach, pancreas, and small and large intestines, ultimately form tributaries of the hepatic portal vein. Venous blood exiting the liver is collected in three major veins (right, middle, and left hepatic veins) which empty into the inferior vena cava. Vascular anatomy of the liver is illustrated in schematic form in Figure 1.3.

Approximately three-quarters of the total blood flow to the liver is venous in origin. The hepatic portal vein supplies venous blood to the liver at a rate of roughly 1000 mL per minute, while the rate of flow through the proper hepatic artery is approximately 280 mL per minute (Zoli et al. 1999). Different physiological pressures exist in the two vascular systems, with 7-10 mmHg in the low pressure portal vein and 80-120 mmHg in the high pressure hepatic artery (Guyton 1976).

The abdominal viscera, including the liver, generally display a high degree of mobility. This mobility of the abdominal organs is attributable to two factors: the presence of the peritoneal membrane and the fact that many abdominal organs are not rigidly fixed in position (Rouhana 2002, Hollinshead 1971). The peritoneum is a thin serous membrane which covers the inner abdominal walls and surrounds or partially surrounds the abdominal viscera. The peritoneal membrane is smooth and secretes a

small amount of serous fluid, which results in low friction between the organs and the walls of the abdominal cavity, and between the organs themselves (Rouhana 2002).

Although the abdominal viscera are not rigidly fixed in position, they also do not "float" unattached within the peritoneal cavity. The peritoneal membrane which lines the abdominal wall "is continuous with and reflected over the organs occupying the abdominal cavity" so that the organs are tethered to the body wall by this double fold of peritoneum (Burdi 1970). The double fold of peritoneum is called a mesentery and provides the main passageway of nerves and blood vessels to and from the abdominal organs. The liver in particular is only partially covered by the peritoneal membrane and is attached inferiorly to the lesser curvature of the stomach and the first part of the duodenum by the lesser omentum (hepatogastric and hepatoduodenal ligaments), a type of mesentery (Burdi 1970).

Some final relevant features of liver anatomy include the ligaments of the liver and the adjacent structures. The liver is supported by five ligaments: the falciform, coronary, left and right triangular, and round ligaments. The falciform and round ligaments connect the anterior surface of the liver to the diaphragm and anterior body wall. The coronary and triangular ligaments attach the superior aspect of the liver to the diaphragm (see Figure 1.1). The anterior and antero-lateral regions of the liver are largely covered by the lower part of the sternum, the right fifth to tenth ribs, and their cartilaginous connections to the sternum (Yoganandan et al. 2001). The upper antero-lateral portion of the liver is also partly covered by the diaphragm and the lower part of

the right lung and pleura. The visceral (inferior/posterior) surface of the liver has impressions or recesses for the stomach, esophagus, duodenum, right kidney, transverse colon, and inferior vena cava (Netter 1997). The ligaments and the structures surrounding the liver play a large role in supporting the liver in its normal anatomical position.

Patterns and Mechanisms of Blunt Liver Injury

Different patterns of blunt liver injury are described in the Abbreviated Injury Scale (AIS), an injury severity scoring system that ranks blunt traumatic injuries on a scale of 0 (no injury) to 6 (maximal injury) (AAAM 1998). Moderate liver injuries (classified as AIS = 2) include subcapsular hematoma over less than 50% of the liver surface, nonexpanding or intraparenchymal hematoma less than 10 cm in diameter, and superficial lacerations less than 3 cm parenchymal depth and less than 10 cm in length. Serious injuries (AIS = 3) include hematoma covering more than 50% of the liver surface or expanding, intraparenchymal hematoma greater than 10 cm in diameter, lacerations greater than 3 cm parenchymal depth, and major bile duct involvement. Severe injuries (AIS = 4) include parenchymal disruption of less than 75% of a hepatic lobe, multiple lacerations more than 3 cm deep, and burst injury (stellate lacerations associated with massive tissue destruction). Critical injuries (AIS = 5) include parenchymal disruption of more than 75% of a hepatic lobe or involving the retrohepatic vena cava or central hepatic veins. Finally, maximal liver injury (AIS = 6) includes hepatic avulsion (total separation of all vascular attachments).

A number of mechanisms have been proposed to describe the causes of blunt liver injury in motor vehicle crashes. During rapid deceleration, the motion of the liver relative to the rest of the body may lead to injury at points of attachment due to stretching of the ligaments and blood vessels beyond their tensile strength (Rouhana 2002). Laceration of the liver may occur due to penetration of fractured ribs (Rouhana 2002). In low velocity impacts, the liver may be injured by compression against the spine or posterior wall of the abdomen (Melvin et al. 1973; Ragsdale and Trunkey 1993).

Rapid increases in internal fluid pressure have also been proposed as an important injury mechanism in fluid-filled solid abdominal organs such as the liver (Mays 1966, Stein et al. 1983). Impact-induced fluid pressure changes within the liver are thought to be associated with compressive and burst injury patterns. To date, previous liver injury biomechanics research has focused on investigating mechanical parameters measured external to the liver (e.g. force or impact velocity) as indicators of liver injury severity, while the association between internal fluid pressure and compressive or burst injury patterns has received little attention.

Previous Liver Injury Biomechanics Research

Several previous studies have focused on the significance of velocity and compression as indicators of abdominal injury in general and liver injury in particular. In a study of impacts applied to surgically mobilized livers in anesthetized Rhesus monkeys, Melvin et al. (1973) reported that the liver stress-strain behavior is sensitive to the rate of loading. In a series of abdominal impact experiments with anesthetized rabbits, Lau

and Viano (1981a) found that when compression was held constant at 16%, hepatic injury increased significantly with increasing impact velocity. Rouhana et al. (1985) reported that the product of maximum pre-impact velocity and maximum compression (V_{max}*C_{max}) was well correlated with abdominal injury in a series of lateral impacts to anesthetized rabbits. Horsch et al. (1985) found that the viscous tolerance criterion, the maximum of V*C as a function of time (Viano and Lau 1985), was well correlated with abdominal injury in a study of steering system impacts to porcine subjects. In an analysis of data from a series of out-of-position airbag impacts to anesthetized swine, Mertz et al. (1997) developed injury risk curves for abdominal injury as a function of maximum rate of abdominal compression.

Impact force and applied pressure have also been investigated as predictors of abdominal injury. Trollope et al. (1973) reported that 0.67 kN of force was associated with ESI > 2 (approximately AIS 3 or 4) liver injury in impacts to surgically exposed primate livers *in vivo*, while 1.56 kN of force was required to produce similar liver injury in impacts to anesthetized intact animals. In the study of surgically mobilized Rhesus monkey livers cited earlier, Melvin et al. (1973) found that 310 kPa applied pressure was associated with moderate (ESI ≥ 3) liver injury. Lau and Viano (1981b) reported that an applied stress of 350 kPa was necessary to produce hepatic surface injury in an investigation of belt-restraint loading in anesthetized beagles. In a series of tests investigating the effects of a force-limiting impact interface on abdominal injury, Rouhana et al. (1986) found that peak force was well correlated with renal injury but

not with hepatic injury. Results from this series of lateral abdominal impacts to anesthetized rabbits showed that the risk of serious abdominal injury did not change significantly with the force-limiting material, although the crushable interface reduced peak applied pressures to one third their previous values. In this study, Rouhana et al. (1986) indicated that "peak [applied] pressure has not proven to be a reliable correlate with injury," while "the rate and the extent of compression are more reliable indicators of soft tissue injury, and particularly of abdominal injury."

The differing conclusions from these studies reveal disagreement on the best predictor of abdominal injury for crash dummies. It is reasonable to believe that this variation could be due to the heterogeneity of the abdominal structure (different injury mechanisms for different organs). It would be beneficial to select an engineering parameter that is easy to measure and to which all the different injury mechanisms could be related for dummy design purposes. Internal pressure can be mathematically related to applied force, applied stress, compression, and velocity in a closed, deformable system. Pressure is also less sensitive to loading direction. These factors could simplify instrumentation in a dummy without sacrificing accuracy in the assessment of injury risk.

Previous Liver Constitutive Models

An understanding of the mechanical deformation behavior of the liver under high strain rate loading conditions could aid in the development of vehicle safety measures to reduce the occurrence of blunt liver injury. In particular, a constitutive

model of human liver mechanical behavior in high strain rate impact loading would be useful for developing finite element representations of the human abdomen that could be used assess the risk of abdominal injury in motor vehicle crash settings.

A few previous studies have developed constitutive models of liver response to different types of loading. Liu and Bilston investigated the mechanical properties of bovine liver under shear loading at low strain (2000) and at moderate to large strain (2002) with strain rates on the order of 0.075/s to 1/s. Results of these experiments were used to develop a model of liver response under moderate to large deformation based on a nonlinear viscoelastic differential model previously developed for brain tissue (Liu and Bilston 2002, Bilston et al. 2001). The model by Liu and Bilston employs a multi-mode upper convected Maxwell model and a Mooney elastic term, along with a nonlinear damping function that depends on shear strain amplitude. This complex model requires ten material constants and successfully captures complex features of liver viscoelastic behavior observed in the shear loading experiments, including strain rate sensitivity, nonlinearity (the relaxation modulus was dependent on strain for shear strains larger than 0.2%), and strain-time inseparability (slope of relaxation modulus vs. time was dependent on applied strain) (Liu and Bilston 2002).

Miller (2000) developed a nonlinear viscoelastic constitutive model of liver tissue based on previously published data from *in vivo* liver compression experiments at high strain rates using anesthetized Rhesus monkeys (Melvin et al. 1973). Miller's proposed model is valid for compressive nominal strains up to 35% and strain rates between 0.2

and 22.5 s^{-1}. Miller's model uses a general viscoelastic material model in which the stress is given by a convolution integral of the relaxation function and strain rate. The relaxation function is expanded using a Prony series. After making several simplifying assumptions, Miller presented an equation for stress that requires only four material constants and one time constant. Comparison of model predictions and experimental stress-elongation data from Melvin et al. (1973) demonstrated high correlation (R^2 = .97-.99).

There are some limitations involved in applying results from the previous studies to the development of computational models of the human liver response to impact loading. Most importantly, none of the previous liver constitutive models were developed from experiments with human liver tissue. In addition, while the loading conditions in the Miller model were applicable to blunt impact loading, strain rates greater than Miller's upper limit of 22.5 s^{-1} could reasonably be expected in the context of motor vehicle crashes. A need exists for a constitutive model of liver stress-strain behavior under high strain rate blunt impact loading based on experimental data from human liver specimens.

Summary

The major points of the preceding discussion are summarized below in order to highlight the significance of the current research.

- Field crash data and clinical studies indicate that blunt liver injury is a significant problem in motor vehicle crashes.
- Current crash dummies assume homogeneity in their response and are not equipped to represent solid abdominal organs located asymmetrically within the human abdomen.
- Previous injury biomechanics studies reveal disagreement on the best predictor of abdominal injury for crash dummies.
- Rapid increases in internal fluid pressure have been proposed as an important injury mechanism in fluid-filled solid abdominal organs such as the liver.
- No previous studies have investigated fluid pressure inside a solid abdominal organ as an indicator of soft tissue injury severity.
- A need exists for a detailed investigation of the statistical relationship between internal fluid pressure and liver injury risk, to provide an experimental basis for improving the ability of crash dummies to assess abdominal injury risk.

- A constitutive model of human liver mechanical behavior in high strain rate impact loading would be useful for developing finite element representations of the human abdomen that could be used to assess the risk of abdominal injury in motor vehicle crash settings.
- None of the previous liver constitutive models were developed from experiments with human liver tissue.

- A need exists for a constitutive model of liver stress-strain behavior under high strain rate blunt impact loading based on experimental data from human liver specimens.

1.2 OBJECTIVES

Experimental Design

The first goal of the analysis presented in Chapter 2 is to provide a theoretical framework for understanding the physical meaning of hydrostatic pressure within the liver and how hydrostatic pressure is related to applied normal stress in the direction of impact. The second goal of Chapter 2 is to describe the statistical methods that were used to investigate the major hypotheses of the research.

Preliminary Experiments

The purpose of the work presented in Chapter 3 is to conduct a preliminary investigation, using porcine *ex vivo* livers as surrogates for human livers, to evaluate whether a significant correlation exists between injury severity and impact-induced pressure changes in the hepatic veins.

The specific objectives of Chapter 3 are:

(1) To develop a porcine *ex vivo* organ experimental model to simulate blunt liver injury.

(2) To validate the experimental model through comparison of injury patterns with clinical examples of blunt liver injury from the CIREN database.

(3) To investigate impact-induced changes in vascular pressure as a predictor of blunt liver injury risk in *ex vivo* porcine livers.

Internal Fluid Pressure as an Indicator of Liver Injury Severity

The purpose of the research presented in Chapter 4 is to investigate the relationship between internal fluid pressure and liver injury severity in impact tests of *ex vivo* human livers and one post-mortem human subject.

The specific objectives of Chapter 4 are:

(1) To characterize the relationship between impact-induced fluid pressures and blunt liver injury in a human *ex vivo* organ experimental model.

(2) To compare human liver tissue pressure (measured in the parenchyma) and vascular pressure (measured in hepatic veins) with other biomechanical variables as predictors of liver injury risk.

(3) To investigate the feasibility of measuring liver vascular pressure in impacts to pressurized full body post-mortem human subjects (PMHS).

Mechanical Behavior of Human Liver in Blunt Impact Loading

The purpose of Chapter 5 is to develop a constitutive model of the stress-strain behavior of human liver tissue under high strain rate blunt impact loading, using strain rates from 19.7 to 62.5 s^{-1}.

The specific objective of Chapter 5 is:

(1) To modify a constitutive model previously developed for finite strain behavior of amorphous polymers (Dupaix and Boyce 2007) to characterize the observed liver mechanical behavior from a series of blunt impact experiments to pressurized *ex vivo* human livers.

Future Work

The purpose of Chapter 6 is to discuss recommended extensions of this research and to summarize the major conclusions of the work.

CHAPTER 2

EXPERIMENTAL DESIGN

ABSTRACT

The following discussion describes the theoretical framework of the study and the statistical methods. The theoretical framework draws from fundamental continuum mechanics concepts to provide support for the idea of a physical relationship between hydrostatic pressure and tissue-level liver injury. The statistical methods include simple linear regression, multiple linear regression, and binary logistic regression. Simple linear regression was used to evaluate relationships between continuous variables for cases involving a single independent predictor, while multiple linear regression was used for cases involving two or more independent predictors. Binary logistic regression was used to evaluate the probability of serious liver injury as a function of a given predictor variable.

2.1 THEORETICAL FRAMEWORK

The starting point for the current study is the idea that tissue level injury is related to tissue stress. The following quote from Y.C. Fung (2002) provides a thorough description of the stress-injury relationship:

> "Trauma to a person is equivalent to the failure of a machine or structure. Generations of engineers have studied the failure of machines and structures, and they have come to the conclusion that everything depends on stress. Every material has a critical value of stress below which it is "safe", and above which it "fails". An external load causes stress everywhere in a structure . . . If the critical stress is exceeded at the weakest spot, then the whole structure may be considered failed, seriously or otherwise. Engineers can design structures against failure. A person has to live with the structure she has. So a person has to understand the stress in one's body under traumatic circumstances."

The second step in the theoretical framework is the hypothesis that in a fluid-filled organ such as the liver, tissue stress is related to hydrostatic pressure through a known relationship from continuum mechanics. This relation is expressed in Equation (2.1) for the simplified example of a cube of homogeneous material subjected to uniaxial compression shown in Figure 2.1:

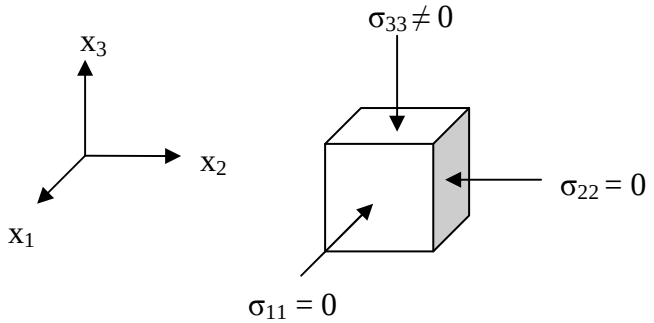

Figure 2.1: Stress state for uniaxial compression

(2.1) $$p = \frac{1}{3} tr\mathbf{T} = \frac{1}{3}\left(\sigma_{11} + \sigma_{22} + \sigma_{33}\right) = \frac{1}{3}\sigma_{33}$$

where: p = hydrostatic pressure (mean normal stress)

σ_{33} = normal stress in loading direction

$\sigma_{11} = \sigma_{22} = 0$

The concepts described above may be used to construct a logical basis for the central hypothesis of the current study: If tissue-level injury is related to tissue stress, and if tissue stress in the liver is related to hydrostatic pressure, then tissue-level injury should be related to hydrostatic pressure. The primary goal of the current research was to demonstrate whether a statistically significant relationship exists between liver injury severity and impact-induced changes in hydrostatic pressure within the liver.

2.2 TEST PLAN

Ex vivo liver biomechanical response and injury data were collected from impact experiments using 19 porcine livers and 14 human livers. The experimental conditions are summarized in Tables 2.1 and 2.2. Experimental conditions were selected with the goal of producing a range of injury severities from AIS 0 to 5. The range of impact energies was based on previous research (Mays 1996), and 30% maximum compression was determined from preliminary experiments using porcine livers.

Number of Subjects	Impact Energy (J)	Impact Velocity (m/s)	Maximum Compression (%)
5	105	3.0	30
3	226	4.3	30
6	250	4.6	30
5	420	6.0	30

Table 2.1: Nominal experimental conditions for 19 porcine liver impact tests

Number of Subjects	Impact Energy (J)	Impact Velocity (m/s)	Maximum Compression (%)
1	20	1.3	30
4	50	2.1	30
3	105	3.0	30
3	250	4.6	30
3	420	6.0	30

Table 2.2: Nominal experimental conditions for 14 human liver impact tests

2.3 STATISTICAL METHODS

In the liver impact experiments conducted for this research, hydrostatic pressure was measured at two sites within re-pressurized liver specimens: (1) inside the hepatic veins (termed “vascular pressure”); and (2) in the parenchyma (termed “tissue pressure”). Several hypotheses were investigated using the statistical methods outlined below. The following discussion is limited to brief examples to illustrate the statistical techniques. Results are described in detail in Chapters 3 and 4.

Hypothesis I: A significant relationship exists between liver injury severity and impact-induced changes in vascular pressure within the porcine liver.

Binary logistic regression is used to determine the association of a categorical response variable (e.g. AIS injury severity score) with different covariates. In the following example, the independent variable is peak vascular pressure, and the binary response variable is the presence/absence of serious (AIS ≥ 3) liver injury. Experimental data from the porcine liver impact test series was used to develop a sigmoidal curve that estimates the probability of serious liver injury as a function of peak vascular pressure (α = .05). The expression for the risk function is given in Equation (2.2). Two model parameters, represented as *a* and *b* in Equation (2.2), are needed to define the risk function. Model parameters were calculated from the experimental data using statistical software (SPSS version 15.0, Chicago, IL). Model goodness of fit was assessed using log likelihood, and pseudo-R^2 was calculated as a secondary measure of the correlation between peak vascular pressure and porcine liver injury severity.

(2.2) $$\text{Probability of AIS} \geq 3 \text{ liver injury} = \frac{e^{a+bx}}{1+e^{a+bx}}$$

where x = measured peak vascular pressure

a , b = model parameters

Results of the binary logistic regression are listed in Table 2.3, and a plot of injury risk versus peak vascular pressure is given in Figure 2.2. Results demonstrated that a

significant correlation exists between peak vascular pressure and injury severity in *ex vivo* porcine livers ($p < .001$, pseudo-$R^2 = .70$).

Model Parameters		Log Likelihood	Odds Ratio*	Significance	Pseudo-R^2
a	*b*				
-9.123	0.070	-5.91	1.072	$p < .001$	0.70

*The odds of serious liver injury increase by a factor of 1.072 when peak vascular pressure increases by one unit.

Table 2.3: Binary logistic regression results for vascular pressure as injury predictor

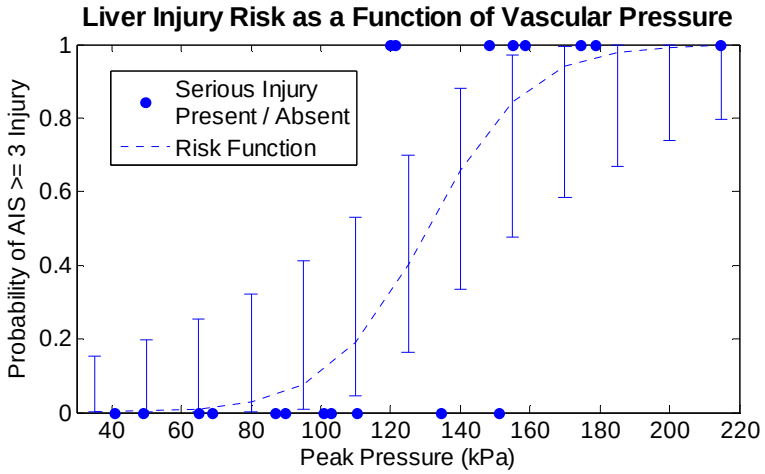

Figure 2.2: Binary logistic regression of peak vascular pressure and injury risk ($p<.001$) in 19 porcine liver impacts. Bars indicate 90% confidence bands for the risk function.

Hypothesis II: A significant relationship exists between liver injury severity and impact-induced changes in tissue pressure within the human liver.

In the *ex vivo* human liver impact test series, binary logistic regression was used to investigate the association of liver injury severity with several biomechanical variables. The following example illustrates the regression analysis of tissue pressure as an indicator of serious liver injury risk. Results of the binary logistic regression are listed in Table 2.4, and a plot of injury risk versus peak tissue pressure is given in Figure 2.3. Results demonstrated that a significant correlation exists between peak tissue pressure injury severity in *ex vivo* human livers ($p<.002$, pseudo-$R^2 = .78$).

Model Parameters		Log Likelihood	Odds Ratio	Significance	Pseudo-R^2
a	*b*				
-5.432	0.113	-2.638	1.132	$p < .002$	0.78

Table 2.4: Binary logistic regression results for tissue pressure as injury predictor

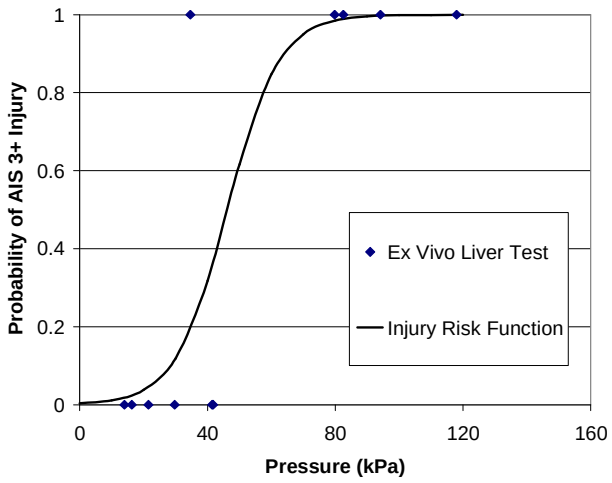

Figure 2.3: Binary logistic regression of peak tissue pressure and injury risk (p<.001) in human liver impacts

Hypothesis III: Measured peak pressure depends on transducer location.

Multiple linear regression is used to study the relationship between two or more independent predictor variables and a dependent variable. The current study employed multiple linear regression ($\alpha = .10$) to determine whether the vertical or radial distances to the pressure sensor from the point of impact were significant predictors of peak vascular pressure in the *ex vivo* human liver impact test series. Strain rate was included as a third predictor variable to control for variation in pressure due to impact velocity. The regression model is given by Equation (2.3), with model parameters listed in Table 2.5. The results demonstrated that vascular pressure was significantly correlated with strain rate and with radial distance from the impact point ($p < .10$). Vascular pressure was not correlated with vertical distance.

(2.3) Pressure (kPa) = $\beta_0 + \beta_1$*Vertical Distance (mm) + β_2*Radial Distance (mm) + β_3*Strain Rate (s^{-1})

Dependent Variable	Multiple Correlation Coefficient (R)	Model Significance (P-value)	Model Coefficients			
			β_0	β_1	β_2	β_3
Vascular Pressure	.84	.001	27.6	-.30	**-.36**	**1.56**

*__Boldface__ indicates that the corresponding variable is a significant correlate with pressure ($p<0.10$)

Table 2.5: Multiple linear regression results for the association between transducer location and peak vascular pressure

Hypothesis IV: Tissue pressure is a measure of hydrostatic pressure within the liver.

Simple linear regressions of tissue pressure versus average stress were obtained for the series of *ex vivo* human liver impact experiments in order to investigate the hypothesis that tissue pressure is a measure of hydrostatic pressure. "Average stress" refers to a calculated estimate of the normal stress at the level of a plane at 50% liver depth as shown in Figure 2.4. (Details of the calculation are given in Chapter 4 and Appendix B.) Since the cross-sectional area of the liver in the horizontal plane varies considerably with depth, the normal stress acting on the liver in the loading direction would be expected to vary with depth as well. It was assumed that the normal stress at the level of 50% liver depth corresponds to the average normal stress across different

depths. The set of resulting trend lines for tissue pressure versus average stress are given in Figure 2.5.

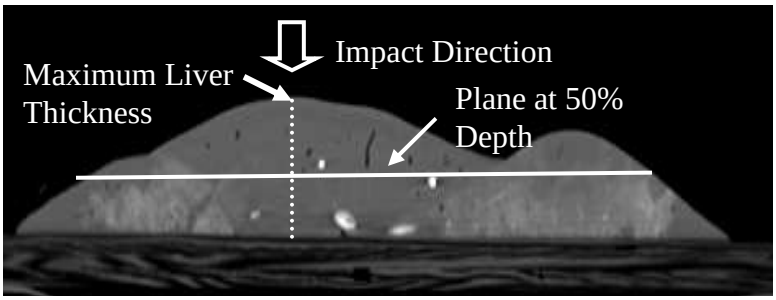

Figure 2.4: Liver CT scan (inferior-superior view) illustrating variation in cross-sectional area as a function of depth

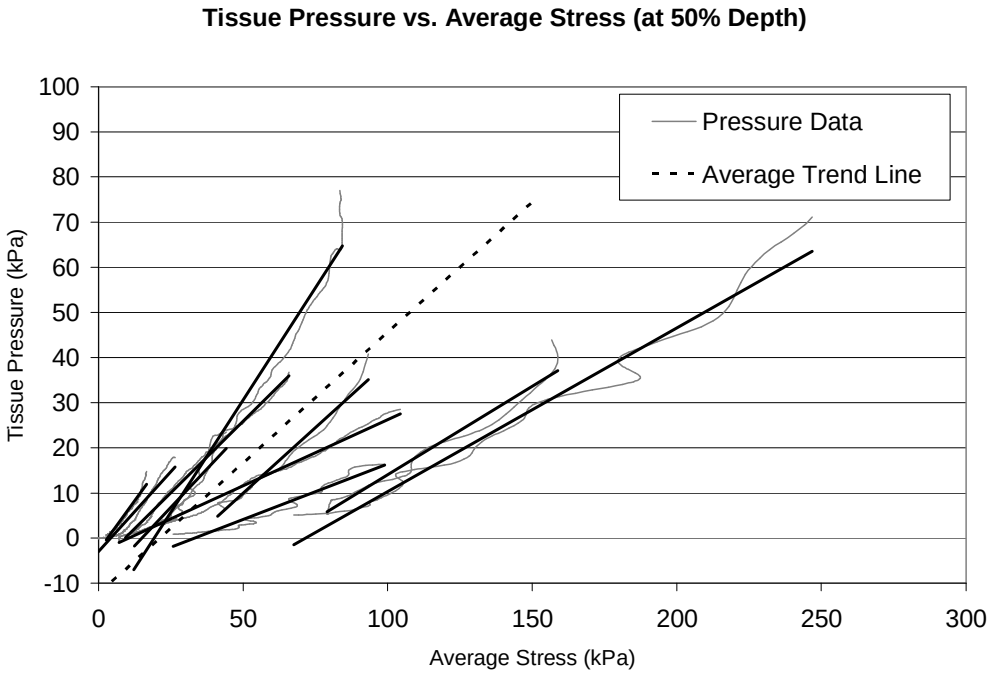

Figure 2.5: Linear regressions of tissue pressure vs. average normal stress. Slope of average trend line was 0.578.

For the set of tissue pressure versus average stress regressions in Figure 2.5, the mean slope value was 0.578. This value was used in Equation (1) to investigate the relationship between tissue pressure and stress. It was assumed that σ_{11} and σ_{22} represent equal lateral normal stresses (σ_L), as shown in Equation (2.4).

(2.4) $$p = \frac{1}{3}(2\sigma_L + \sigma_{33}) = (.578)\sigma_{33}$$

$$\sigma_L = (.367)\sigma_{33}$$

Given the assumption that tissue pressure is equivalent to hydrostatic pressure, this analysis indicates that a compressive normal stress of $(.367)\sigma_{33}$ acts on the lateral surfaces of the liver during impact loading. This outcome is reasonable since the structure of the liver is not homogeneous. The liver has a connective tissue capsule that acts to resist the lateral expansion of the parenchyma due to the Poisson effect. Overall, the results of Figure 2.5 and Equation (2.4) are consistent with the interpretation that tissue pressure is a measure of hydrostatic pressure within the liver.

CHAPTER 3

EVALUATING INTRAVASCULAR PRESSURE AS AN INDICATOR OF INJURY SEVERITY IN AN *EX VIVO* PORCINE MODEL OF BLUNT LIVER TRAUMA

ABSTRACT

The objectives of this study were to develop an *ex vivo* organ model to simulate blunt liver injury and to investigate impact-related pressure changes as a predictor of injury risk. Knowledge of the relationship between fluid pressure changes and the likelihood of liver injury could be used to enhance the design of crash test dummies used in vehicle safety testing. Excised porcine livers (n = 19) were instrumented with pressure sensors in the hepatic veins and perfused with normal saline at physiologic temperature and pressures. A drop tower was used to apply blunt impact at varying velocities (3-6 m/s). Injury severity scores were assigned according to the AIS. Experimental liver injuries produced in this model were consistent with those observed in motor vehicle accident victims documented in the Crash Injury Research and Engineering Network (CIREN) database. A significant binary logistic regression model was obtained for peak vascular pressure as a predictor of serious (AIS $\geq$ 3) liver injury in blunt impacts to *ex vivo* porcine livers.

3.1 BACKGROUND

Field accident studies have shown that the liver is among the most frequently injured abdominal organs in both frontal and side impact collisions (Elhagediab and Rouhana 1998; Rouhana and Foster 1985; Bondy 1980). In clinical studies, the mortality rates associated with blunt hepatic trauma range from 9-17% overall and may be as high as 67% if the injury involves the retrohepatic vena cava or hepatic veins (Christmas 2005, Hurtuk 2006, John et al. 1992). These statistics indicate that liver injury is a significant problem in motor vehicle crashes.

Previous studies have analyzed the relationship between liver injury and numerous physical parameters, including energy (Mays 1966), applied pressure (Walfisch et al. 1980), impact force (Talantikite 1993), velocity (Lau et al. 1981), compression (Rouhana et al. 1986), and the product of velocity and compression (Rouhana et al. 1985). A trend that emerges from a review of previous literature is that injury to soft abdominal tissues is strongly associated with both the rate and extent of compression (Rouhana et al. 1986). The rate dependence of the liver's mechanical behavior (Melvin et al. 1973) is a likely factor contributing to this trend.

Rapid increases in internal fluid pressure have been proposed as an important injury mechanism in fluid-filled solid abdominal organs such as the liver (Mays 1966, Stein et al. 1983). Impact-induced fluid pressure changes within the liver are thought to be associated with compressive and burst injury patterns. Burst injury is a severe form of blunt liver trauma characterized by stellate lacerations and extensive damage to the

liver's internal architecture. To date, previous liver injury biomechanics research has focused on investigating mechanical parameters measured external to the liver (e.g. force or impact velocity) as indicators of liver injury severity, while the association between internal fluid pressure and compressive or burst injury patterns has received little attention.

The purpose of the present study was to investigate whether a significant correlation exists between injury severity and impact-induced pressure changes in the hepatic veins of *ex vivo* porcine livers. Knowledge of a significant relationship between internal fluid pressure and liver injury severity could be used to enhance the injury prediction capabilities of anthropomorphic dummies used in vehicle safety testing.

The objectives of the study are:

(1) To develop a porcine *ex vivo* organ experimental model to simulate blunt liver injury.

(2) To validate the experimental model through comparison of injury patterns with clinical examples of blunt liver injury from the CIREN database.

(3) To investigate impact-induced changes in vascular pressure as a predictor of blunt liver injury risk in *ex vivo* porcine livers.

3.2 METHODS

Basis for Experimental Technique

Results from a number of studies indicate that the physiological perfusion pressure within the liver plays an important role in the liver's response to blunt trauma, with regard to both injury outcomes and mechanical behavior. A study of blunt liver injury by Mays (1966) showed that reproducing the hemodynamic pressure in the cadaver liver was important for the pathogenesis of burst injury. More recently, Liu and Bilston (2002) reported a discrepancy between liver mechanical response data measured under *in vitro* conditions (Liu and Bilston 2002, Seki et al. 1998, Wang et al. 1992) as compared to data obtained *in vivo* (Melvin et al. 1973). The authors suggested that this discrepancy may be due to a strong effect of perfusion on the biomechanical properties of very soft tissues such as the liver (Liu and Bilston 2002). A study of *in vivo* and *ex vivo* porcine livers investigated the effect of perfusion on liver mechanical properties (Kerdok et al. 2006). This study found that the viscoelastic properties of the liver change with perfusion and that the mechanical behavior of perfused *ex vivo* livers closely approximated the *in vivo* behavior (Kerdok et al. 2006). In light of this literature, an *ex vivo* perfusion system was developed to reproduce physiological pressures in the vasculature of porcine liver specimens subjected to blunt impact in the present series of experiments.

A study of blunt abdominal trauma in anesthetized primate and porcine subjects reported an association between impactor cross-sectional area and the type of liver

injury produced (Trollope 1973). In that study a variety of impactor sizes were investigated. The authors observed that impactor surfaces with small cross-sectional area relative to the liver surface were more likely to produce localized surface lacerations, while large cross-sectional area impactors were more likely to produce burst injury. A flat rigid impactor with large cross-sectional area relative to the liver surface was chosen for the present study in order to increase the likelihood of compressive and burst injury outcomes and to avoid surface lacerations due to concentrated stresses near the edges of a narrow impactor.

The range of impact energies used in the present study was selected with the intent of producing a range of injury severities in the porcine liver equivalent to 0 (no injury) to 5 (major parenchymal disruption of a hepatic lobe) on the Abbreviated Injury Scale (AIS) (AAAM 1998). A prior study involving drop tests of cadaver livers injected with barium and saline (Mays 1966) reported that impact energies of 37-46 J produced tears and lacerations to Glisson's capsule without evidence of vascular or biliary damage (AIS 2). Energies of 144-182 J produced deeper lacerations and occasional disruption of small arteries or bile ducts (AIS 3). Higher energies in the range of 386-488 J resulted in burst injury and extensive pulpefaction of the liver with severe disruption of tertiary divisions of the portal vein, hepatic artery, and bile ducts (AIS 4 and 5). Results of this prior study were used to guide the selection of impact energy levels in the present investigation. It should be noted that in the study by Mays cited above the impacts were applied by dropping cadaver livers from varying heights onto a concrete surface,

while in the present study an impact plate was dropped onto porcine livers using a drop tower technique.

Test Matrix and Instrumentation

Impact tests were conducted on nineteen *ex vivo* porcine livers. Porcine livers were selected as test specimens because the organ mass is similar to that of humans. The specimens were acquired from a local meat-processing facility and were harvested immediately after the animal was sacrificed. All specimens were packed in ice until testing began, and all specimens were tested within twelve hours of death in order to minimize post-mortem degradation of the tissue. The average liver mass with gallbladder attached was 1496 ± 254 g.

The mass of the impact plate (23.4 kg) was constant for all tests, and the nominal impact velocities were calculated from the drop heights required to achieve the desired impact energies. Nominal maximum compression of the liver was held constant at 30% in order to minimize the number of variables. A pilot investigation showed that varying impact energy within the range shown in Table 3.1 while holding compression constant at 30% produced the desired range of injury severities in porcine livers. Table 3.1 summarizes test conditions for the nineteen porcine liver impact tests conducted in the present study.

Number of Subjects	Impact Energy (J)	Impact Velocity (m/s)	Nominal Maximum Compression (%)
5	105	3.0	30
3	226	4.3	30
6	250	4.6	30
5	420	6.0	30

Table 3.1: Test matrix for porcine liver impact tests

Prior to the impact event each liver was weighed and photographed. Specimens were instrumented with three miniature pressure-measuring catheters (Model SPR-524, Millar Instruments, Houston, TX) in three hepatic veins through the opening of the vena cava, as illustrated in Figure 3.1. A pre-test CT scan was obtained for each specimen in order to determine the locations of the pressure sensors and to evaluate the initial condition of the hepatic arterial and portal venous systems using radio-opaque contrast material. An example of a reconstructed pre-test CT scan is shown in Figure 3.2.

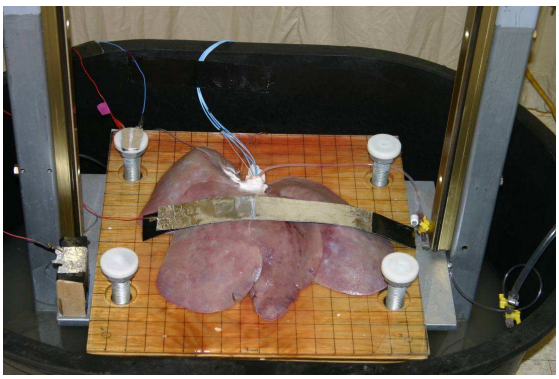

Figure 3.1: Instrumented porcine liver in base of drop tower

Figure 3.2: Reconstructed pre-test CT image showing three pressure sensors in hepatic veins of a porcine liver specimen. Contrast material was injected into the hepatic artery and portal vein.

Drop Tower Design and Perfusion System

After specimen preparation was complete, the impact test was conducted using a drop tower technique. A 23.4 kg impact plate made of steel and aluminum was released from varying heights using an electromagnetic trigger mechanism. High density plastic slip bearings were secured to the sides of the plate to interact with two guide rails on opposite sides of the tower. An accelerometer was mounted to the impact plate. A contact sensor was used to synchronize the data acquisition system with initiation of the impact event. Compression was limited to 30% of the maximum height of the liver through the use of adjustable-height brake columns. The drop tower design is shown in Figure 3.3.

The perfusion system shown in Figure 3.4 was developed to produce vascular pressures within the physiologic range in the *ex vivo* porcine livers. Constant fluid level

reservoirs of normal saline solution were positioned at appropriate heights to supply constant pressures of 100 mmHg in the hepatic artery and 9 mmHg in the portal vein. Each liver was perfused with heated saline (33-37 °C) for forty-five to sixty minutes prior to the impact.

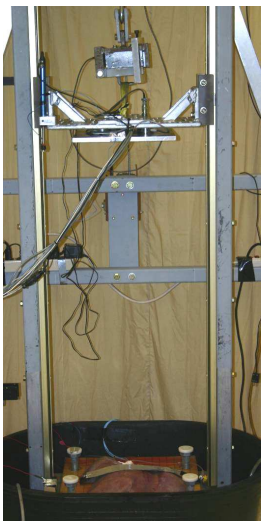

Figure 3.3: Drop tower

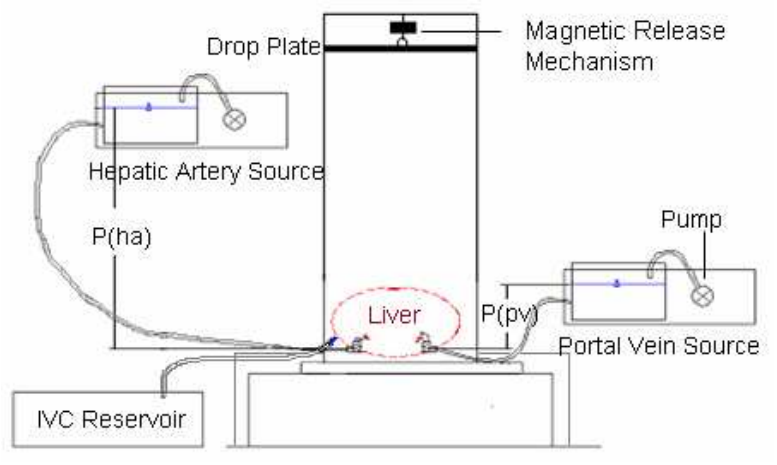

Figure 3.4: Schematic of perfusion system

Injury Analysis

Following the impact event visual inspections were performed to identify signs of injury. A trauma surgeon assigned injury severity scores according to a modified version of the AIS (AAAM 1998). The scoring system is summarized in Table 3.2.

AIS 0	No Injury
AIS 2	Superficial Lacerations Subcapsular Hematoma Over ≤ 50% of Surface
AIS 3	Deep Laceration Duct or Vascular Involvement Hematoma Over >50% of Surface or Expanding
AIS 4	Multiple Deep Lacerations "Burst Injury" (Stellate Lacerations, Shattering of Parenchyma)
AIS 5	Parenchymal Disruption of >75% of a Hepatic Lobe Involvement of Retrohepatic Vena Cava or Central Hepatic Veins
AIS 6	Hepatic Avulsion

Table 3.2: Modified AIS for ranking porcine liver injury severity

A search of the Crash Injury Research and Engineering Network (CIREN) database was conducted to identify photographs of liver injury patterns sustained by victims of motor vehicle crashes. These images were used to assess whether the injury outcomes produced in the porcine experimental model were consistent with blunt liver injuries observed clinically.

Data Processing and Statistical Methods

Data was collected at a sampling frequency of 20 kHz. Impact velocities were calculated by integrating the measured plate acceleration up to the time of impact. Impact energies were determined from the plate mass and the calculated impact velocity.

Binary logistic regression ($\alpha = .05$) was used to evaluate the probability of serious (AIS ≥ 3) liver injury as a function of peak vascular pressure and as a function of impact

velocity. Statistical significance was assessed using the log likelihood test, and pseudo-R^2 was calculated to evaluate the correlation between peak pressure and liver injury severity. Equation (3.1) is the expression for the risk function. Peak pressures were measured experimentally, and model parameters *a* and *b* were calculated using a statistical software package (SPSS version 15.0, Chicago, IL).

(3.1) Probability of AIS ≥ 3 liver injury $= \frac{e^{a+bx}}{1+e^{a+bx}}$

where x = peak pressure

a , b = model coefficients

3.3 RESULTS

Experimental injury outcomes of varying severities are shown in Figure 3.5 in conjunction with similar injury patterns in CIREN cases. Injury outcomes ranged from AIS 0 to AIS 5. Figures 3.5A and 3.5B show superficial lacerations to the liver capsule. Figures 3.5C and 3.5D illustrate a burst injury pattern with stellate lacerations and shattering of the parenchyma. Figures 3.5E and 3.5F show massive disruption of a hepatic lobe. These images demonstrate that the experimentally induced liver injuries in the porcine model were consistent with injury patterns observed in motor vehicle crash victims documented in the CIREN database.

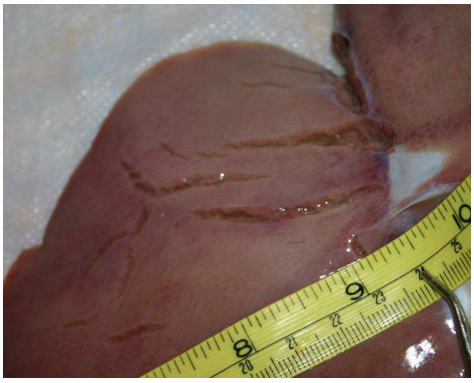

Figure 3.5A: AIS 2 injury in porcine liver

Figure 3.5B: AIS 2 injury in CIREN case

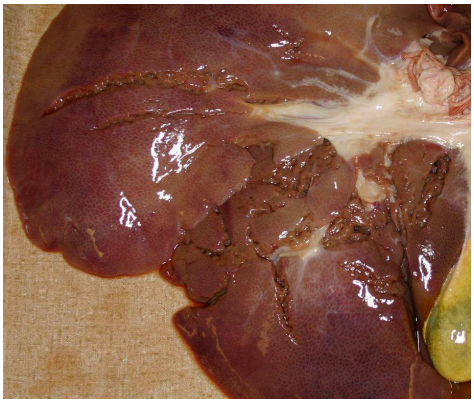

Figure 3.5C: AIS 4 injury in porcine liver

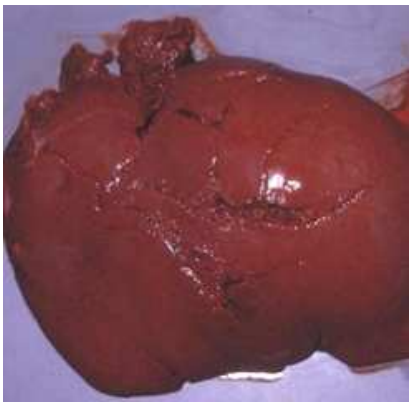

Figure 3.5D: AIS 4 injury in CIREN case

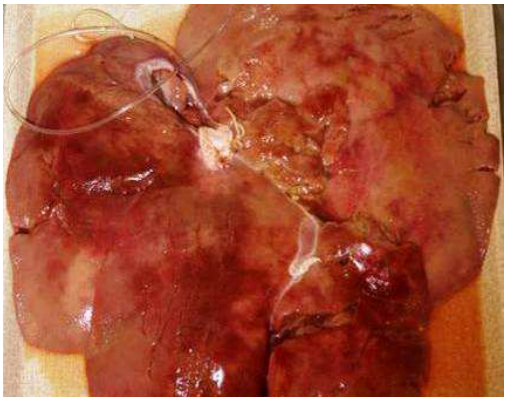

Figure 3.5E: AIS 5 injury in porcine liver

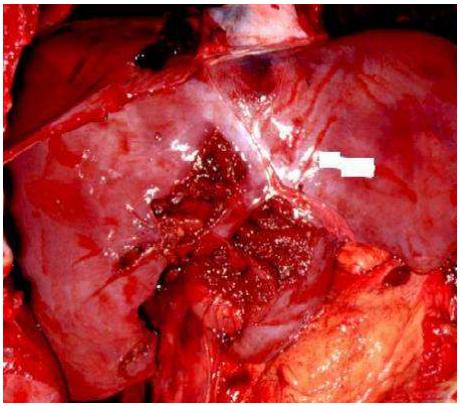

Figure 3.5F: AIS 5 injury in CIREN case

Figure 3.5: Injuries in porcine model compared to CIREN cases

Measured impact velocities, peak vascular pressures, and AIS scores for all tests are presented in Table 3.3. Binary logistic regression model parameters are given in Table 3.4. Peak vascular pressure was a significant predictor of serious injury ($p < .001$), and peak pressure was well correlated with injury severity (pseudo-$R^2 = 0.70$). In this porcine liver impact test series, a peak vascular pressure of 130 kPa (975 mmHg) was associated with a 50% probability of AIS ≥ 3 liver injury. The calculated odds ratio indicated that the odds of serious liver injury increase by a factor of 1.072 when the peak vascular pressure increases by one unit (kPa). A plot of liver injury risk as a function of peak vascular pressure is given in Figure 3.6, including 90% confidence bands for the calculated risk function.

Impact velocity also was a significant predictor of serious injury ($p < .001$), and the correlation with injury severity was slightly higher for impact velocity (pseudo-$R^2 = 0.72$) than for peak pressure. An impact velocity of 4.5 m/s was associated with a 50% probability of serious liver injury. The odds ratio for impact velocity was 53.24. A plot of impact pressure versus injury risk is shown in Figure 3.7, including 90% confidence bands for the risk function. The 90% confidence bands were wider for impact velocity as an indicator of injury than for peak pressure.

Specimen Number	Impact Energy (J)	Impact Velocity (m/s)	Peak Pressure (kPa)	AIS
PL04250	237	4.5	120	3
PL05105	105	3.0	65	0
PL06250	237	4.5	134	2
PL07420	394	5.8	148	5
PL08105	105	3.0	41	0
PL09420	380	5.7	155	4
PL10105	98	2.9	49	0
PL11250	248	4.6	159	3
PL12420	380	5.7	174	5
PL13105	105	3.0	90	0
PL14250	237	4.5	103	2
PL15420	394	5.8	179	4
PL16105	98	2.9	69	2
PL17250	227	4.4	87	2
PL18420	341	5.4	214	5
PL19226	197	4.1	121	3
PL20226	197	4.1	101	2
PL21226	197	4.1	151	2
PL23250	216	4.3	110	2

Table 3.3: Results of porcine liver impacts

Independent Variable	Model Parameters		Log Likelihood	Odds Ratio	Significance	Pseudo-R^2
	a	*b*				
Peak Pressure (kPa)	-9.123	0.070	-5.91	1.072	$p < .001$	0.70
Impact Velocity (m/s)	-18.031	3.975	-5.67	53.24	$p < .001$	0.72

Table 3.4: Binary logistic regression results

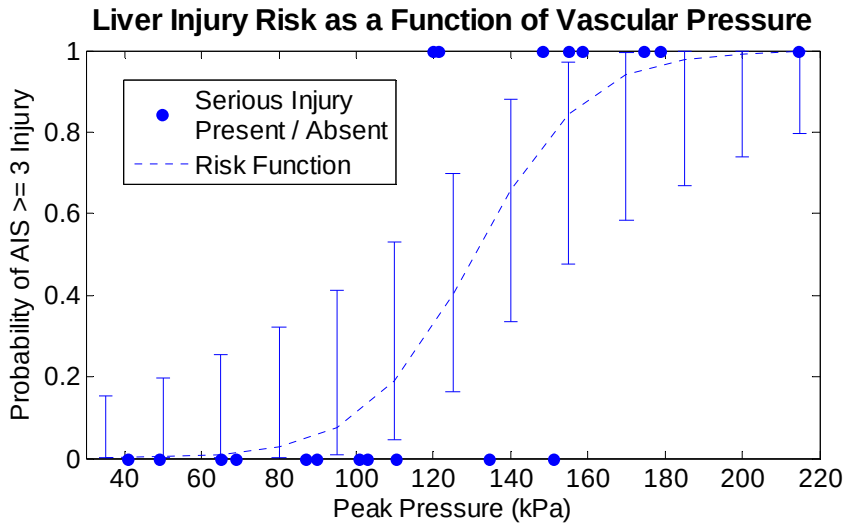

Figure 3.6: Binary logistic regression of peak vascular pressure and injury risk in 19 porcine liver impacts. Bars indicate 90% confidence bands for the risk function.

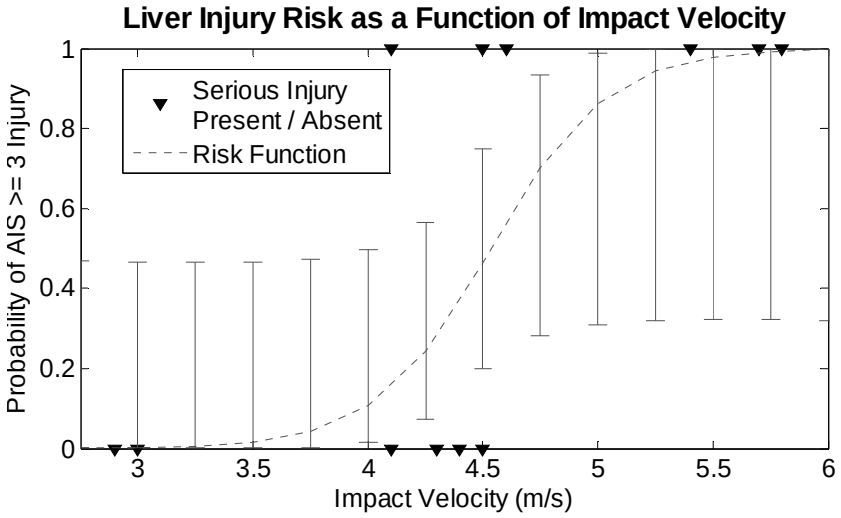

Figure 3.7: Binary logistic regression of impact velocity and injury risk in 19 porcine liver impacts. Bars indicate 90% confidence bands for the risk function.

3.4 DISCUSSION

The injury patterns produced in this series of blunt impacts to re-pressurized porcine livers were remarkably consistent with the types of hepatic trauma documented in CIREN cases. In particular, the porcine experimental model in the current study successfully reproduced compressive and burst injury outcomes. Generating burst injury in the perfused porcine liver experimental model supports previous findings that hemodynamic pressures are necessary for the occurrence of burst injury mechanisms in the liver (Mays 1966).

In the series of *ex vivo* porcine liver impacts presented in this study, nominal maximum compression of the liver was held constant at 30%. Under these conditions, binary logistic regression analysis demonstrated that impact velocity was well correlated with liver injury severity (pseudo-R^2 = .72, $p < .001$). This finding is consistent with previous liver injury research. In a series of impacts to anesthetized rabbits, Lau and Viano reported an increase in liver injury severity with increasing impact velocity when antero-posterior abdominal compression was held constant at 16% (1981a). The relatively wide 90% confidence bands at the low and high ends of the velocity range in Fig. 3.7 were attributed to the fact that the impact velocity values are clustered in three groupings corresponding to the energy levels in the test matrix. A more uniform distribution of impact velocities across the test range would likely narrow the 90% confidence bands in future testing.

The novel injury predictor presented in this study is vascular pressure. Peak vascular pressure was a significant predictor of injury ($p < .001$) and was well correlated with liver injury severity (pseudo-$R^2 = .70$). Peak pressure performed approximately as well as impact velocity as an indicator of liver injury severity, with tighter 90% confidence bands and similar correlations and p-values. The importance of peak vascular pressure over impact velocity as an injury indicator is that vascular pressure is related to the liver's *response* to the impact event, while impact velocity is an independent variable in the experimental design. Because of this relationship to liver response, impact-induced changes in vascular pressure could be used to investigate a detailed injury mechanism that relates the physical conditions inside the liver with mechanical failure of the liver's structural components.

Since the present study was conducted using *ex vivo* porcine livers, the applicability of the results to human livers is unknown at this time. Several important differences exist between human and porcine livers, including organ geometry and connective tissue content. Porcine livers are broad, relatively flat organs with five lobes, while human livers have only four lobes and have a more rounded globular shape (see Figs. 3.1 and 3.5). At a microscopic level, hepatic lobules in the porcine liver have clearly delineated connective tissue boundaries, while hepatic lobules in the human liver are not as well-defined. This higher connective tissue content in porcine livers could contribute to increased stiffness in the organ's response to impact and injury as compared to human livers. The findings of the present study demonstrate that a

significant relationship exists between vascular pressure and blunt liver injury in re-pressurized *ex vivo* porcine livers. Further testing is needed to determine if a similar relationship holds true in human livers.

3.5 CONCLUSIONS

Experimental blunt liver injuries produced in this *ex vivo* porcine model were consistent with those observed in motor vehicle crash victims. The liver vascular system was re-pressurized using a perfusion system, and compressive and burst injury outcomes were observed. Significant binary logistic regression models were obtained for peak vascular pressure and for impact velocity as indicators of injury severity ($p < .001$). Similar correlations with injury severity were obtained for vascular pressure and for impact velocity (pseudo-R^2 = .70 and .72, respectively). A 50% probability of AIS ≥ 3 liver injury was associated with a peak vascular pressure of 130 kPa (975 mmHg) and an impact velocity of 4.5 m/s at 30% compression. Since vascular pressure is related to the liver's mechanical response to an impact event, it could be used to investigate an injury mechanism that links physical conditions within the liver to mechanical failure of the liver capsule and internal architecture. In addition, an understanding of the relationship between fluid pressure within the liver and the probability of serious liver injury could be used to enhance the abdominal injury prediction capabilities of anthropomorphic dummies used in vehicle safety testing.

CHAPTER 4

USING FLUID PRESSURE TO PREDICT BLUNT LIVER INJURY RISK: IMPACT TESTS OF EX VIVO HUMAN LIVERS AND ONE POST-MORTEM HUMAN SUBJECT

ABSTRACT

Liver trauma research suggests that rapidly increasing internal pressure plays a role in causing blunt liver injury. Knowledge of the relationship between pressure and the likelihood of liver injury could be used to enhance the design of crash test dummies. The objectives of this study were (1) to characterize the relationship between impact-induced pressures and blunt liver injury in an *ex vivo* organ experimental model; (2) to compare human liver tissue pressure and vascular pressure with other biomechanical variables as predictors of liver injury risk; and (3) to investigate the feasibility of measuring liver vascular pressure in impacts to pressurized full body post-mortem human subjects (PMHS). Test specimens included 14 *ex vivo* human livers and 1 full body PMHS. Specimens were perfused with normal saline solution at physiological pressures, and a drop tower applied blunt impact at varying energies. Impact-induced pressures were measured by transducers inserted into the hepatic veins and the parenchyma (caudate lobe) of *ex vivo* specimens. Experimentally induced liver injuries

were consistent with those documented in the Crash Injury Research and Engineering Network (CIREN) database. Binary logistic regression analysis demonstrated that tissue pressure measured in the parenchyma was the best indicator of serious liver injury risk ($p = .002$, Pseudo-$R^2 = .78$). A peak tissue pressure of 48 kPa was correlated to 50% risk of serious (AIS ≥ 3) liver injury. A burst injury mechanism directly related to hydrostatic pressure is postulated for the *ex vivo* liver loaded dynamically in a drop test experiment.

4.1 BACKGROUND

Several studies have investigated the incidence of abdominal injuries in motor vehicle crashes (Ricci 1980; Rouhana and Foster 1985; Elhagediab and Rouhana 1998; Augenstein et al. 2000). Results from these studies indicate that abdominal injuries comprise only 3-5% of the total number of injuries due to automotive crashes. However, abdominal injuries account for increasingly higher proportions of more severe injury categories. For example, Elhagediab and Rouhana (1998) reported that abdominal injuries constituted 8% of AIS ≥ 3 injuries, 16.5% of AIS ≥ 4 injuries, and 20.5% of AIS ≥ 5 injuries in a review of frontal impacts in the NASS database for the years 1988 through 1994. A similar pattern was observed in studies by Ricci (1980), Rouhana and Foster (1985), and Augenstein et al. (2000). The vehicle contact points associated with abdominal injury include the steering wheel, belt, airbag, armrest, side interior, and instrument panel.

Solid organs such as the liver, spleen, and kidney are the most frequently injured abdominal organs in both frontal and side impact collisions (Rouhana and Foster 1985; Elhagediab and Rouhana 1998). According to clinical studies, the reported mortality rate for blunt liver injury ranges from 9-17% overall and increases to 30% if operative intervention is required (Christmas et al. 2005; Hurtuk et al. 2006). For liver injuries involving the inferior vena cava or hepatic veins, the mortality rate is as high as 67% (John et al. 1992). These statistics indicate that blunt liver injury is a significant problem in motor vehicle crashes. To date, no existing crash dummy is equipped to represent solid abdominal organs located asymmetrically in the human abdomen (Tamura et al. 2002). All existing instrumented abdominal components in crash dummies assume homogeneity in their response. A need exists for detailed investigations of the injury mechanisms and mechanical response of the individual solid abdominal organs in blunt impact loading.

Several previous studies have focused on the importance of velocity and compression as indicators of abdominal injury in general and liver injury in particular. In a study of impacts applied to surgically mobilized livers in anesthetized Rhesus monkeys, Melvin et al. (1973) reported that the liver stress-strain behavior is sensitive to the rate of loading. In a series of abdominal impact experiments with anesthetized rabbits, Lau and Viano (1981a) found that when compression was held constant at 16%, hepatic injury increased significantly with increasing impact velocity. Rouhana et al. (1985) reported that the product of maximum pre-impact velocity and maximum compression

(V_{max}*C_{max}) was well correlated with abdominal injury in a series of lateral impacts to anesthetized rabbits. Horsch et al. (1985) found that the viscous tolerance criterion, the maximum of V*C as a function of time (Viano and Lau 1985), was well correlated with abdominal injury in a study of steering system impacts to porcine subjects. In an analysis of data from a series of out-of-position airbag impacts to anesthetized swine, Mertz et al. (1997) reported that the rate of abdominal compression was well correlated with injury.

Impact force and applied pressure have also been investigated as predictors of abdominal injury. Trollope et al. (1973) reported that 0.67 kN of force was associated with ESI > 2 (approximately AIS 3 or 4) liver injury in impacts to surgically exposed primate livers *in vivo*, while 1.56 kN of force was required to produce similar liver injury in impacts to anesthetized intact animals. In the study of surgically mobilized Rhesus monkey livers cited earlier, Melvin et al. (1973) found that 310 kPa applied stress was associated with moderate (ESI ≥ 3) liver injury. Lau and Viano (1981b) reported that an applied stress of 350 kPa was necessary to produce hepatic surface injury in an investigation of belt-restraint loading in anesthetized beagles. In a series of tests investigating the effects of a force-limiting impact interface on abdominal injury, Rouhana et al. (1986) found that peak force was well correlated with renal injury but not with hepatic injury. Results from this series of lateral abdominal impacts to anesthetized rabbits showed that the risk of serious abdominal injury did not change significantly with the force-limiting material, although the crushable interface reduced

peak applied pressures to one third their previous values. In this study, Rouhana et al. (1986) indicated that "peak [applied] pressure has not proven to be a reliable correlate with injury," while "the rate and the extent of compression are more reliable indicators of soft tissue injury, and particularly of abdominal injury."

The purpose of the present study is to investigate the relationship between internal fluid pressure and liver injury severity. Rapid increases in internal fluid pressure have been proposed as an important injury mechanism in fluid-filled solid abdominal organs such as the liver (Mays 1966, Stein et al. 1983). A small number of previous studies have investigated fluid pressure in association with the abdomen. Prasad and Daniel (1984) used peak aortic blood pressure as a measure of abdominal compression in airbag tests of anesthetized swine. In developing a prototype pregnant abdomen for the small-female Hybrid III anthropomorphic test device (ATD), Rupp et al. (2001) correlated peak pressures inside a fluid-filled bladder component with the risk of adverse fetal outcome. No previous studies have investigated fluid pressure inside a solid abdominal organ as an indicator of soft tissue injury severity.

The objectives of the present study are:

(1) To characterize the relationship between impact-induced fluid pressures and blunt liver injury in an *ex vivo* organ experimental model.

(2) To compare human liver tissue pressure (in parenchyma) and vascular pressure with other biomechanical variables as predictors of liver injury risk.

(3) To investigate the feasibility of measuring liver vascular pressure in impacts to pressurized full body post-mortem human subjects (PMHS).

4.2 METHODS

Ex Vivo Organ Tests

Test specimens included 14 livers from unembalmed post-mortem human subjects (PMHS) (Table 4.1). Liver specimens were excluded from the study if the donor had a history of liver disease, known exposure to HIV or HBV, cancer with liver metastasis, abdominal or thoracic trauma, communicable disease or sepsis at the time of death. All specimens were tested within 36 hours of death. The average age was 67 ± 16 years with a range of 36 to 92 years. The average liver mass (with gallbladder attached) was 1992 ± 921 grams.

Subject ID	Age (years)	Height (cm)	Body Mass (kg)	Gender	Liver Mass (g)
HL01	77	163	72.5	Female	1588
HL02	36	188	172.3	Male	4660
HL03	73	183	81.6	Male	1367
HL04	59	157	77.1	Female	1745
HL05	81	185	99.8	Male	1760
HL07	72	178	77.1	Male	2948
HL08	51	183	99.8	Male	2139
HL09	47	191	76.2	Male	1722
HL10	63	183	88.4	Male	2293
HL11	71	160	81.6	Female	1646
HL12	91	163	54.4	Female	995
HL13	92	168	71.6	Male	1147
HL14	74	163	128.3	Female	1545
HL15	55	173	88.0	Male	2330

*HL06 excluded from analysis due to abnormal pressures in bile duct system.

Table 4.1: Subject characteristics

The test conditions are summarized in Table 4.2. Nominal impact energies ranged from 20 to 420 J. Impact velocities ranged from 1.0 to 5.7 m/s. The maximum compression of the liver at its highest point was limited to approximately 30% for all tests, with an average of 31.5 ± 6%. Experimental conditions were selected with the goal of producing a range of injury severities. Impact energies were based on previous research (Mays 1966) and 30% compression was determined from preliminary experiments using porcine livers.

Number of Liver Specimens	Nominal Impact Energy (J)	Average Maximum Compression (%)	Average Impact Velocity (m/s)
1	20	20	1.0
4	50	32	1.7
3	105	29	2.7
3	250	33	4.3
3	420	35	5.4

Table 4.2: Experimental conditions for 14 human liver impact tests

Drop Tower Design. A drop tower was used to apply blunt impact to the isolated liver specimens. The drop tower included a 23.4 kg two-layered impact plate composed of steel (upper layer) and aluminum (lower layer). Plate instrumentation is illustrated in Figure 4.1. An accelerometer was mounted to the aluminum layer. Three load cells were mechanically coupled to both layers and were mounted in a triangular arrangement at 120 degree intervals. The fourth load cell was mechanically isolated from the lower aluminum layer. It was mounted in the center of the upper plate and capped so that the loading surface was flush with the flat impact surface. The cross-sectional area of the loading surface of the isolated load cell was 5.1 cm^2, and the total cross-sectional area of the aluminum impact surface was 1006 cm^2. The arrangement was such that the total impact force was transmitted completely through the four load cells.

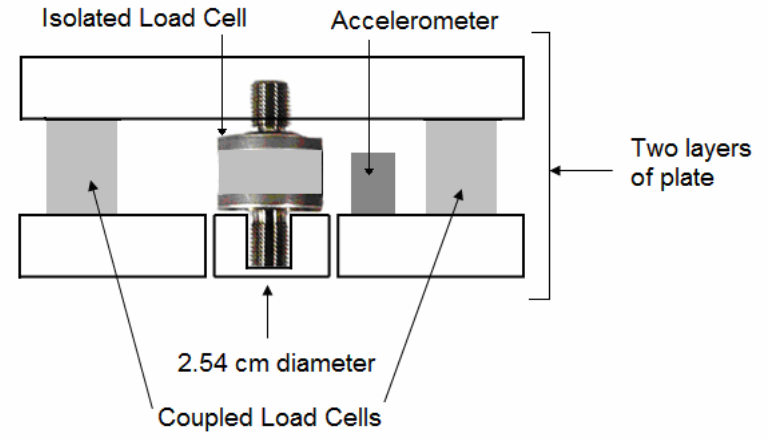

Figure 4.1: Instrumentation of drop plate

The liver was positioned in the drop tower so that the highest point on the liver was aligned with the isolated load cell in the center of the plate. Force from the isolated load cell was divided by the load cell cross-sectional area (5.1 cm^2) to calculate the stress applied locally at the high point of the liver. A linear variable displacement transducer (LVDT) mounted to the tower platform was used to record the displacement time history. Strain was calculated from the displacement of the liver at its highest point using Equation (4.1), as illustrated in Figure 4.2:

$$\varepsilon(t) = \frac{\Delta h(t)}{h_i} \tag{4.1}$$

Strain rate was calculated from the impact velocity divided by the pre-test liver height, since the velocity of the drop plate during liver compression was nearly constant. Calculated values for applied stress, compressive strain, and strain rate acting locally in the region of maximum liver height are nominal values and do not take into account the

stress and strain distributions associated with the complex three-dimensional geometry of the liver.

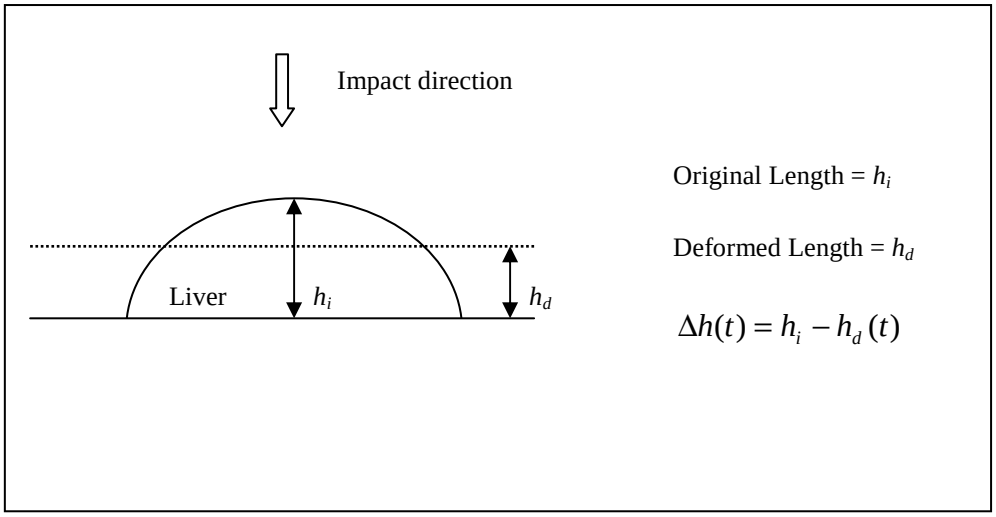

Figure 4.2: Nominal compressive strain calculated from displacement of highest point on liver divided by pre-test liver height

The drop tower experimental set up is shown in Figure 4.3. The plate was released from the desired height using an electromagnetic trigger mechanism. High density plastic slip bearings were secured to the sides of the plate to interact with the two guide rails on opposite sides of the tower so that alignment of the plate with respect to the liver could be maintained with minimal frictional loss. A contact sensor triggered the data acquisition system at the start of the impact event. Compression was limited to a nominal 30% of the maximum height of the liver through the use of adjustable-height brake columns.

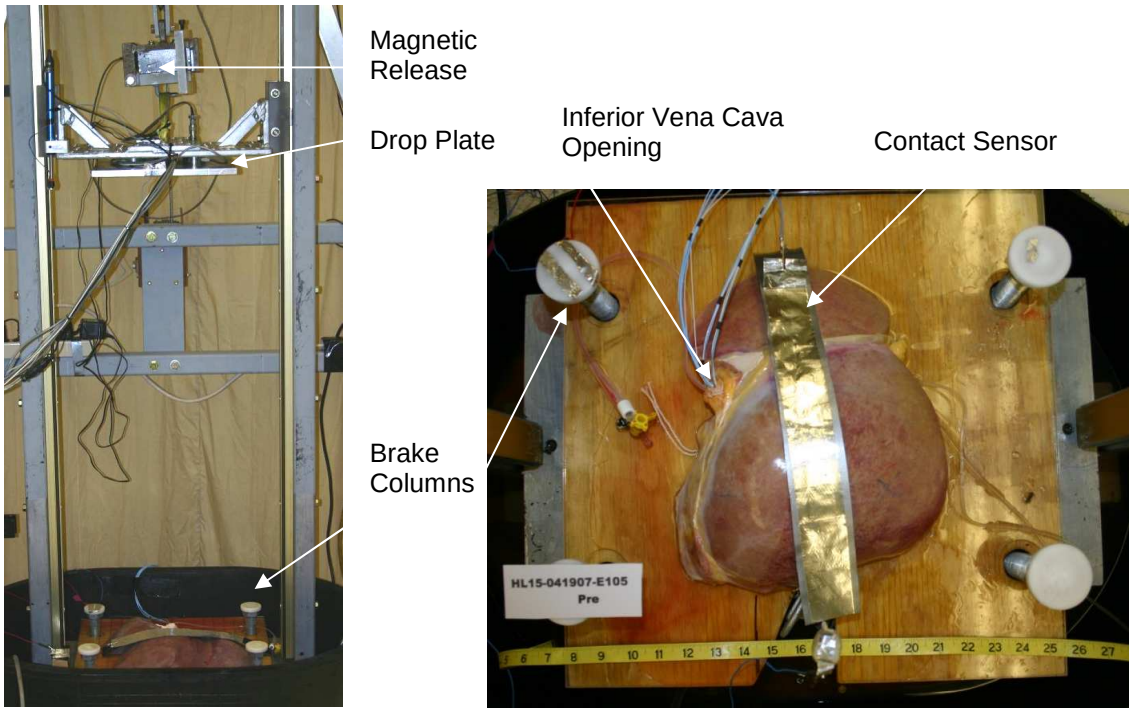

Figure 4.3A: Drop tower

Figure 4.3B: Instrumented liver positioned in drop tower base

Figure 4.3: Experimental set up

Perfusion System. An *ex vivo* liver perfusion system was developed to reproduce physiological pressures in the liver vascular system and tissue. Previous research has demonstrated that the viscoelastic properties of the liver change with perfusion and that the mechanical behavior of perfused *ex vivo* liver closely approximates the *in vivo* behavior (Kerdok et al. 2006). The perfusion system is illustrated in schematic form in Figure 4.4. Liver specimens were perfused with heated (33-37 °C) normal saline solution for 45 to 60 minutes prior to testing. The saline sources for the hepatic artery and hepatic portal vein were positioned at appropriate heights to provide constant pressures of 100 mmHg in the hepatic artery and 9 mmHg in the hepatic portal vein.

The normal physiological pressure range in the hepatic portal vein is 7-10 mmHg (Guyton 1976). A Foley catheter was inserted into the inferior vena cava to serve as a drainage route for perfusate fluid. A state of equilibrium was assumed when the maximum thickness of the liver reached a stable value. The pre-test static pressure in the hepatic venous system was calculated from the height of the fluid column inside the Foley catheter draining the inferior vena cava. The surface of the liver was hydrated and maintained at a stable temperature by continuously pouring heated saline over the organ surface prior to the test.

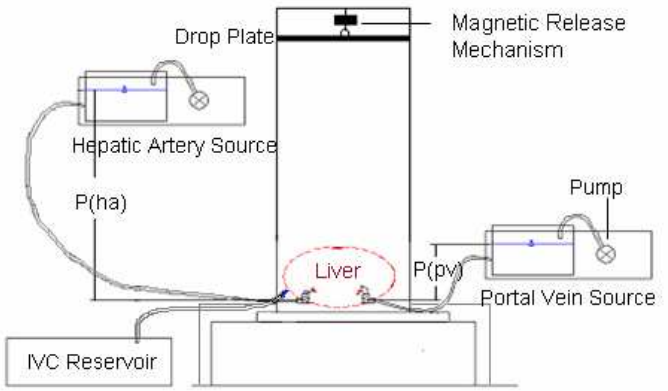

Figure 4.4: *Ex vivo* liver perfusion system

Specimen Instrumentation. Liver specimens were instrumented with miniature pressure-measuring catheters (Model SPR-524, Millar Instruments, Houston, TX) with a natural frequency over 10 KHz, a range of 386 kPa, and a diameter of 1.2 mm. The sensors are designed for constant temperature, non-flow, in-fluid applications. To

ensure accurate pressure measurements, the sensors were pre-soaked at temperature within the perfused liver for at least 45 minutes to minimize temperature effects. Hydrostatic pressure was maintained by the fluid columns as shown in Figure 4.4. It was assumed that no flow was present during the impact event because (1) the valve on the outflow tube draining the inferior vena cava was closed immediately prior to the test; and (2) the speed of the impact event was not believed to allow sufficient time for fluid to escape the liver through other mechanisms.

Three miniature pressure sensors were inserted into three different hepatic veins through the opening of the inferior vena cava on the liver's superior surface, as shown in Fig. 4.3B. In 11 of the 14 livers, a cannula was used to insert a fourth miniature pressure sensor into the parenchyma from the visceral surface of the liver. Fluid pressure measurements from the hepatic vein sensors will be termed "vascular pressure", and fluid pressure measurements from the parenchymal caudate lobe sensor will be termed "tissue pressure". The caudate lobe was chosen as the site of tissue pressure measurement because with the liver positioned in the drop tower the caudate lobe is aligned vertically with the point of maximum thickness. The positions of all pressure sensors in three dimensions were determined from pre-test CT scans of each liver specimen.

PMHS Trial

One fixed-back PMHS upper abdominal impact test was conducted in order to investigate the feasibility of measuring liver vascular pressure in impacts to re-

pressurized unembalmed PMHS. The mass and height of the subject were 80 kg and 157 cm, respectively. The subject was female, 91 years of age, and was screened for all of the exclusion criteria applied in the selection of *ex vivo* liver specimens described previously.

PMHS Instrumentation and Vascular Pressurization. A midline incision was made in the abdomen. A double-balloon Foley catheter with an attached pressure sensor was inserted in the abdominal aorta and positioned so that the gap between the balloons was located at the level of the celiac trunk (the source of arterial supply to the liver). A single-balloon Foley catheter with an attached pressure sensor was inserted into the superior mesenteric vein and advanced until the balloon was located in the hepatic portal vein just proximal to the porta hepatis. All catheter placement was accomplished under fluoroscopic guidance. The incision was sutured closed after catheter placement was complete.

A second incision was made in the right side of the neck. Three miniature pressure transducers were positioned in the hepatic veins through an opening in the internal jugular vein. The locations of the pressure transducers were confirmed using fluoroscopy, and the incision was sutured closed. A third small incision was made in the superficial tissue over the sternum in order mount an accelerometer to the body of the sternum using small screws.

A pressurization trial was conducted prior to the impact test. The external ends of the catheters were connected to the appropriate saline reservoirs of the liver

perfusion system (as shown in Fig. 4.4). Catheter balloons were inflated and valves to the saline reservoirs were opened. Pressure changes in the abdominal aorta, hepatic portal vein, and hepatic veins were recorded for 3 minutes. Room temperature (21 °C) saline was used for pressurization due to the sensitivity of the miniature pressure sensors to rapid fluctuations in temperature. The core temperature of the subject was monitored using a thermocouple in the abdominal aorta, and the saline temperature was adjusted accordingly.

Impact Test Conditions. The drop tower modifications for the PMHS full body impact test are shown in Figure 4.5. A flat rectangular rigid impact face, 15.2 cm by 40.6 cm, was mounted to the drop plate used in the *ex vivo* liver tests. Instrumentation of the drop plate consisted of the coupled load cells and accelerometer as described for the previous test series. Total mass of the drop plate was 59 kg and the target impact velocity was 5.4 m/s. These parameters were selected to approximate the impact energy applied to PMHS subjects in the fixed-back, rigid bar mid-abdomen impact tests conducted by Hardy et al. (2001). That test series included 6 m/s impacts with a 48 kg impactor, amounting to 864 J of energy available at impact.

The subject was oriented in a supine position on a rigid platform and, like the *ex vivo* tests, an anterior impact was applied using the drop tower. The center of the impact face was aligned 2 cm below the xyphoid process to maximize interaction with the liver's anatomical position. The impact plate interaction with the upper abdomen is

illustrated in Figure 4.6. A necropsy was performed following the test to evaluate injuries to the thorax and abdomen.

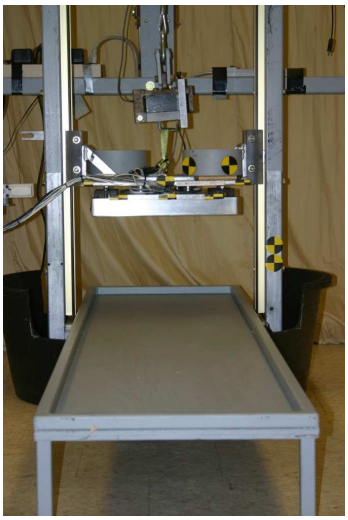

Figure 4.5: Drop tower modified for PMHS full body impact test

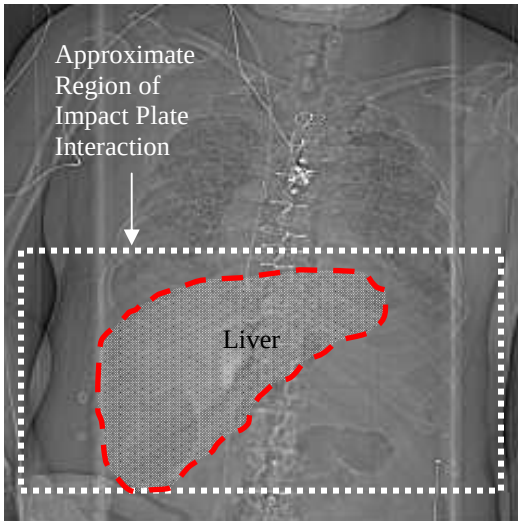

Figure 4.6: CT topogram illustrating approximate anatomical position of liver with respect to rigid impact plate

Injury Analysis

Following the impact test each liver was inspected for injuries on the organ surface and in the organ interior. Injury severity scores were assigned by a trauma surgeon according to the Abbreviated Injury Scale (AIS) as summarized in Table 4.3 (AAAM 1998). A search of the Crash Injury Research and Engineering Network (CIREN) database was conducted to ascertain whether the experimentally produced injury patters were consistent with blunt liver injuries seen in motor vehicle crash victims.

AIS 0	No Injury
AIS 2	Superficial Lacerations Subcapsular Hematoma Over $\leq$ 50% of Surface
AIS 3	Deep Laceration Duct or Vascular Involvement Hematoma Over >50% of Surface or Expanding
AIS 4	Multiple Deep Lacerations "Burst Injury" (Stellate Lacerations, Shattering of Parenchyma)
AIS 5	Parenchymal Disruption of >75% of a Hepatic Lobe Involvement of Retrohepatic Vena Cava or Central Hepatic Veins
AIS 6	Hepatic Avulsion

Table 4.3: Summary of liver injury patterns and corresponding AIS values

Data Processing and Statistical Methods

Data was collected at a sampling frequency of 20 kHz, and force and acceleration data channels were filtered at 1650 Hz (CFC 1000). Force measurements were compensated for the mass and inertia of the plate between the load cells and the liver

and scaled using the technique described by Eppinger (1976), with the average liver mass used as the reference mass:

(4.2) $$F_{scaled} = \left(\frac{M_{ref}}{M_i} \right)^{\frac{2}{3}} F_i$$

M_{ref} = average liver mass
M_i = liver mass of i^{th} subject
F_i = Force measurement of i^{th} subject

Binary logistic regression ($\alpha = .05$) was used to calculate the risk of serious (AIS ≥ 3) liver injury associated with measured experimental values for vascular pressure, tissue pressure, force, velocity, compression, $V_{max}*C_{max}$, impact energy, strain rate, and applied stress. The force acting on the liver was calculated from the acceleration and load data according to the procedure described in Appendix A. $V_{max}*C_{max}$ was defined as the product of maximum pre-impact velocity and maximum compression as described by Rouhana (1985). Logistic regressions were calculated separately for peak values of all variables up to the time of maximum plate displacement (maximum liver compression). The candidate injury predictors were ranked according to log likelihood values, which were used to evaluate the fit of the logistic regression models.

Multiple linear regression ($\alpha = .10$) was used to investigate whether the location of the pressure transducer influenced the measured peak vascular pressure or peak tissue pressure. Specifically, the regression model investigated whether vertical distance and radial distance from the impact point were significant predictors of peak pressure. A strain rate term was included in the model to control for the variation in

peak pressure associated with impact velocity. Vertical and radial distances were calculated from three dimensional coordinates assigned to all pressure transducer locations in the CT scans of the liver specimens. An illustration of radial and vertical distance is given in Figure 4.7.

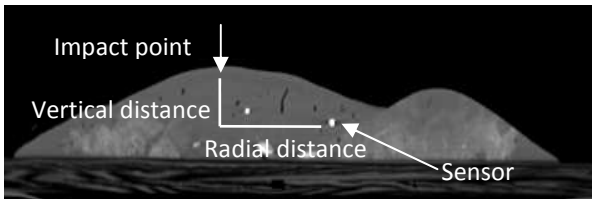

Figure 4.7: Vertical and radial distance from impact point to pressure sensor location determined by CT scan

If tissue pressure is a measure of hydrostatic pressure, then the relationship between experimental measurements of tissue pressure and normal stress should correspond to the theoretical relationship between hydrostatic pressure and stress. Simple linear regression ($\alpha = .05$) was used to investigate the relationship between tissue pressure and normal stress. The means and standard deviations were calculated for the slopes and y-intercept values of the resulting trend lines. Additional linear regressions were calculated for slope versus strain rate and y-intercept versus strain rate to investigate the possibility of rate dependence in the stress-tissue pressure relationship.

Normal Stress Calculations

Because of the complex three-dimensional geometry of the liver, the true normal stress in the loading direction will vary with liver depth just as the liver cross-sectional area in the horizontal plane varies with depth (see Figure 4.8). The applied normal stress measured locally at the highest part of the liver is likely to overestimate the average normal stress for the liver as a whole. Similarly, the normal stress at the base of the liver, at the site of maximum cross-sectional area, is likely to underestimate the average normal stress. Since the actual average normal stress is unknown, the normal stresses measured at the highest part of the liver (σ_h) and at the liver base (σ_b) were used as upper and lower bounds for the average normal stress.

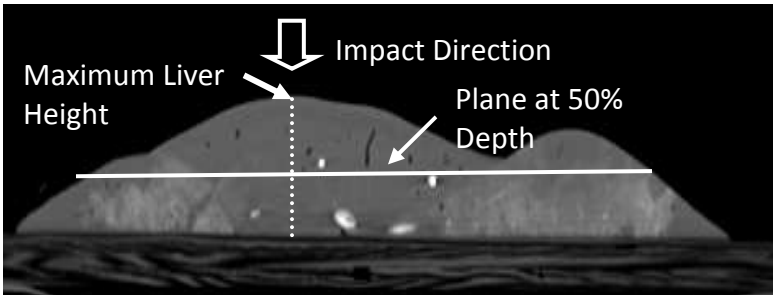

Figure 4.8: Liver CT scan illustrating change in cross-sectional area as a function of depth

The normal stress acting at the site of maximum liver height, σ_h, was calculated by dividing the force from the isolated load cell at the center of the impact plate by the load cell cross-sectional area, as described previously. To calculate the normal stress at the liver base, σ_b, it was necessary to determine the cross-sectional area of the liver

base for each specimen from pre-test photographs using image analysis software (ImageJ version 1.34s, National Institutes of Health, USA) as illustrated in Figure 4.9.

Figure 4.9: Pre-test liver photo with free-hand outline for area calculation using image analysis software

The normal stress at the liver base was then calculated by multiplying the applied stress at maximum liver height, σ_h, by the appropriate ratio of cross-sectional areas:

(4.3) $$\sigma_b = \frac{A_h}{A_b}\sigma_h$$

where A_b = area of liver base

$$A_h = \frac{F_{total}}{\sigma_h}$$

The value of A_h was approximated as a constant value for each specimen using the slope of the trend line for total force versus σ_h, as shown in the example in Figure 4.10.

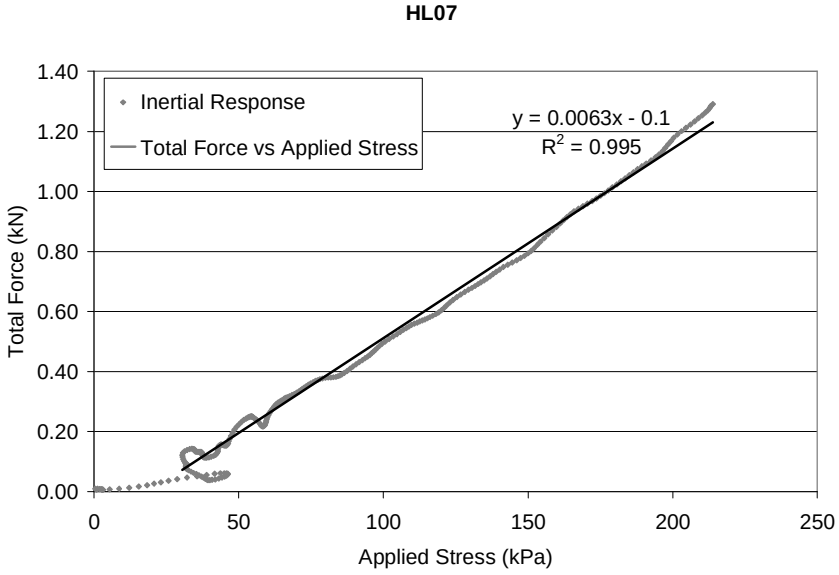

Figure 4.10: Example of A_h calculation from slope of trend line excluding inertial response in the early part of the curve. For test HL07, A_h = .0063 m^2.

In addition to determining upper and lower bounds for the average stress from σ_h and σ_b, a direct estimate of average normal stress was calculated by estimating the cross-sectional area at 50% liver depth, A_{avg}, using an equivalent sphere calculation as described in Appendix B. The measured normal stress at the highest part of the liver, σ_h, was multiplied by the appropriate ratio of cross-sectional areas to calculate the estimated average normal stress, using Equation (4.4):

$$\sigma_{avg} = \frac{A_h}{A_{avg}} \sigma_h \quad (4.4)$$

4.3 RESULTS

Table 4.4 summarizes the experimental data from the impact tests. Pressure time histories are shown in Appendix C. Plots of normal stress measured at the highest part of the liver versus nominal strain are given in Appendix D.

Injury Analysis

Comparisons of experimental injury results with CIREN images revealed that the laboratory-produced liver injuries were consistent with injuries in motor vehicle crash victims. Experimental injury outcomes included shallow lacerations of the liver capsule, deep lacerations, burst-type stellate lacerations, and intra-parenchymal damage. The two most frequent experimental injury outcomes, right lobe lacerations and intra-parenchymal damage, are shown and contrasted with similar CIREN cases in Figure 4.11. Injury results for all tests are listed in Table 4.5.

Subject	Peak Tissue Pressure (kPa)	Peak Vascular Pressure (kPa)	Impact Energy (J)	Strain Rate (1/s)	Velocity (m/s)	Peak Strain (%)	V_{max} *C_{max} (m/s)	Scaled Peak Applied Stress (kPa)	Scaled Peak Force (N)
HL01	N/A*	88.1	217	55.4	4.3	39.0	1.68	N/A	2580
HL02	N/A*	80.5	215	45.9	4.3	32.0	1.37	245	3966
HL03	14.0	67.5	211	47.1	4.2	28.2	1.20	445	9223
HL04	94.2	132.5	380	65.8	5.7	43.1	2.45	557	5799
HL05	N/A*	41.9	91	31.3	2.8	31.0	.86	212	7106
HL07	41.4	32.0	38	19.9	1.8	29.0	.52	216	4847
HL08	29.7	68.2	29	18.0	1.6	31.6	.49	379	3218
HL09	41.8	14.9	38	21.0	1.8	34.1	.61	587	5941
HL10	79.9	52.4	36	19.7	1.7	32.3	.56	223	5090
HL11	118.0	100.8	248	52.7	4.6	26.6	1.22	483	14307
HL12	21.5	5.7	11	12.1	1.0	20.0	.20	202	3262
HL13	82.6	78.5	317	68.9	5.2	36.6	1.90	646	18302
HL14	34.7	10.8	84	28.0	2.7	30.5	.82	488	4283
HL15	16.4	30.6	86	30.8	2.7	25.6	.69	352	7406

*Tissue pressure was not recorded during these tests.

Table 4.4: Results from *ex vivo* liver impacts and PMHS test

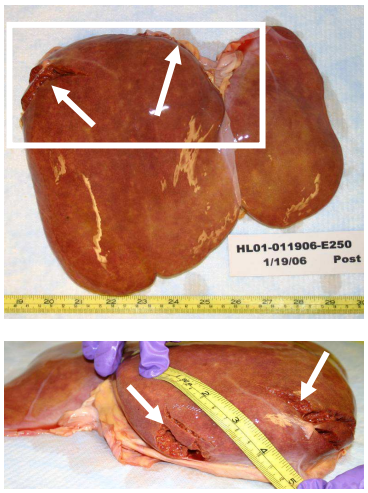

Figure 4.11A: Right lobe lacerations in *ex vivo* test

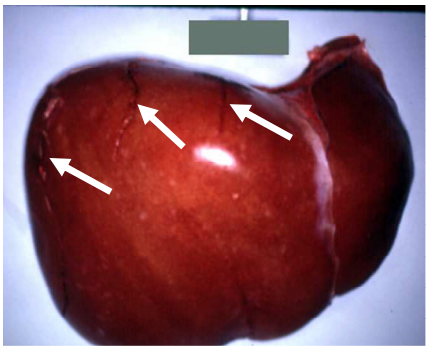

Figure 4.11B: Right lobe lacerations in CIREN case

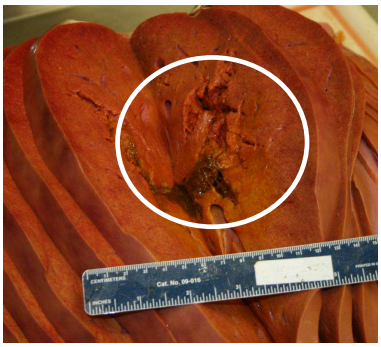

Figure 4.11C: Intra-parenchymal damage in *ex vivo* test

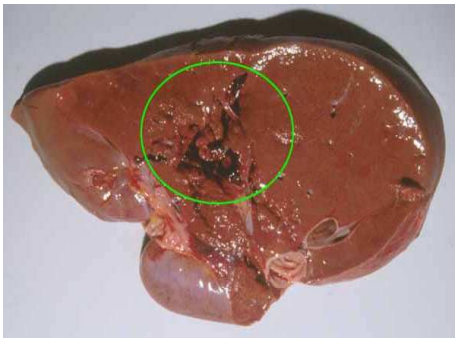

Figure 4.11D: Intra-parenchymal damage in CIREN case

Figure 4.11: Experimental injuries (A, C) compared to similar injury patterns in CIREN cases (B, D)

Subject	AIS	Injury Description
HL01	3	One deep and one superficial laceration on superior aspect of right lobe (9 and 5 cm); Three superficial lacerations on posterior aspect of right lobe (2, 5, and 6 cm)
HL02	3	One superficial laceration on superior aspect of right lobe (4 cm); One superficial laceration on lateral aspect of right lobe (10 cm); Moderate internal damage in right lobe (8 cm)
HL03	2	One superficial laceration on superior aspect of right lobe (8 cm); Minor internal damage (2 cm)
HL04	4	Two deep lacerations on right lobe (5 and 6 cm); Five superficial lacerations on right lobe (2, 3, 4, 5, and 5 cm); Burst injury of right lobe
HL05	3	Five superficial lacerations on right lobe (3, 5, 5, 6, and 7 cm); Moderate internal damage (5 cm)
HL07	2	One superficial laceration on lateral aspect of right lobe (4 cm); One superficial laceration on posterior aspect of right lobe (7 cm)
HL08	2	Superficial capsule laceration on posterior aspect of right lobe (7 cm); Minor internal damage in right lobe (2 cm)
HL09	2	Superficial right lobe laceration (4 cm)
HL10	3	Three lacerations on anterior aspect of right lobe (5, 7, 9 cm); Moderate internal damage in right lobe (5 cm)
HL11	3	Two right lobe lacerations (8 and 4 cm); Moderate internal damage (3 cm)
HL12	2	Laceration on lateral aspect of right lobe continuing to posterior aspect (7 cm)
HL13	4	Seven lacerations on anterior aspect of right lobe (2, 2, 3, 3, 5, 5, 6 cm); One laceration on posterior aspect of right lobe (2 cm); Severe internal damage (10 cm)
HL14	3	Three lacerations on anterior aspect of right lobe (6, 6, 8 cm); The 8 cm laceration extended to the posterior aspect of right lobe; Moderate internal damage in right lobe (5 cm)
HL15	2	No surface lacerations; Minor internal damage in right lobe (3 cm)
PMHS test	4	One superficial laceration on anterior aspect of left lobe (6 cm); Extensive maceration of posterior aspect of right lobe extending into left lobe

Table 4.5: Injury outcomes for *ex vivo* liver impacts and PMHS test

Binary logistic regression was performed to determine the association of serious (AIS ≥ 3) liver injury with different covariates. Output of each model is summarized in Table 4.6, including log likelihoods, odds ratios, p-values, and pseudo-R^2 values. Log likelihoods were used to evaluate which predictors best fit the data, with smaller absolute values indicating better fit. Tissue pressure was the best indicator of liver injury risk ($p = .002$) followed by $V_{max}*C_{max}$ ($p = .009$). Several other significant predictors were moderately associated with injury risk, including strain rate, impact velocity, impact energy, compression, and vascular pressure. Applied stress and force were not significantly associated with liver injury risk. Plots of tissue and vascular pressure versus probability of AIS ≥ 3 liver injury are given in Figure 4.12, and injury risk curves for all other significant predictors are given in Appendix E.

The peak vascular pressure recorded in the PMHS impact test is shown with the *ex vivo* vascular pressure data and injury risk curve in Figure 4.12B. The pressure recorded in the PMHS injury case was consistent with injurious levels of vascular pressure in the *ex vivo* liver tests.

Predictor Variable	Units	Log Likelihood	Odds Ratio*	P-value	Pseudo-R^2
Tissue Pressure	kPa	-2.638	1.132	.002	.79
V_{max}*C_{max}	(m/s)*compression fraction	-6.106	49.946	.009	.52
Strain Rate	1/s	-6.825	1.094	.019	.43
Velocity	m/s	-6.826	2.926	.019	.43
Impact Energy	J	-6.968	1.014	.023	.42
Compression	%	-7.310	1.328	.034	.37
Vascular Pressure	kPa	-7.508	1.038	.043	.34
Applied Stress	kPa	-8.824	1.003	.585	.03
Scaled Force	N	-9.149	1.000	.364	.08

*The odds of serious liver injury increase by a factor of the odds ratio when the predictor variable increases by one unit.

Table 4.6: Binary logistic regression results for risk of AIS ≥ 3 liver injury in *ex vivo* tests

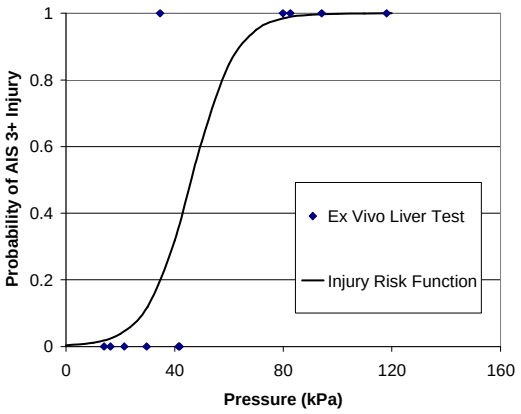

Figure 4.12A: Tissue pressure vs. injury risk

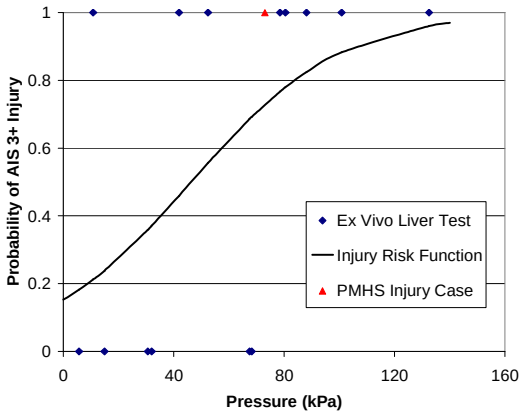

Figure 4.12B: Vascular pressure vs. injury risk

Figure 4.12: Probability of serious liver injury as a function of tissue and vascular pressure

Effect of Sensor Location on Peak Pressure

Multiple linear regression was used to determine whether the vertical or radial distances to the pressure sensor from the point of impact were correlated with peak

vascular or tissue pressure. Strain rate was included as a predictor to control for variation in pressure due to impact velocity. Results are given in Table 4.7. A significant dependence on transducer location was found for peak vascular pressure but not for peak tissue pressure. Vascular pressure was significantly correlated with radial distance from the impact point ($p < .10$). The radial distance coefficient was a negative value, indicating a decrease in peak vascular pressure with increasing radial distance from the impact point. Vertical distance was not a significant predictor of peak vascular pressure. Tissue pressure was not significantly correlated with either radial or vertical distance. The regression model is given in Equation (4.5).

Dependent Variable	Multiple Correlation Coefficient (R)	Model Significance (ANOVA p-value)	Model Coefficients			
			β_0	β_1	β_2	β_3
Vascular Pressure	.84	.001	27.6	-.30	**-.36**	**1.56**
Tissue Pressure	.88	.022	-7.1	.48	-.44	**1.76**

*__Boldface__ indicates that the corresponding variable is a significant correlate with pressure ($p < .10$).

Table 4.7: Multiple linear regression results for the association between transducer location and peak vascular or tissue pressure

(4.5) Pressure (kPa) = $\beta_0 + \beta_1$*Vertical Distance (mm) + β_2*Radial Distance (mm) + β_3*Strain Rate (s^{-1})

Tissue Pressure and Normal Stress

Simple linear regression was performed to investigate the relationship between tissue pressure and normal stresses measured at maximum liver height (σ_h), at the liver base (σ_b), and at 50% liver depth (σ_{avg}). Data points from the early inertial loading phase were excluded from analysis. Separate regressions were performed for each test, and the average results are given in Table 4.8. Figures 4.13 – 4.15 show the tissue pressure versus normal stress regressions for each of the three normal stress measurements.

Normal Stress Value	Mean Slope	Mean Y-intercept	Mean Correlation Coefficient (R)	Significance (for all tests)
σ_h	.21 ± .08	-12.3 ± 9.3	.96 ± .03	$p < .05$
σ_b	1.27 ± .49	-12.3 ± 9.3	.96 ± .03	$p < .05$
σ_{avg}	.578 ± .25	-12.3 ± 9.3	.96 ± .03	$p < .05$

*Tests HL01, HL02, and HL05 were excluded because tissue pressure was not measured in those tests.
*Test HL03 was excluded because tissue pressure was measured in a different location than the caudate lobe directly below the impact.

Table 4.8: Average results for linear regressions of tissue pressure vs. normal stress

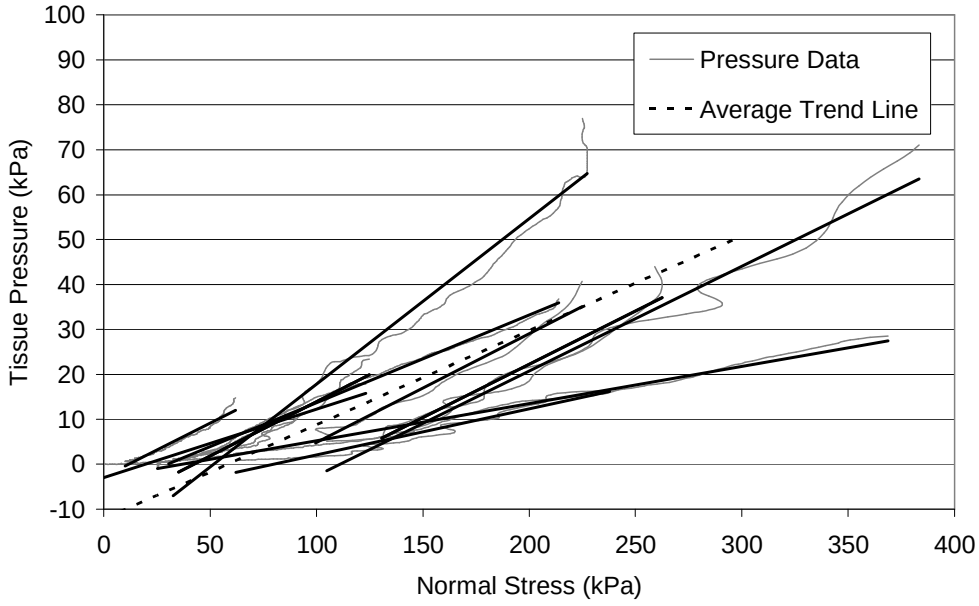

Figure 4.13: Tissue pressure vs. normal stress measured at maximum liver height (σ_h). Average slope = 0.21 ± .08.

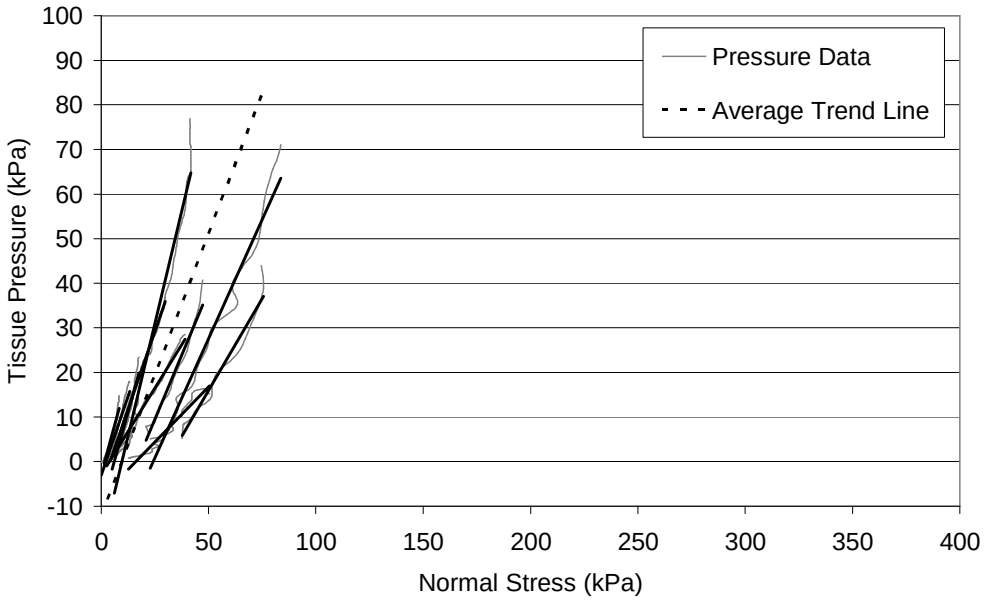

Figure 4.14: Tissue pressure vs. normal stress at liver base (σ_b). Average slope = 1.27 ± .49.

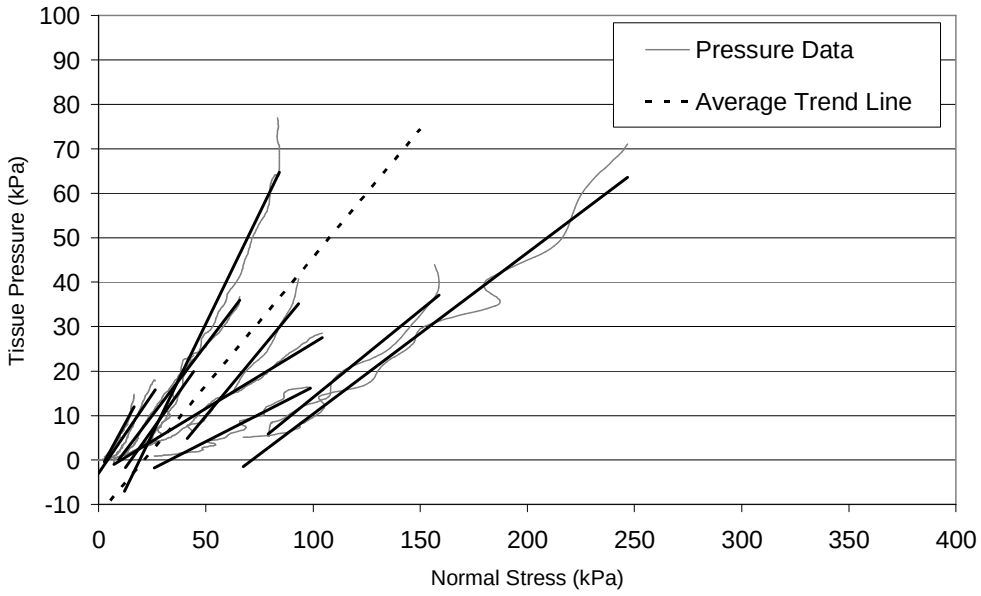

Figure 4.15: Tissue pressure vs. normal stress at 50% liver depth (σ_{avg}). Average slope = .578 ± .25.

As expected, normal stresses acting locally in the region of liver maximum height (σ_h) were generally high resulting in a lower average slope, while normal stresses at the liver base (σ_b) were lower resulting in a higher average slope. Estimated average normal stresses at 50% liver depth (σ_{avg}) fell between the upper and lower bounds given by σ_h and σ_b, respectively. All regressions were highly correlated (R = .96 ± .03) and statistically significant ($p < .05$).

Within a given plot for Figures 4.13 – 4.15, the slopes of the trend lines were relatively consistent across all impact tests while the y-intercept values were more variable. Additional linear regressions were calculated to determine if variation in slope or y-intercept values was rate dependent. Results from these analyses are shown in

Table 4.9. The slopes of the tissue pressure-normal stress relationships were not correlated with strain rate ($p > .05$), but y-intercept was significantly correlated with strain rate ($p = .001$, $R = .86$). Additionally, the y-intercept values given in Table 4.6 were identical for the three normal stress measurements. This pattern was attributed to the fact that all three measurements of normal stress were proportional to σ_h, the stress measured by the load cell at the highest part of the liver (anterior surface). It appears that σ_h exhibited a viscous step response while the tissue pressure measured near the base of the liver (posterior surface) did not exhibit an obvious step response. It is not known why this step phenomenon was absent from the tissue pressures, but it is hypothesized that the step response is diffused as the pressure wave passes through the liver.

Linear Regression Model	Correlation Coefficient (R)	P-Value
Slope vs. Strain Rate	.12	>.05
Y-intercept vs. Strain Rate	.86	.001

Table 4.9: Correlation of strain rate with slope and y-intercept of tissue pressure vs. normal stress trend lines

PMHS Trial

In the single PMHS full body impact the vascular system was pressurized and the liver was instrumented and impacted *in situ*. The injuries observed were consistent with a crushing or burst injury mechanism with considerable tissue destruction. The pressures measured by the vascular transducers were similar to those measured in *ex*

vivo tests as shown in Figure 4.12B. Some experimental complications occurred including low core temperature and leakage within the abdominal cavity; however, pressures were measured successfully within the *in situ* liver, and the overall results indicate that the approach is applicable to PMHS full body impacts.

4.4 DISCUSSION

Analysis of Injury Risk

Overall, the binary logistic regression results listed in Table 4.4 are highly consistent with previous studies (Rouhana 1985, Lau and Viano 1981a, Mertz et al. 1997, Rouhana 1986). The importance of both the rate and extent of compression are clearly apparent. Impact energy and strain rate were highly correlated to velocity in this study since the impactor mass was kept constant and the compression was limited to roughly 30% for most tests. Accordingly, it is not surprising that strain rate, velocity, and impact energy showed roughly equivalent correlations with injury. Taking the limited variation in compression into account with V_{max}*C_{max} resulted in one of the best indicators of liver injury in this series of experiments. Compression alone was also a significant predictor of injury risk, but the strength of correlation was relatively low (Pseudo-R^2 = .37). The lack of significant association between force or applied stress and liver injury is consistent with some previous work (Rouhana 1986), although other studies have reported significant correlations between force and abdominal injury risk (Viano et al. 1989).

The injury predictors in Table 4.4 that are novel to this study include tissue pressure and vascular pressure. Tissue pressure was the best indicator of liver injury risk of all the parameters investigated in this work. Tissue pressure may be considered as a measure of impact-induced fluid pressure changes inside the liver. It is reasonable to expect that fluid pressure changes inside a fluid-filled solid organ such as the liver would be well correlated with injury. In addition, the location of the tissue pressure sensor relative to the impact site was very consistent from one test to the next. Multiple regression analysis confirmed that pressure sensor location was not a significant source of variation in the peak tissue pressure data. It is likely that tissue pressure was a better indicator of injury risk than vascular pressure because tissue pressure measurements did not include significant variation due to sensor location.

Vascular pressure was also significantly correlated with liver injury, although the correlation coefficient was low (Pseudo-R^2 = .34). Like tissue pressure, vascular pressure is a measure of impact-induced changes in fluid pressure. However, unlike tissue pressure, the locations of the vascular pressure sensors were not controlled. The vascular pressure sensor locations were somewhat arbitrary based on the branching patterns of the hepatic veins draining into the inferior vena cava. The influence of sensor location on peak vascular pressure was demonstrated in the multiple regression analysis, which revealed that peak vascular pressure was significantly correlated with radial distance from the impact point. The peak vascular pressure decreased as the

distance from the impact point increased. This variation due to position likely contributed to the weaker correlation of vascular pressure with injury risk.

Hydrostatic Pressure Analysis

This study hypothesizes that tissue pressure and vascular pressure are measures of hydrostatic pressure inside the liver. A known theoretical relationship exists between hydrostatic pressure and normal stress:

$$p = \frac{tr(\mathbf{T})}{3} = \frac{(\sigma_{11} + \sigma_{22} + \sigma_{33})}{3} \quad (4.6)$$

where hydrostatic pressure p (mean normal stress) is equal to the mean of the diagonal terms of the Cauchy stress tensor $\mathbf{T}$. The direction of impact was taken to be the negative x_3 direction, and the liver was compressed with no constraints on the liver's lateral surfaces.

Tissue pressure was selected as the simplest case with which to test the hydrostatic pressure hypothesis, because the tissue pressure data did not include significant variation due to sensor location since it was measured roughly in vertical alignment with the point of impact. The mean slope value (0.578) for tissue pressure versus average normal stress from Figure 4.15 was used in Equation (4.6). It was assumed that σ_{11} and σ_{22} represent equal lateral normal stresses (σ_L) and that $\sigma_{33} = \sigma_{avg}$, as shown in Equation (4.7):

(4.7) $$p = \frac{1}{3}(2\sigma_L + \sigma_{avg}) = (.578)\sigma_{avg}$$

$$\sigma_L = (.367)\sigma_{avg}$$

This analysis indicates that a compressive normal stress of $(.367)\sigma_{avg}$ acts on the lateral surfaces of the liver during impact loading. This outcome is reasonable since the structure of the liver is not homogeneous. The liver has a connective tissue capsule that acts to resist the lateral expansion of the parenchyma due to the Poisson effect. Overall, the results of Figure 4.15 and Equation (4.7) are consistent with the interpretation that tissue pressure is a measure of hydrostatic pressure within the liver.

Comparison of Tissue Pressure with Vascular Pressure

Table 4.5 showed that radial distance and strain rate were significantly correlated to the peak vascular pressure measured during the impact, while vertical distance from the impact point was not significantly correlated. Therefore, a second multiple regression was conducted using only radial distance and strain rate as independent variables. The resulting formula ($R = 0.84$, $p < .0001$) was:

(4.8) Peak Vascular Pressure (kPa) = 13.95 - 0.42 (Radial Distance, mm) + 1.60 (Strain Rate, s^{-1})

To determine whether the vascular pressure was measuring the same phenomenon as the tissue pressure, Equation (4.8) was used to calculate spatially-

adjusted vascular pressures from the peak vascular pressure values listed in Table 4.4 (for cases in which caudate lobe tissue pressures were recorded for comparison). Radial distance was set to zero in Eq. (4.8) while the measured strain rate was applied for each test. Spatially-adjusted vascular pressures will be termed "midline" pressures.

Results, shown in Figure 4.16, indicate that: (1) the peak tissue pressure and peak midline vascular pressure are linearly related; and (2) the peak values are redundant measures of the pressure wave occurring in the liver, since the slope is nearly unity (slope = 1.08, R^2 =0.33) when the regression line is constrained to pass through zero. The R^2 value of 0.33 is relatively low; however, if a potential outlier point from test HL15 is excluded, the slope remains constant while R^2 increases to 0.60.

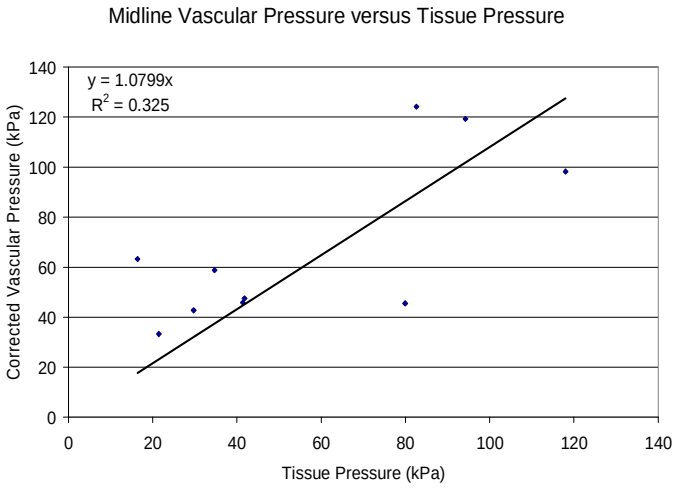

Figure 4.16: Tissue pressure measured at midline versus vascular pressure adjusted to midline using strain rate and radial distance from the midline

Based on this linear relationship and consequential assumption that the sensors located within the vasculature and caudate lobe are indeed measuring the same pressure phenomenon due to impact, a modified binary logistic regression was generated for midline vascular pressure as a predictor of serious liver injury risk. Results were compared to the tissue pressure risk curve as shown in Figure 4.17.

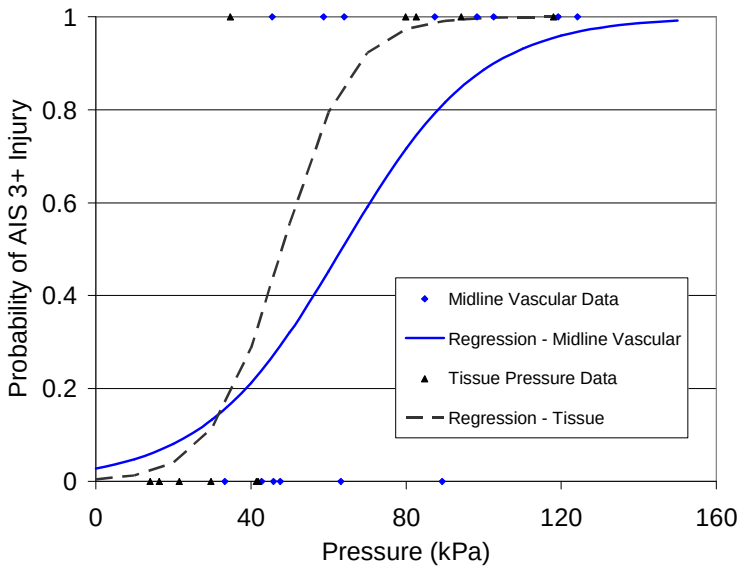

Figure 4.17: Modified liver injury risk curve using midline vascular pressures calculated from Eq. (8)

The correlation of midline vascular pressure to injury risk (log likelihood = -6.825, $p = 0.019$, pseudo-$R^2 = .43$) improved in comparison to the logistic regression results for measured vascular pressure shown in Table 4.6. The peak midline vascular pressure threshold for 50% risk of serious liver injury was 64 kPa while the peak tissue pressure

threshold was 48 kPa. Tissue pressure remained a stronger correlate than midline vascular pressure.

The differences between peak midline vascular and tissue pressures could be attributed to the fact that the tissue pressure data was based on direct measurements and consistent placement below the liver impact point, while the vascular pressures were calculated from a regression relationship using strain rate as the only predictor (with radial distance set to zero). In addition, it is possible that fluid flow occurs in the vessels during impact and affects the measured vascular pressure. Nonetheless, the linear relationship between tissue pressure and adjusted vascular pressure, with both significantly correlated to liver injury, is encouraging for being able to estimate a pressure associated with a liver injury occurring anywhere within the liver structure. This could also be beneficial for instrumentation placement in a fluid-filled abdominal component within a dummy. It should be noted that the regression models given in Eqs. (4.5) and (4.8), which describe the effect of spatial position on measured pressures within the liver, are applicable to the *ex vivo* liver loading conditions used in the current series of impact experiments. In future work, a combined approach involving three-dimensional computational modeling and PMHS full body impacts is needed to develop a more detailed understanding of the dynamic pressure distribution within the impacted three-dimensional *in situ* liver.

It has been shown that the adjusted midline vascular pressures correlate with the tissue pressures measured at the “midline”, with a slope approaching unity (Figure

4.16). It was also demonstrated that, on average, tissue pressure was equal to 57.8% of the average normal stress, or $(0.578)\sigma_{avg}$, indicating a lateral compressive stress of $(.367)\sigma_{avg}$ which is a reasonable estimate of the resistance to lateral expansion of the liver due to the connective tissue capsule. These findings represent supporting evidence that tissue pressure and vascular pressure are measures of hydrostatic pressure within the liver.

Because the peak vascular and tissue pressures provide strong logistic regression relationships with injury it can be postulated that hydrostatic pressure is involved in the mechanism of blunt liver injury. All but one of the livers in this test series sustained surface lacerations indicative of a capsule-burst injury pattern that is likely to be caused by rapid increases in hydrostatic pressure within the liver. It is plausible that the capsule lacerations occur due to pressure overload and are followed by subsequent parenchymal damage that occurs after the protective capsule is compromised.

It should be noted that the estimate of lateral stress, $\sigma_L = (.367)\sigma_{avg}$, is dependent on the ratio of tissue pressure to average normal stress (Figure 4.15), which in turn is dependent on the estimate of average normal stress (Eq. (4.4) and Appendix B). While estimating the normal stress in the loading direction on a plane at 50% liver depth seems to be a reasonable approach for approximating the average normal stress, the actual normal stress is not known. This analysis is intended to support the use of vascular and tissue pressures as measures of hydrostatic pressure indicative of liver injury risk. The lateral stress estimate is not used in any way.

Limitations

A limitation of this study is the relatively small sample size of 14 subjects. The limited sample size contributes to wide 95% confidence bands for the injury risk functions listed in Appendix B (confidence bands not shown). In addition, the injury risk function for tissue pressure versus AIS ≥ 3 injury would benefit from additional data points in the transition region between 40 and 70 kPa, in the pressure range near 50% probability of serious injury (48 kPa). It was anticipated that the tests at mid-range impact energies would generate peak tissue pressures across the transition region, but the measured tissue pressures instead resulted in a gap of 38 kPa between cases with and without serious injury.

4.5 CONCLUSIONS

The conclusions of this study were as follows:

(1) Tissue pressure was found to be the strongest correlate to human liver injury in this impact configuration. A peak tissue pressure of 48 kPa was correlated to 50% risk of serious (AIS ≥ 3) liver injury.

(2) Peak vascular pressure also was significantly correlated with injury, and the correlation improved when peak vascular pressure was adjusted for sensor location (aligned with the liver impact point/midline). A peak midline vascular pressure of 64 kPa was correlated to a 50% risk of serious injury (AIS ≥ 3) liver injury.

(3) The pressure sensors were shown to measure hydrostatic pressure because: (1) midline vascular pressure was equivalent to measured tissue pressure; and (2) the ratio of tissue pressure to average applied stress (0.578) indicated a compressive lateral stress situation that is both reasonable and compatible with experimental observation.

(4) V_{max}*C_{max} correlated well with injury, with 0.82 m/s indicating a 50% risk of serious injury (AIS ≥ 3) liver injury. Significant binary logistic regression models also were obtained for strain rate, velocity, impact energy, and compression as predictors of serious (AIS ≥ 3) liver injury.

(5) The liver injuries resulting from impact tests with pressurized *ex vivo* livers were consistent with patterns of blunt liver trauma observed in motor vehicle crash victims documented in the CIREN database.

(6) In the PMHS fully body impact the liver was instrumented successfully *in situ* with pressure transducers in the hepatic veins. The vascular pressure recorded in the PMHS injury case was consistent with the injury risk function developed from the *ex vivo* liver tests.

(7) A burst injury mechanism directly related to hydrostatic pressure is postulated for the *ex vivo* liver loaded dynamically in a drop test experiment.

CHAPTER 5

CONSTITUTIVE MODEL OF RATE DEPENDENT STRESS-STRAIN BEHAVIOR OF HUMAN LIVER TISSUE IN BLUNT IMPACT LOADING

ABSTRACT

Studies of field crash data demonstrate that blunt liver injury is a significant problem in motor vehicle crashes. An understanding of the mechanical deformation behavior of the liver under high strain rate loading conditions could aid in the development of vehicle safety measures to reduce the occurrence of blunt liver injury. The purpose of this study was to develop a constitutive model of the stress-strain behavior of human liver tissue in blunt impact loading. Experimental stress and strain data was obtained from impact tests of 12 unembalmed human livers using a drop tower technique. A constitutive model previously developed for finite strain behavior of amorphous polymers was adapted to model the observed liver behavior. The elements of the model include a nonlinear spring in parallel with a linear spring and nonlinear dash-pot. The model captures three features of liver stress-strain behavior in impact loading: (1) a relatively stiff initial modulus, (2) a rate-dependent yield or rollover to

viscous “flow” behavior, and (3) strain hardening at large strains. Six material properties were used to define the constitutive model. This study represents a novel application of polymer mechanics concepts to understand the rate dependent large strain behavior of human liver tissue under high strain rate loading. Applications of this research include finite element simulations of injury-producing liver or abdominal impact events.

5.1. BACKGROUND

The liver is one of the most frequently injured abdominal organs in motor vehicle crashes (Rouhana and Foster 1985, Elhagediab and Rouhana 1998). Clinical research has shown that blunt liver injury is associated with mortality rates as high as 30% in cases requiring operative intervention (Hurtuk 2006). An understanding of the mechanical deformation behavior of the liver under high strain rate loading conditions could aid in the development of vehicle safety measures to reduce the occurrence of blunt liver injury. In particular, a constitutive model of human liver mechanical behavior in high strain rate impact loading would be useful for developing finite element representations of the human abdomen that could be used to assess the risk of abdominal injury in motor vehicle crash settings.

A few previous studies have developed constitutive models of liver response to different types of loading. Liu and Bilston investigated the mechanical properties of bovine liver under shear loading at low strain (2000) and at moderate to large strain (2002) with strain rates on the order of 0.075 to 1 s^{-1}. Results of these experiments

were used to develop a model of liver response under moderate to large deformation based on a nonlinear viscoelastic differential model previously developed for brain tissue (Liu and Bilston 2002, Bilston et al. 2001). The model by Liu and Bilston employs a multi-mode upper convected Maxwell model and a Mooney elastic term, along with a nonlinear damping function that depends on shear strain amplitude. This complex model requires ten material constants and successfully captures complex features of liver viscoelastic behavior observed in the shear loading experiments, including strain rate sensitivity, nonlinearity (the relaxation modulus was dependent on strain for shear strains larger than 0.2%), and strain-time inseparability (slope of relaxation modulus versus time was dependent on applied strain) (Liu and Bilston 2002).

Miller (2000) developed a nonlinear viscoelastic constitutive model of liver tissue based on previously published data from *in vivo* liver compression experiments at high strain rates using anesthetized Rhesus monkeys (Melvin et al. 1973). Miller's proposed model is valid for compressive nominal strains up to 35% and strain rates between 0.2 and 22.5 s^{-1}. Miller's model uses a general viscoelastic material model in which the stress is given by a convolution integral of the relaxation function and strain rate. The relaxation function is expanded using a Prony series. After making several simplifying assumptions, Miller presented an equation for stress that requires only four material constants and one time constant. Comparison of model predictions and experimental stress-elongation data from Melvin et al. (1973) demonstrated high correlation (R^2 = .97-.99).

There are some limitations involved in applying results from the previous studies to the development of computational models of the human liver response to impact loading. Most importantly, none of the previous liver constitutive models were developed from experiments with human liver tissue. In addition, while the loading conditions in the Miller model were applicable to blunt impact loading, strain rates greater than Miller's upper limit of 22.5 s^{-1} could reasonably be expected in the context of motor vehicle crashes. The purpose of the present study was to develop a constitutive model of the stress-strain behavior of human liver tissue under high strain rate blunt impact loading, using strain rates from 19.7 to 62.5 s^{-1}. A constitutive model previously developed for finite strain behavior of amorphous polymers (Dupaix and Boyce 2007) was modified and applied to characterize the observed liver mechanical behavior from a series of blunt impact experiments to pressurized *ex vivo* human livers.

5.2 METHODS

Liver Impact Experiments

Specimen Characteristics. Liver specimens from 12 unembalmed cadavers were tested within 36 hours of death. Liver specimens were excluded from the study if the donor had a history of liver disease, known exposure to HIV or HBV, cancer with liver metastasis, abdominal or thoracic trauma, or communicable disease or sepsis at the time of death. The average age was 67 ± 16 years, with a range of 36 to 92 years. The average liver mass (with gallbladder attached) was 1992 ± 921 grams.

Perfusion of Vascular System. The vascular system of each specimen was perfused with heated (33-37 °C) normal saline solution for at least 45 minutes prior to testing. Pressures in the appropriate physiological range were applied to each of the two major vessels supplying the liver, with constant pressures of 100 mmHg in the hepatic artery and 9 mmHg in the hepatic portal vein, respectively. Previous research has demonstrated that the viscoelastic properties of the liver change with perfusion and that the mechanical behavior of perfused *ex vivo* livers closely approximates the *in vivo* behavior (Kerdok et al. 2006).

Experimental Conditions. A drop tower, shown in Figure 5.1, was used to apply blunt impact at varying velocities ranging from 1.6 to 5.7 m/s. Maximum compression was limited to a nominal 30% of the maximum height of the liver through the use of adjustable-height brake columns. The 30% maximum compression limit is consistent with the upper bound of compressive nominal strain used by Miller (2000). Impact test conditions are summarized in Table 5.1.

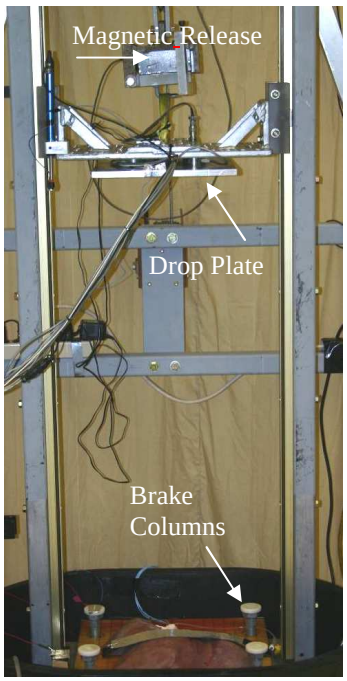

Number of Liver Specimens	Average Maximum Compression (%)	Average Impact Velocity (m/s)	Average Strain Rate (s^{-1})
4	32	1.7	19.7
5	29	3.3	36.6
3	35	5.2	62.5

Table 5.1: Experimental conditions for liver impact tests

Figure 5.1: Drop tower design

Stress and Strain Measurements. Forces were recorded by a 2.5 cm diameter load cell that was mechanically isolated from the liver-impacting surface of the two-layered drop plate, as shown in Figure 5.2. The load cell was mounted in the center of the upper plate and capped so that the loading surface was flush with the flat impact surface. The liver was positioned in the drop tower so that the highest point on the liver was aligned with the isolated load cell in the center of the plate. Force from the isolated load cell was divided by the load cell cross-sectional area (5.1 cm^2) to calculate the applied stress acting at the site of maximum liver height.

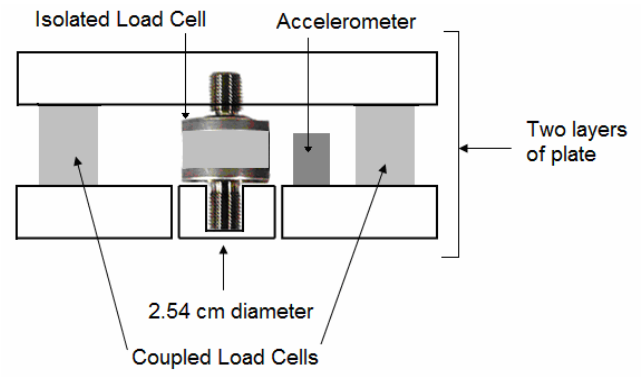

Figure 5.2: Drop plate instrumentation

A linear variable displacement transducer (LVDT) mounted to the tower platform was used to record the displacement time history. The velocity of the drop plate during liver compression was nearly constant, producing ramp displacement time histories similar to those shown in Figure 5.3. Nominal compressive strain was calculated by dividing the displacement of the highest point on the liver by the pre-test liver height, as illustrated in Figure 5.4. Strain rate was calculated by dividing the constant velocity during liver compression by the pre-test liver height. All data was collected at a sampling rate of 20 kHz using a PC-based data acquisition system (Model WE7000, Yokagawa Electric Corporation, Tokyo).

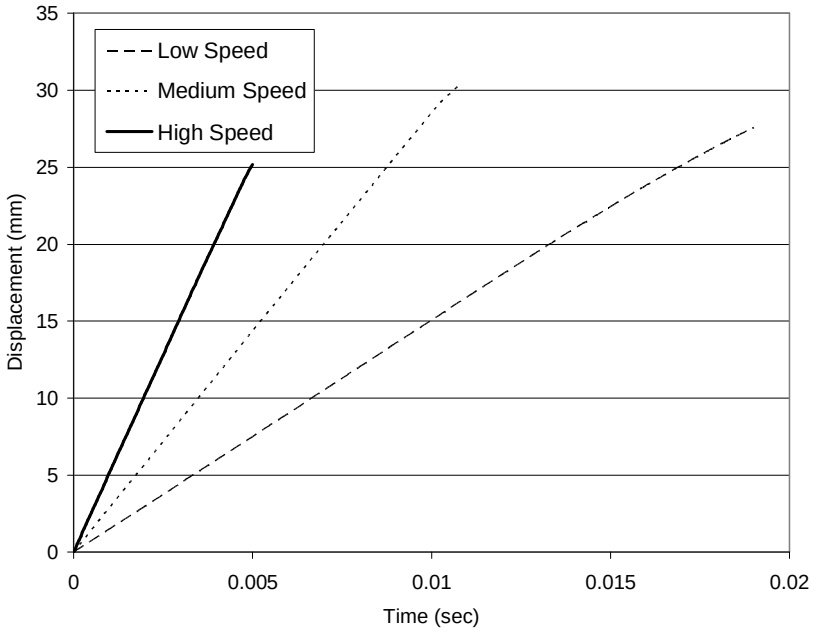

Figure 5.3: Typical ramp displacement time histories for three impact speeds

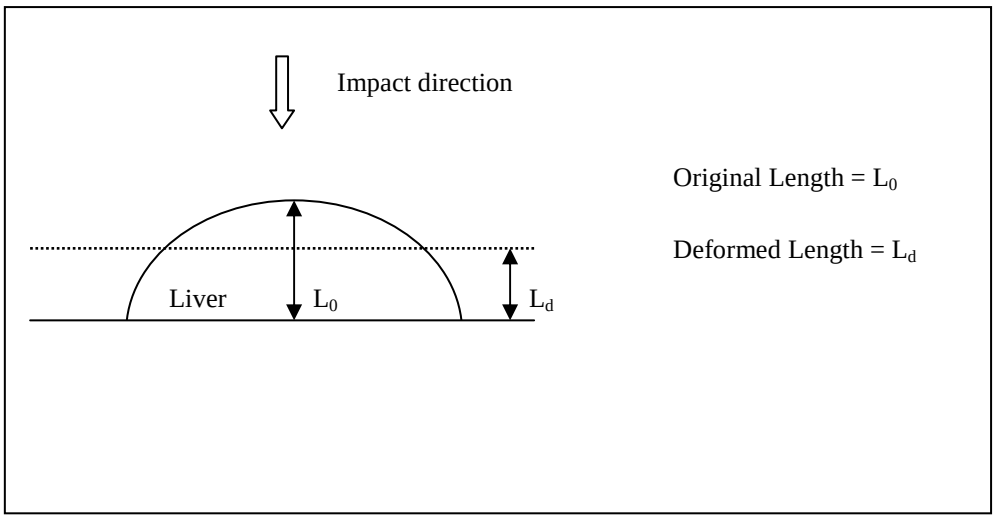

Figure 5.4: Nominal compressive strain calculated from displacement of highest point on liver divided by pre-test liver height: $\varepsilon = (L_0-L_d)/L_0$

The stress and strain measurements obtained from the *ex vivo* liver impacts represent average values that are subject to certain limitations. The measured applied stress and nominal compressive strain acting locally in the region of maximum liver height do not take into account the stress and strain distributions associated with the complex three-dimensional geometry of the liver. Although testing un-perfused liver tissue samples cut to precise shapes would help to address this issue, the method of testing whole perfused organs was preferred for two reasons: (1) previous studies have demonstrated that physiological perfusion has a significant effect on liver mechanical properties; and (2) average properties at the whole organ level may be more appropriate for finite element simulations of injury-producing impact interactions between the abdomen and vehicle components.

Rationale for Constitutive Model Selection

Liver Stress-Strain Behavior. Figure 5.5 illustrates typical applied stress versus nominal compressive strain behavior for each of the strain rates tested. (Stress-strain plots of all tests are given in Appendix D.) Several features of liver stress-strain behavior in impact loading are apparent. First, an inertial response occurs early in the event as the mass of liver tissue at rest is suddenly accelerated after initial contact with the impact plate. This inertial response becomes more pronounced at higher impact velocities and corresponding higher strain rates. A second feature of liver stress-strain behavior is the relatively stiff initial modulus followed by a yield or rollover to viscous flow behavior. A

striking rate-dependence exists in the stress value corresponding to yield and onset of flow behavior. A third feature of the stress-strain response is nonlinear strain hardening at large strains. The increase in stiffness at larger strains is similar in appearance to an exponential curve.

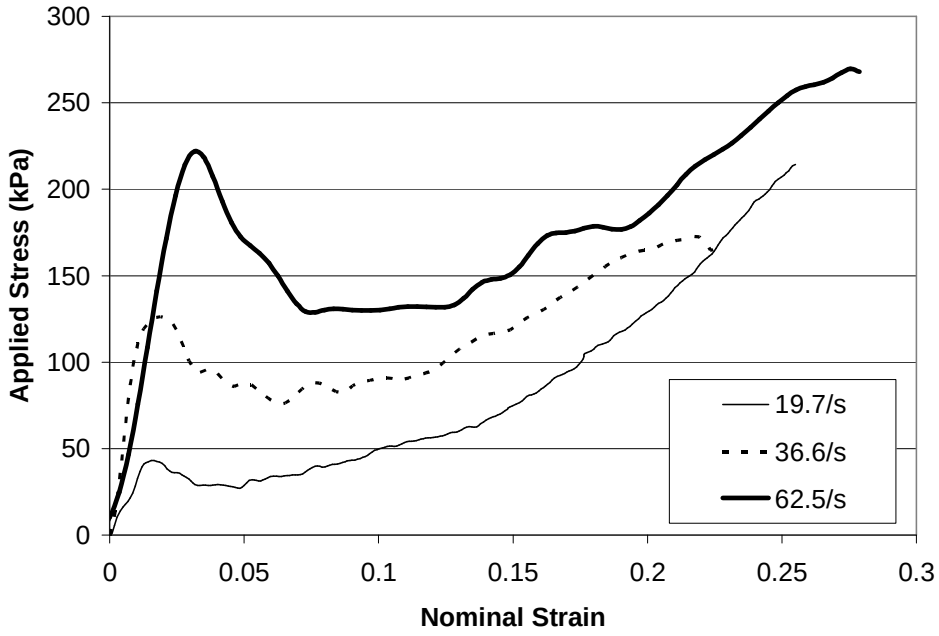

Figure 5.5: Stress-strain behavior of human liver in impact loading at different strain rates

Constitutive Model Selection. A previously developed model of the finite strain behavior of amorphous polymers by Dupaix and Boyce (2007) was selected as the basis for a constitutive model of the liver because it captures the key features of liver stress-strain response in impact loading as described above. These features include: (1) a relatively stiff initial modulus, (2) a rate-dependent yield or rollover to viscous flow behavior, and (3) strain hardening at large strains. The inertial response was excluded from the

current model. Similarities between the stress-strain behavior of amorphous polymers in uniaxial compression and human liver in blunt impact loading can be observed in Figures 5.5 and 5.6.

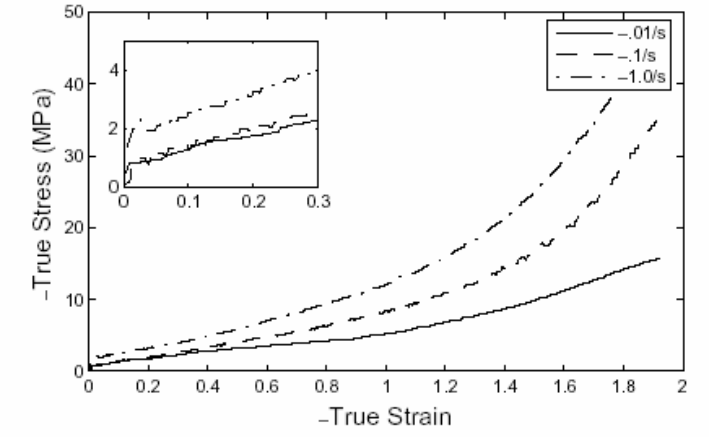

Figure 5.6: Uniaxial compression data for amorphous polymer, from Dupaix and Boyce (2005)

The constitutive model developed in this work capitalizes on similarities between the mechanical behavior of amorphous polymers and soft biological tissue such as the liver. Although the microscopic structure of the liver is very different from that of an amorphous polymer, some similarities do exist. The connective tissue framework of the liver is composed largely of collagen, a biological polymer. This connective tissue framework, illustrated in Figure 5.7, may be considered as roughly analogous to the polymer chain network concept that is employed to explain amorphous polymers' resistance to deformation, as shown in Figure 5.8.

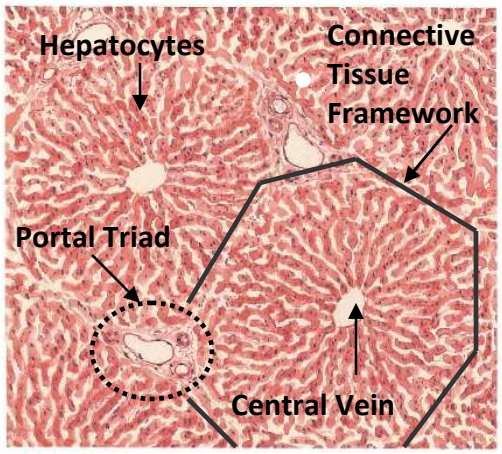

Figure 5.7A: Liver lobule surrounded by connective tissue (Netter 1997)

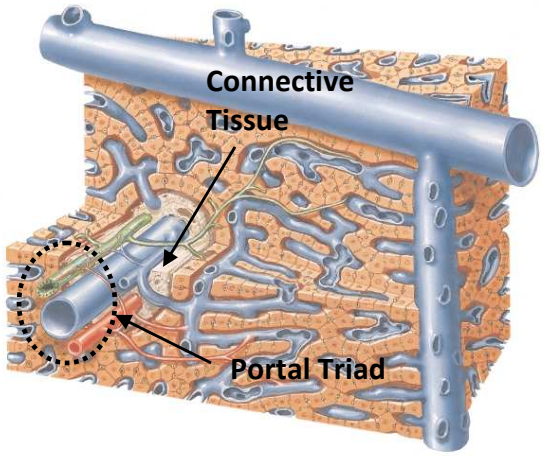

Figure 5.7B: Close up of connective tissue surrounding portal triad (Netter 1997)

Figure 5.7: Connective tissue network surrounding liver lobules

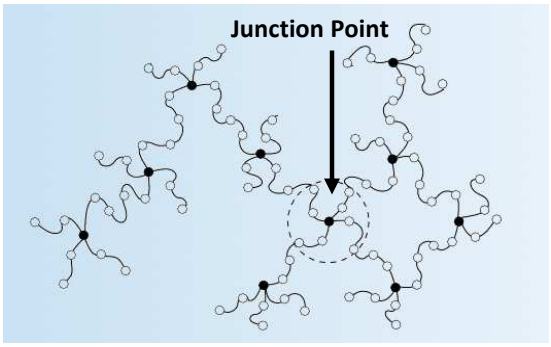

Figure 5.8A: Illustration of polymer chain network (from Satmarel et al. 2005)

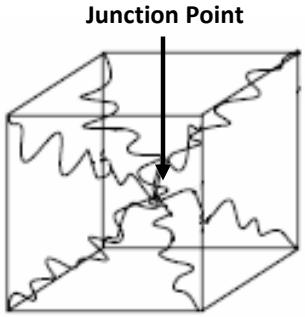

Figure 5.8B: Eight-chain network model (Arruda and Boyce 1993, image from Dupaix and Boyce 2007)

Figure 5.8: Schematic representations of polymer chain network concept

Constitutive Model of Human Liver Tissue

Introduction. The proposed liver constitutive model is shown in schematic form in Figure 5.9. The left side of the model includes a linear spring that contributes to the initial stiffness of the material, in series with a nonlinear dashpot that captures the rate dependent finite stress at which the material transitions to viscous flow behavior. This finite stress value is termed the yield or flow stress. The right side of the model includes a nonlinear spring that causes stiffening at large strains and is a secondary contributor to the initial stiffness.

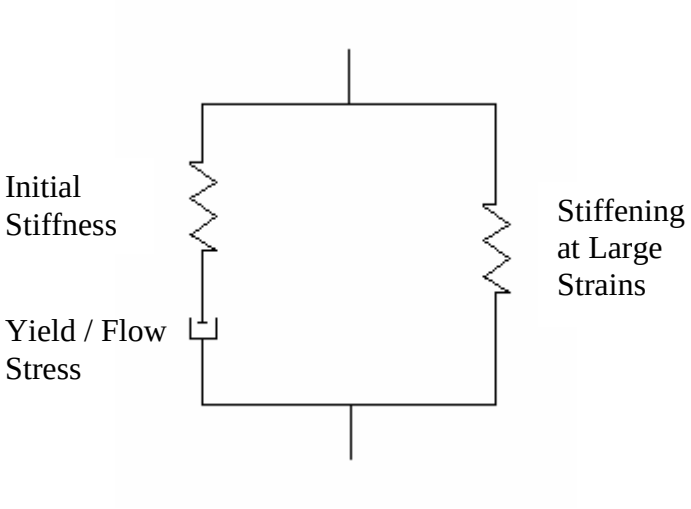

Figure 5.9: Schematic representation of liver constitutive model

The relevant equations, developed in detail in Dupaix and Boyce (2007), are summarized here. The resistances from the left and right sides of the model are represented in parallel, so the deformation gradient for each side is equal to the total deformation gradient:

(5.1) $\mathbf{F}_L = \mathbf{F}_R = \mathbf{F}$

where $\mathbf{F} = \dfrac{\partial \mathbf{x}}{\partial \mathbf{X}}$

$\mathbf{X}$ = reference position of a material point

$\mathbf{x}$ = current position of a material point

Left Side Resistance. The resistance to deformation given by the left side of the model will be addressed first. The deformation gradient $\mathbf{F}_L$ is decomposed in a multiplicative manner into elastic and plastic components as shown in Equation (5.2) (Lee 1969):

(5.2) $\mathbf{F}_L = \mathbf{F}_L^e \mathbf{F}_L^p$

Polar decomposition is used to decompose the elastic and plastic components into stretch and rotation components:

(5.3) $\mathbf{F}_L^e = \mathbf{V}_L^e \mathbf{R}_L^e$ and $\mathbf{F}_L^p = \mathbf{V}_L^p \mathbf{R}_L^p$

The velocity gradient $\mathbf{L}_L$ describes the rate kinematics, with

(5.4) $\mathbf{L}_L = \dot{\mathbf{F}}_L \mathbf{F}_L^{-1}$

The elastic and plastic components of the deformation gradient are substituted into Equation (5.4), yielding:

(5.5) $$\mathbf{L}_L = \dot{\mathbf{F}}_L^e \mathbf{F}_L^{e^{-1}} + \mathbf{F}_L^e \dot{\mathbf{F}}_L^p \mathbf{F}_L^{p^{-1}} \mathbf{F}_L^{e^{-1}} = \mathbf{L}_L^e + \tilde{\mathbf{L}}_L^p$$

The plastic velocity gradient $\tilde{\mathbf{L}}_L^p$ includes a symmetric rate of plastic strain $\tilde{\mathbf{D}}_L^p$ and an antisymmetric plastic spin $\tilde{\mathbf{W}}_L^p$ as shown in Equation (6). The plastic spin in the loaded configuration is prescribed to be zero, $\tilde{\mathbf{W}}_L^p = 0$ (see Boyce et al. 1989).

(5.6) $$\tilde{\mathbf{L}}_L^p = \tilde{\mathbf{D}}_L^p + \tilde{\mathbf{W}}_L^p$$

Equation (5.7) provides the constitutive description of the rate of plastic straining:

(5.7) $$\tilde{\mathbf{D}}_L^p = \dot{\gamma}_L^p \mathbf{N}_L$$

where $\mathbf{N}_L = \dfrac{1}{\sqrt{2}\tau_L} \mathbf{T}_L'$ is the normalized deviatoric stress

$$\tau_L = \left[\frac{1}{2} tr(\mathbf{T}_L' \mathbf{T}_L') \right]^{\frac{1}{2}}$$

$$\mathbf{T}_L' = \mathbf{T}_L - \frac{1}{3} tr(\mathbf{T}_L) \mathbf{I}$$

The Cauchy stress $\mathbf{T}_L$ is related to the elastic deformation gradient by a linear elastic model (Equation (5.8)):

(5.8) $$\mathbf{T}_L = \frac{1}{J_L}\,\mathscr{S}^{\mathrm{e}}\,[\ln \mathbf{V}_L^e]$$

where J_L = det $\mathbf{F}_L^e$ = the volume change

$\mathscr{S}^{\mathrm{e}}$ = fourth order tensor of elastic constants

$\ln \mathbf{V}_L^e$ = Hencky strain (Anand 1979)

The fourth order tensor of elastic constants is defined by Equation (5.9):

(5.9) $$\mathscr{S}^{\mathrm{e}} = 2\mu J + \frac{3K - 2\mu}{3}\,\mathbf{1} \otimes \mathbf{1}$$

where J = fourth order identity matrix

1 = second order identity matrix

K = bulk modulus

μ = shear modulus

In the original model by Dupaix and Boyce (2007) the bulk and shear moduli were strongly dependent on rate and temperature, as appropriate for the amorphous polymers characterized in that work. In the present study the bulk and shear moduli were assumed to be constant within the narrow range of strain rates tested, and temperature dependence was excluded because specimen temperatures (33-37 °C) were maintained near physiological levels.

The plastic strain rate $\dot{\gamma}_L^p$ is governed by Equation (5.10):

$$\dot{\gamma}_L^p = \dot{\gamma}_{0L} \exp\left[-\frac{\Delta G\left(1 - \frac{\tau_L}{s}\right)}{k\theta} \right] \tag{5.10}$$

where $\dot{\gamma}_{0L}$ = pre-exponential factor

ΔG = activation energy (must be overcome for flow to begin)

s = 0.15 μ = shear resistance (see Argon 1973)

k = 1.38 x 10^{-23} = Boltzmann's constant

θ = 300 K = absolute temperature

Equations (5.1) - (5.10) comprise the constitutive prescription for the elements on the left side of the model in Figure 5.9.

Right Side Resistance. The resistance to deformation of the right side of the model is given by a single nonlinear spring, with $\mathbf{F}_R^e = \mathbf{F}$. The stress in the spring element, $\mathbf{T}_{R,}$ is calculated using the Arruda-Boyce eight-chain rubber elasticity model (Arruda and Boyce 1993a, b), which describes the nonlinear stress arising from stretching a network of polymer chains arranged as shown in Figure 5.8B. In brief, the Arruda-Boyce expression for network stress serves two purposes: (1) it determines the slope of the stress-strain curve after rollover to viscous flow behavior, and (2) it provides the functionality that the stress increases dramatically as the stretch approaches a critical value near the finite limit of extensibility of the polymer chains. For application to liver connective tissue, a "polymer chain" is analogous to a collagen segment between junction points within the collagen network.

The effective stretch of each chain in the network is given by the root-mean square of the distortional applied stretch:

(5.11) $$\bar{\lambda}_{ch} = \left[\frac{1}{3} tr\left(\bar{\mathbf{B}}_R^e\right)\right]^{\frac{1}{2}}$$

where $\bar{\mathbf{B}}_R^e = \bar{\mathbf{F}}_R^e \left(\bar{\mathbf{F}}_R^e\right)^T$

$$\bar{\mathbf{F}}_R^e = \left(J_R\right)^{\frac{-1}{3}} \mathbf{F}_R^e$$

$$J_R = \det \mathbf{F}_R^e$$

The stress $\mathbf{T}_R$ is given by Equation (5.12):

$$\mathbf{T}_R = \frac{1}{J_R}\frac{nk\theta}{3}\frac{\sqrt{N}}{\overline{\lambda}_{ch}}\,\mathscr{L}^{-1}\left[\frac{\overline{\lambda}_{ch}}{\sqrt{N}}\right]\,[\overline{\mathbf{B}}_R^e - (\overline{\lambda}_{ch})^2\mathbf{I}] \tag{5.12}$$

where n = chain density

k = Boltzmann's constant

θ = absolute temperature

$\mathscr{L}^{-1}$ = the inverse Langevin function given by $\mathscr{L}(\beta) = \coth(\beta) - (1/\beta)$

N = number of rigid links between junction points

The product $nk\theta$ gives a rubbery modulus proportional to the slope of the stress-strain curve in the region after the onset of flow and before significant strain hardening has occurred. The inverse Langevin function is derived from a non-Gaussian probability function. As the effective stretch $\overline{\lambda}_{ch}$ approaches $\sqrt{N}$ the stress increases dramatically, because $\mathscr{L}^{-1}[\overline{\lambda}_{ch}/\sqrt{N}]$ approaches an asymptote at $\overline{\lambda}_{ch} = \sqrt{N}$. See Appendix F for calculation of the limiting value of N from the maximum principal stretch of the liver during impact.

Equations (5.1), (5.11), and (5.12) comprise the constitutive prescription for the right side of the model. The total stress acting on the system is the sum of the stresses on the left and right sides:

(5.13) $\mathbf{T} = \mathbf{T}_L + \mathbf{T}_R$

Determination of Material Constants

Values for the six material constants of the liver constitutive model are listed in Table 5.2. Material constants were determined by fitting the model parameters to experimental data as described in the following sections.

Behavior	Property	Symbol	Value	Units
Initial Elastic	Shear modulus	μ	3.416	MPa
	Bulk modulus	K	169.7	MPa
Flow Stress	Pre-exponential factor	$\dot{\gamma}_{0L}$	2.76 x 10^{9}	s^{-1}
	Activation energy	ΔG	7.87 x 10^{-20}	J
Strain Stiffening	Rubbery modulus	$nk\theta$	39.0	kPa
	Junction point density	N	1.23	none

Table 5.2: Constitutive model parameters

Initial Elastic Behavior. Young's modulus E was calculated for all tests from the linear portion of the initial elastic response (see Appendix D). Values for E are listed in Table

5.3. The average Young's modulus, E = 10.18 MPa, was used to calculate the shear modulus and bulk modulus using Equations (5.14) and (5.15). E was approximated as a constant because no significant trend was detected over the relatively narrow range of strain rates tested, as shown in Figure 5.10. For a broader strain rate range, the model could easily be extended to capture variation in E as a function of strain rate. Since the liver is a fluid-filled solid organ, a Poisson's ratio of ν = .49 was assumed in order to approximate near incompressibility.

(5.14) $$\mu = \frac{E}{2(1+\nu)}$$

(5.15) $$K = \frac{E}{3(1-2\nu)}$$

Subject	E (MPa)
HL02	38.60
HL03	13.42
HL04	7.67
HL05	10.36
HL07	3.31
HL08	0.58
HL09	2.89
HL10	3.03
HL11	22.89
HL13	8.19
HL14	6.81
HL15	4.40
	Mean = 10.18
	StDev = 10.78

Table 5.3: E values from experimental data

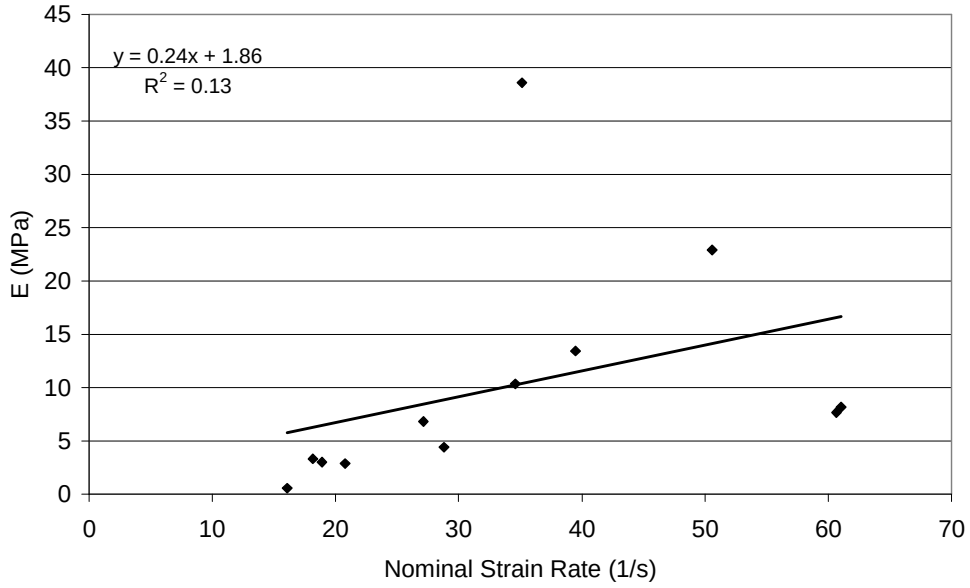

Figure 5.10: Least-squares linear fit of experimental data indicates low correlation (R^2 = .13) between *E* and strain rate over the narrow range of strain rates tested

Flow Stress. Model parameters governing flow stress behavior were determined using Equation (10). The intersection of an exponential fit of each stress-strain curve with its initial linear elastic region was used to determine the axial stress, σ, at which the stress-strain curve yields or transitions to flow behavior. As an example, Figure 5.11 illustrates the determination of axial yield stress for test HL02. The initial flow stress τ_L was approximated from the axial yield stress using $\tau_L = \sigma/\sqrt{3}$. The plastic strain rate $\dot{\gamma}_L^p$ was approximated as $\sqrt{3}\dot{\varepsilon}$, with $\dot{\varepsilon}$ being the axial strain rate. The constants $\dot{\gamma}_{0L}$ and ΔG were determined from a least-squares linear fit of the experimental data, as shown

in Figure 5.12. The slope and intercept of the linear fit were applied to Equation (5.10) to determine values for $\dot{\gamma}_{0L}$ and ΔG as given in Table 5.2.

For application to lower strain rates, the model could be modified through the introduction of a second line of different slope, as indicated in Figure 5.12. Previous studies (Mulliken and Boyce 2006; Roetling 1965; Rietsch and Bouette 1990; Moy et al. 2003) have reported that some polymer materials such as polycarbonate and poly(methyl methacrylate) (PMMA) exhibit an increased sensitivity to strain rate beyond a transition threshold, producing a two-phase response similar to that proposed in Figure 5.12. Further testing at low strain rates is needed to investigate whether human liver tissue exhibits this type of two-phase response and to determine the threshold strain rate at which the transition occurs.

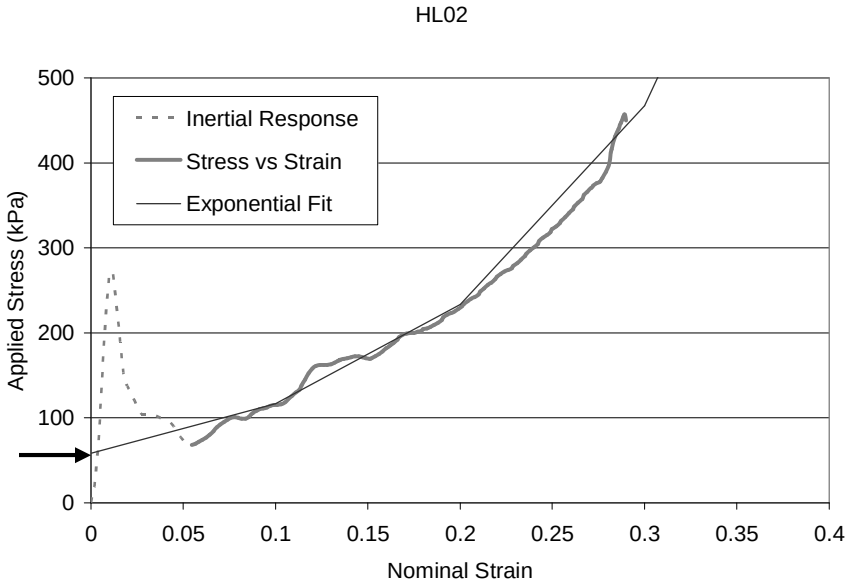

Figure 5.11: Exponential fit of stress-strain experimental data from test HL02, excluding inertial response. Arrow indicates axial yield stress, σ.

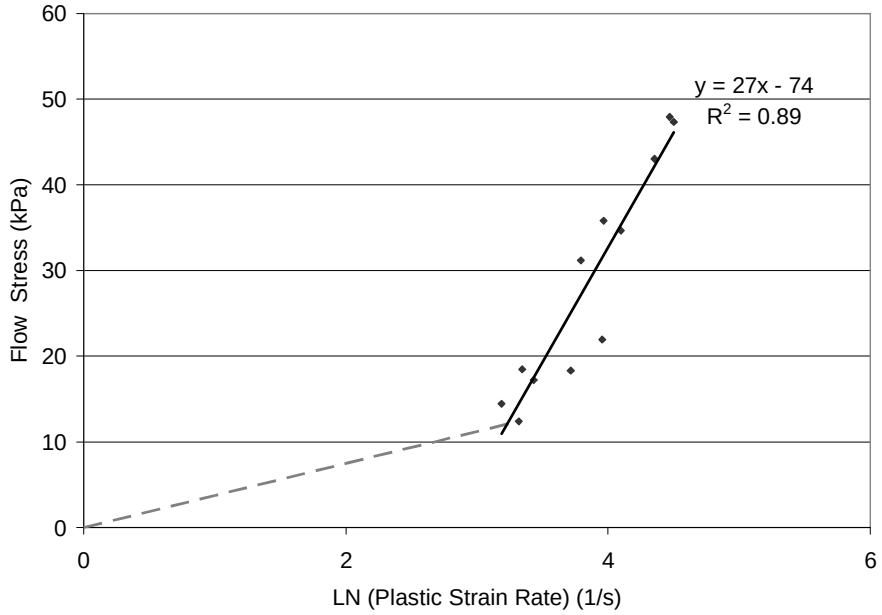

Figure 5.12. Least-squares linear fit of experimental data (black line), used to calculate model parameters $\dot{\gamma}_{0L}$ and ΔG. Gray dashed line indicates possible change in slope for application to lower strain rates.

Strain Stiffening. Strain stiffening behavior is governed by the rubbery modulus $nk\theta$ which is proportional to the initial hardening slope, and by the parameter *N* which is related to the finite limit of chain extensibility. Fitting to experimental data across all strain rates gives:

$nk\theta$ = 39 kPa

N = 1.23

5.3 RESULTS

Comparing Model Results with Experimental Data

Figure 5.13 illustrates model results for all strain rates. The effect of strain rate on model response closely approximates the rate dependence of the experimental data as shown in Figure 5.5. Figures 5.14 - 5.16 provide direct comparisons of model predictions versus experimental data for each individual strain rate. These plots illustrate good agreement between model and experiment across all strain rates tested.

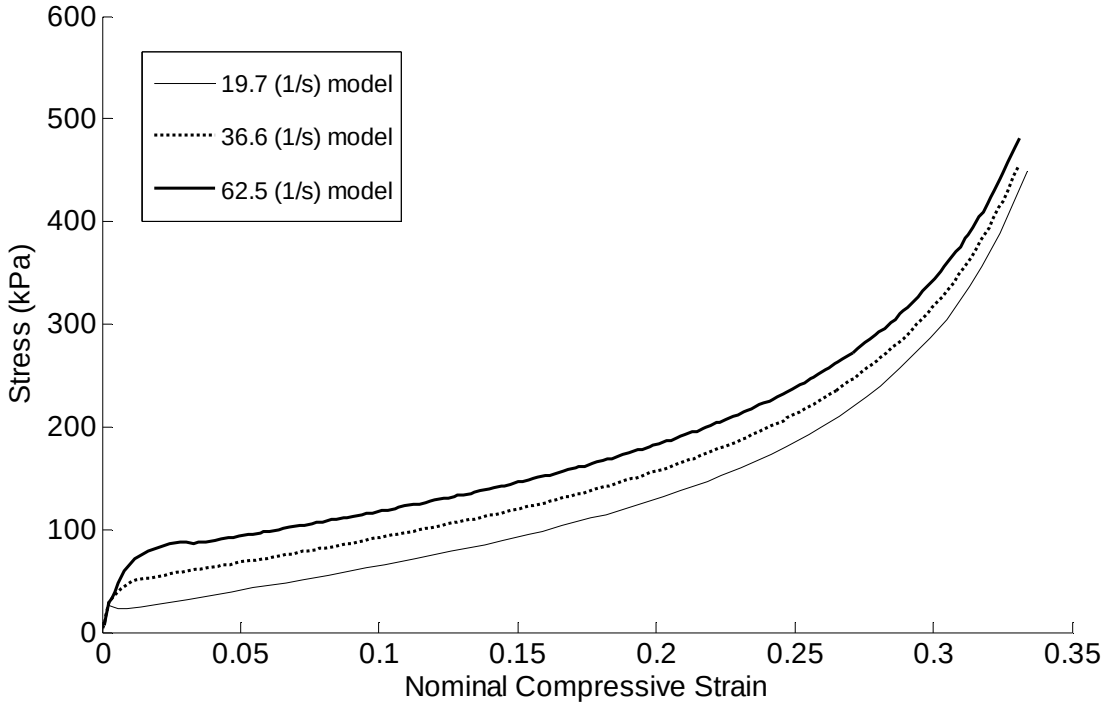

Figure 5.13: Model results for three strain rates

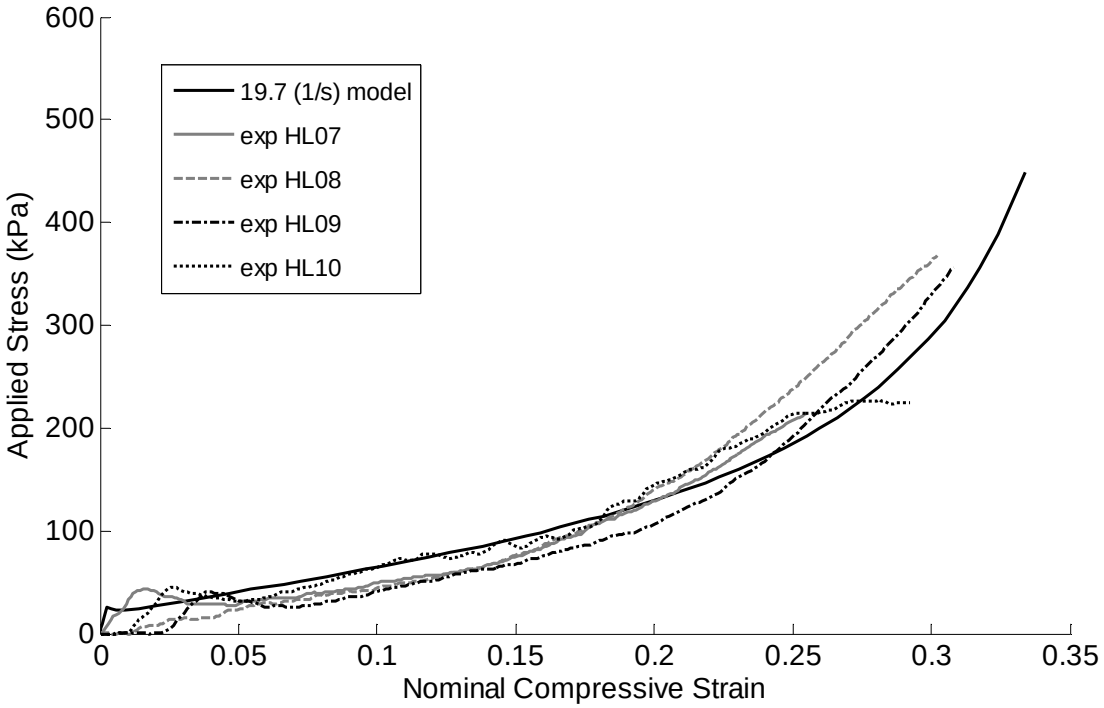

Figure 5.14: Comparison of model prediction and experimental data for 19.7 s^{-1} strain rate

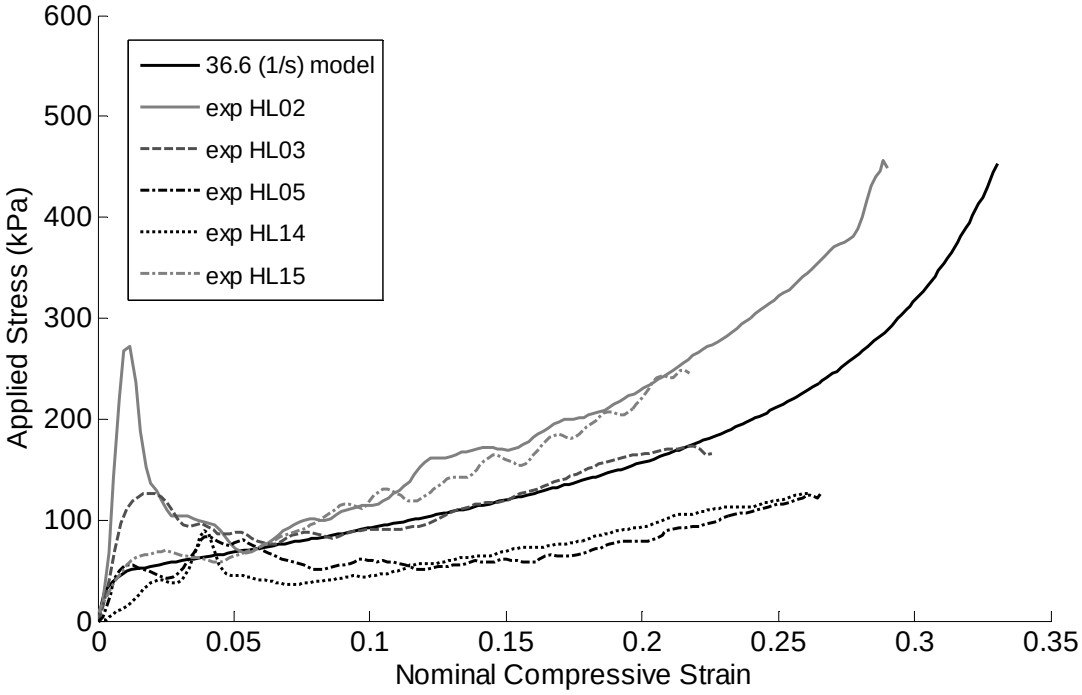

Figure 5.15: Comparison of model prediction and experimental data for 36.6 s^{-1} strain rate

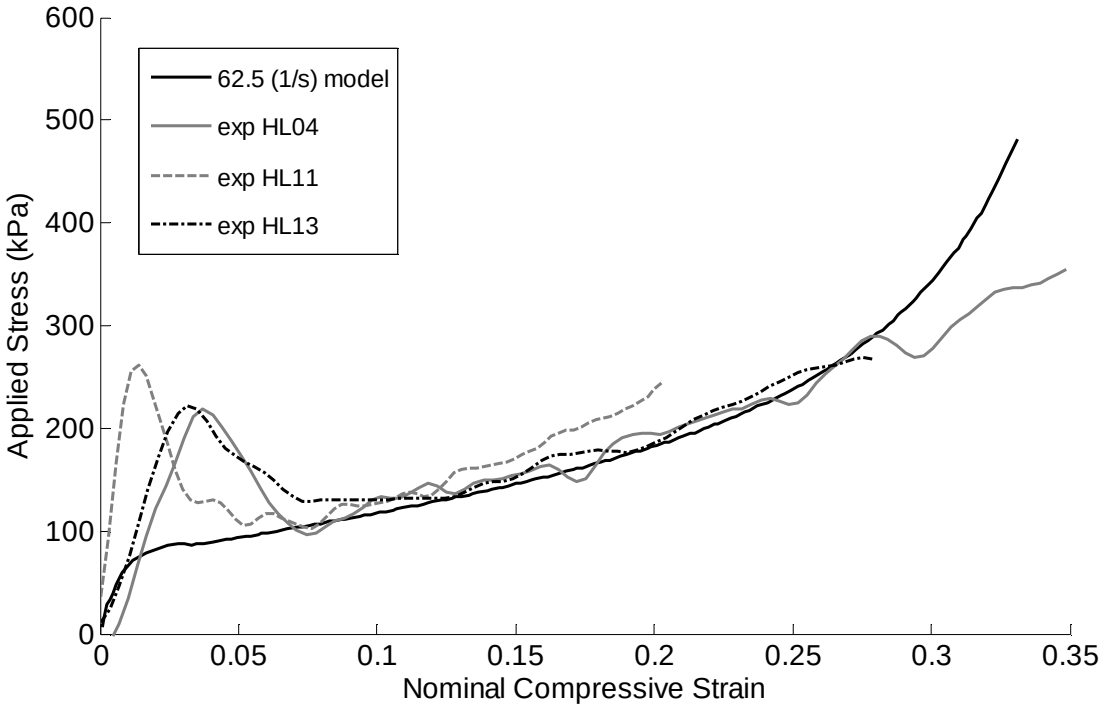

Figure 5.16: Comparison of model prediction and experimental data for 62.5 s^{-1} strain rate

5.4 DISCUSSION

The constitutive model was highly effective at capturing many features of the stress-strain behavior of human liver in high strain rate impact loading. These features include the initial elastic response, the rate-dependent yield to viscous flow behavior, and the nonlinear strain hardening that begins gradually and increases dramatically at large strains. Overall there was excellent agreement between model predictions and experimental data. Even in cases involving greater variability in the biological data, such as Figure 5.15, the model-predicted stress-strain response fell near the center of the corridor created by the data.

This study represents a novel application of polymer mechanics concepts to understand the rate dependent large strain behavior of human liver tissue under high strain rate loading. Applications of this research include finite element simulations of injury-producing liver or abdominal impact events. In addition, the constitutive modeling and experimental techniques developed in this work could be applied to investigate the behavior of a variety of soft biological tissues with fine collagenous frameworks similar to that of the liver. Future work will investigate possible model refinements for application to a broader range of strain rates. Specific modifications may include rate dependence of Young's modulus and incorporation of a transition threshold to capture a possible two-phase response.

5.5 CONCLUSIONS

The conclusions of this study were as follows:

(1) A constitutive model was developed that captures the rate dependent stress-strain behavior of human liver tissue under high strain rate impact loading.

(2) The model capitalizes on similarities between the mechanical behavior of amorphous polymers and soft biological tissue such as the liver.

(3) The model is relatively simple, includes only six material constants, and could be applied to develop finite element representations of the human abdomen for simulating impact-induced blunt abdominal trauma.

CHAPTER 6

CONCLUSION

6.1 FUTURE WORK

Post-Mortem Human Subject Testing

The results of the *ex vivo* human liver impact series demonstrated that peak pressures measured inside the liver were significant indicators of liver injury severity. Tissue pressure in particular was the best correlate with liver injury risk among the nine variables studied in the *ex vivo* experiments. These findings have considerable potential value for improving the design of crash dummy abdominal components. However, it is unknown at the present time whether these findings are representative of the liver response to impact under *in vivo* conditions. The liver boundary conditions in the *ex vivo* experiments were dramatically different from *in vivo* boundary conditions, and it is reasonable to expect that the complex and unique constraints imposed by the liver's anatomical attachments and nearby abdominal structures would influence the liver's biomechanical response to blunt impact. Therefore, it is recommended that a series of abdominal impact experiments of post-mortem human subjects (PMHS) be completed to investigate the applicability of the *ex vivo* experimental results to full body impacts. A

critical feature of the recommended PMHS test series is the pressurization of the liver vascular system, because previous research has demonstrated that certain injury mechanisms, such as burst injury, cannot be reproduced in un-pressurized cadaver livers (Mays 1966).

As a first step toward the recommended PMHS test series, two PMHS impact experiments were conducted to investigate the feasibility of (1) pressurizing the liver vascular system; and (2) measuring impact-induced pressure changes in the hepatic veins and liver parenchyma of cadaver subjects. The experimental protocol for the first PMHS test is described in section 4.2. For the second PMHS test the same protocol was used, with the addition of a pressure transducer inserted in the caudate lobe through the midline abdominal incision in order to measure tissue pressure.

Injury Results. Liver injuries observed in the PMHS tests are shown in Figures 6.1 and 6.2. Left lobe lacerations were observed in both cases. Massive tissue disruption of the posterior / visceral aspect of the liver was documented in subject PMHS01. Neither specimen showed right lobe lacerations or evidence of significant intra-parenchymal damage. In general these injury patterns differ from trends observed in the *ex vivo* experiments, in which the most common injury outcomes included internal damage and lacerations of the diaphragmatic aspect of the right lobe (see Figures 4.7 and 4.8). A likely explanation of the PMHS injury patterns is that the left lobe lacerations in both cases and the damage to the posterior aspect of the liver in PMHS01 resulted from

compression of the midline portion of the liver against the spine as the impact plate loaded the upper abdomen in the anterior-posterior direction. Liver injury resulting from anterior-posterior compression against the spine is a recognized injury mechanism in motor vehicle crash victims (Rouhana 2002), but it is a relatively rare occurrence. Interestingly, the injury outcomes observed in the *ex vivo* experiments more closely resembled the more common types of blunt liver injury observed in the clinical setting, which include right lobe lacerations and intra-parenchymal hematoma. It is possible that a method of impact application that more closely approximates loading conditions in motor vehicle crashes would produce more realistic liver injury patterns in future PMHS tests.

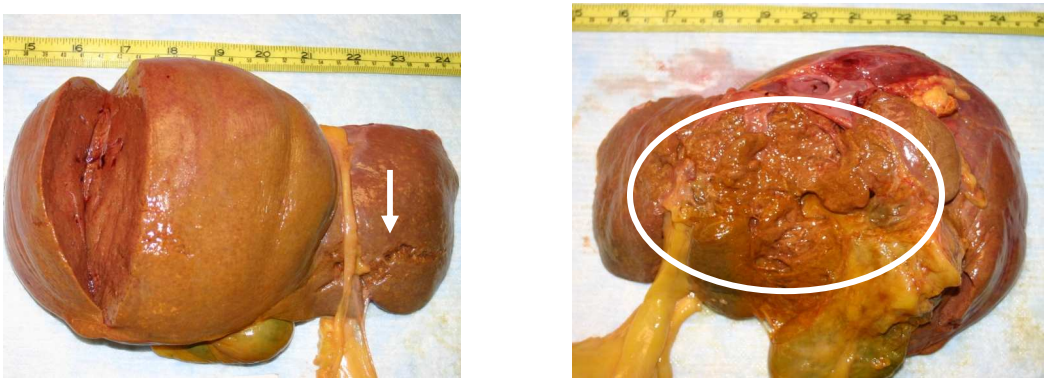

6.1A: Left lobe laceration, anterior surface 6.1B: Massive parenchymal disruption, posterior surface

Figure 6.1: AIS 4 liver injuries from subject PMHS01

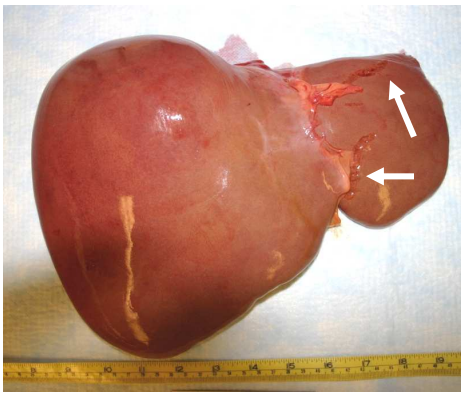

6.2A: Left lobe lacerations, anterior surface

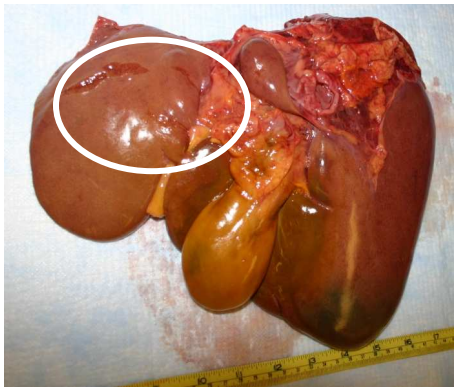

6.2B: Left lobe lacerations, posterior surface

Figure 6.2: AIS 3 liver injuries from subject PMHS02

Pressure-Injury Relationships. The peak values of vascular pressure (in hepatic veins) and tissue pressure (in caudate lobe) from the PMHS tests are shown in Figures 6.3 and 6.4 in conjunction with *ex vivo* results. For both vascular and tissue pressure measured in the PMHS livers, the results were consistent with the injury risk functions developed from the *ex vivo* experiments. This finding provides support for the applicability of the *ex vivo* injury risk functions to future PMHS tests results.

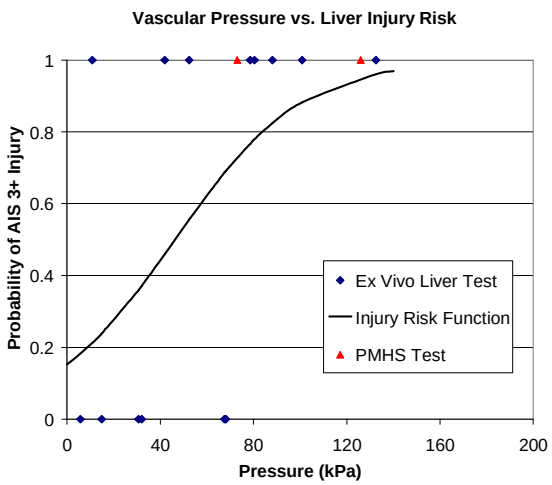

Figure 6.3: Vascular pressure data and risk function

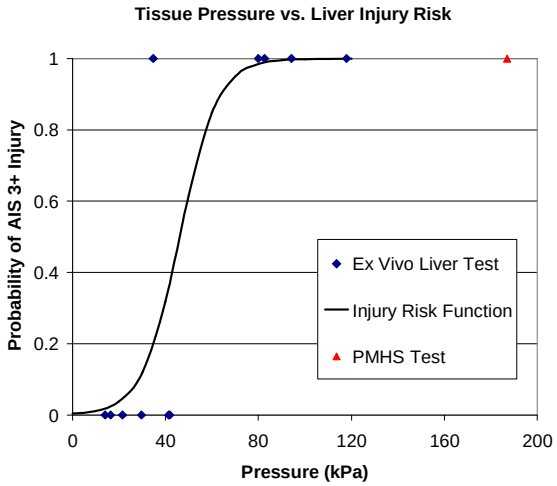

Figure 6.4: Tissue pressure data and risk function

Vascular Pressurization. During the pressurization trials, measured pressures inside the abdominal aorta were well below the target physiological levels of 100 mmHg for both subjects. Inspection of the Foley catheters after removal from the abdominal aorta revealed that the balloons were damaged and no longer functional. Calcified atherosclerotic plaques were clearly detectable along the length of the aorta for both subjects. It is likely that interaction of the inflated balloons with the relatively sharp plaques resulted in balloon puncture and subsequent failure to reach the desired vascular pressure due to insufficient obstruction of the targeted segment of the aorta. Foley catheters within the abdominal aorta are shown in Figure 6.5, and evidence of aortic plaque is shown in Figure 6.6. For future tests, it is recommended to utilize a secondary means of obstructing the targeted region of the aorta, such as suturing or clamping, to compensate for possible balloon failure.

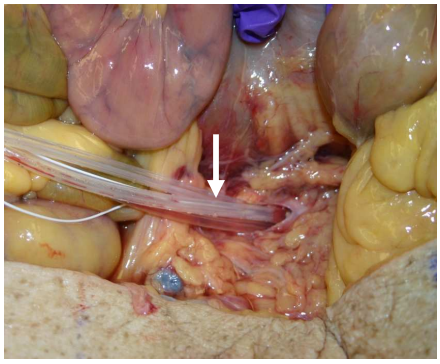

Figure 6.5: Foley catheters in abdominal aorta

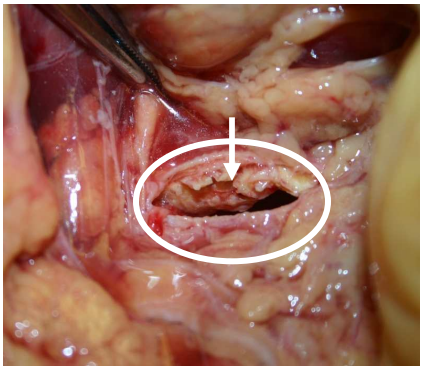

Figure 6.6: Atherosclerotic plaque inside aorta

Conclusions from PMHS Trials. The PMHS tests demonstrated a successful instrumentation technique for obtaining measurements of vascular pressure and intra-parenchymal pressure within the liver of a cadaver subject. Measured pressure values were consistent with the injury risk functions developed from the *ex vivo* liver impact tests. Further testing is needed to improve the vascular pressurization technique and to demonstrate conclusively that the *ex vivo* relationship between pressure and liver injury is applicable to PMHS impact test results.

Computational Modeling

The liver constitutive model developed in this work characterized the mechanical behavior and material properties of the *ex vivo* human liver in blunt impact loading. These results could be applied to develop a computational model of the liver that would be a valuable addition to finite element representations of the human abdomen used in crash safety research. Model geometry could be developed from the available CT scans

of the liver specimens, and the model could be validated extensively using the wealth of experimental data collected during the *ex vivo* impacts. This type of model would enable more thorough investigation of a number of interesting issues that cannot be addressed through other means, such as characterizing stress wave propagation through the complex three-dimensional shape of the liver and relating stresses and strains at specific locations in the liver to the likelihood of injury occurrence at those locations. Understanding the high strain rate load-deformation behavior of a structure as complex as the liver could contribute to a better understanding of soft tissue injury at the structural level.

6.2 SUMMARY

In Chapter 1, a review of previous literature demonstrated that:

(1) A need exists for a detailed investigation of the statistical relationship between internal fluid pressure and liver injury risk, to provide an experimental basis for improving the ability of crash dummies to assess abdominal injury risk.

(2) A need exists for a constitutive model of human liver stress-strain behavior under high strain rate blunt impact loading, to develop improved finite element models of the human abdomen used in crash safety research.

The research presented in this work addressed these needs through a series of blunt impact experiments with *ex vivo* porcine and human livers and post-mortem human subjects.

The major conclusions of this research are:

(1) Vascular pressures measured in hepatic veins and tissue pressures measured in the liver parenchyma are both statistically significant indicators of liver injury severity in *ex vivo* liver impacts.

(2) Tissue pressure had the highest correlation with liver injury among the nine candidate predictor variables investigated in the *ex vivo* liver experiments.

(3) Linear regressions of tissue pressure and average normal stress were applied to calculate an estimate of the compressive normal stress on the lateral surfaces of the liver due to the liver capsule. On average, the lateral stress was found to be 37% of the normal stress in the loading direction. These results are consistent with the interpretation that tissue pressure is a measure of hydrostatic pressure within the liver.

(4) Experimental blunt liver injuries produced in the *ex vivo* impacts were consistent with injuries observed in motor vehicle crash victims documented in the Crash Injury Research and Engineering (CIREN) database.

(5) A constitutive model was developed that captures the rate dependent stress-strain behavior of human liver tissue under high strain rate impact loading.

These results could be applied to improve the abdominal injury assessment capabilities of both anthropomorphic crash dummies and finite element human body models used in vehicle safety research.

REFERENCES

American Association for Automotive Medicine. (1998) The abbreviated injury scale, 1990 revision, update 1998. Des Plaines, IL: AAAM. p.31.

Anand, L. (1979) On H. Hencky's approximate strain energy function for moderate deformations. Journal of Applied Mechanics 46: 78-82.

Argon, A.S. (1973) A theory for the low-temperature plastic deformation of glassy polymers. Philosophical Magazine 28: 839-865.

Arruda, E.M., Boyce, M.C. (1993a) Evolution of plastic anisotropy in amorphous polymers during finite straining. International Journal of Plasticity 9(6):697-720.

Arruda, E.M., Boyce, M.C. (1993b) A three-dimensional constitutive model for the large stretch behavior of rubber elastic materials. Journal of the Mechanics and Physics of Solids 41(2):389-412.

Augenstein, J., Bowen, J. Perdeck, E., Singer, M., Stratton, J., Horton, T., Rao, A., Digges, K., Malliaris, A., and Steps, J. (2000) Injury patterns in near-side collisions, SAE #2000-01-0634. SAE 2000 World Congress, Society of Automotive Engineers, Warrendale, PA.

Bilston, L.E., Liu, Z., Phan-Thien, N. (2001) Large strain behavior of brain tissue in shear: some experimental data and differential constitutive model. Biorheology 38: 335-345.

Boyce, M.C., Weber, G.G., Parks, D.M. (1989) On the kinematics of finite strain plasticity. Journal of the Mechanics and Physics of Solids 37(5):647-665.

Burdi, A.R. (1970) Thoracic and abdominal anatomy. In: Huelke DF, ed. Human anatomy, impact Injuries, and human tolerances. New York: Society of Automotive Engineers. pp. 52-68.

Christmas, A.B., Wilson, A.K., Manning, B., Franklin, G.A., Miller, F.B., Richardson, J.D., Rodriguez, J.L. (2005) Selective management of blunt hepatic injuries including nonoperative management is a safe and effective strategy. Surgery 138(4): 606-610.

Dupaix, R.B., Boyce, M.C. (2007) Constitutive modeling of the finite strain behavior of amorphous polymers in and above the glass transition. Mechanics of Materials 39: 39-52.

Dupaix, R.B., Boyce, M.C. (2005) Finite strain behavior of poly(ethylene terephthalate) (PET) and poly(ethylene terephthalate)-glycol (PETG). Polymer 46(13):4827-4838.

Elhagediab, A.M., Rouhana, S.W. (1998) Patterns of abdominal injury in frontal automotive crashes. 16th International ESV Conference Proceedings, pp. 327-337. NHTSA, Washington, DC.

Eppinger, R.H. (1976) Prediction of thoracic injury using measurable experimental parameters. 6th International ESV Conference Proceedings, pp. 770-780. NHTSA, Washington, DC.

Fung, Y.C. (2002) The application of biomechanics to the understanding of injury and healing. In: Nahum AM and Melvin JW, eds. Accidental injury: biomechanics and prevention, 2nd edition. New York: Springer-Verlag. pp. 1-11.

Guyton, A.G. (1976) Textbook of medical physiology. W.B. Saunders, Philadelphia.

Hardy, W.H., Schneider, L.H., Rouhana, S.W. (2001) Abdominal impact response to rigid-bar, seatbelt, and airbag loading. Stapp Car Crash Journal 45: 375-406.

Hollinshead, WH. (1971) Anatomy for surgeons: volume 2-the thorax, abdomen, and pelvis, 2nd ed. New York: Harper and Row.

Horsch, J.D., Lau, I.V., Viano, D.C., Andrzejak, D.V. (1985) Mechanism of abdominal injury by steering wheel loading. Proc. 29th Stapp Car Crash Conference, pp. 69-78. Society of Automotive Engineers, Warrendale, PA.

Hurtuk, M., Reed, R.L. II, Esposito, T.J., Davis, K.A., Luchette, F.A. (2006) Trauma surgeons practice what they preach: The NTDB story on solid organ injury management. Journal of Trauma 61(2): 243-255.

John, T.G., Greig, J.D., Johnstone, A.J., Garden, O.J. (1992) Liver trauma: A 10-year experience. British Journal of Surgery 79(12): 1352-1356.

Lau, V.K., Viano, D.C. (1981a) Influence of impact velocity on the severity of nonpenetrating hepatic injury. Journal of Trauma 21(2): 115-123.

Lau, V.K., Viano, D.C. (1981b) An experimental study on hepatic injruy from belt-restraint loading. Aviation Space and Environmental Medicine 52(10): 611-617.

Lee, E.H. (1969) Elastic-plastic deformation at finite strains. Journal of Applied Mechanics 36: 1-6.

Liu, Z., Bilston, L.E. (2002) Large deformation shear properties of liver tissue. Biorheology 39: 735-742.

Liu, Z., Bilston, L.E. (2000) On the viscoelastic character of liver tissue: experiments and modelling of the linear behavior. Biorheology 37: 191-201.

Mays, E.T. (1966) Bursting injuries of the liver. Archives of Surgery 93: 92-103.

Melvin, J.W., Stalnaker, R.L., Roberts, V.L., Trollope, M.L. (1973) Impact injury mechanisms in abdominal organs. Proc. 17th Stapp Car Crash Conference, pp. 115-126. Society of Automotive Engineers, Warrendale, PA.

Mertz, H.J., Prasad, P., Irwin, A. (1997) Injury risk curves for children and adults in frontal and rear collisions. Proc. 41st Stapp Car Crash Conference, pp. 13-30. Society of Automotive Engineers, Warrendale, PA.

Miller, K. (2000) Constitutive modelling of abdominal organs. Journal of Biomechanics 33: 367-373.

Moy, P., Weerasooriya, T., Hsieh, A., Chen, W. (2003) Strain rate response of a polycarbonate under uniaxial compression. In: Proceedings of the SEM Conference on Experimental Mechanics.

Mulliken, A.D., Boyce, M.C. (2006) Mechanics of the rate-dependent elastic-plastic deformation of glassy polymers from low to high strain rates. International Journal of Solids and Structures 43: 1331-1356.

Netter, FH. (1997) Atlas of human anatomy, 2nd ed. East Hanover, NJ: Novartis. p.270.

Prasad, P., Daniel, R.P. (1984) A biomechanical analysis of head, neck, and torso injuries to child surrogates due to sudden torso acceleration. Proc. 28th Stapp Car Crash Conference, pp. 25-40. Society of Automotive Engineers, Warrendale, PA.

Ragsdale J, Trunkey DD. (1993) Injuries to the liver and extrahepatic ducts. In: Blaidsell FW, Trunkey DD, eds. Abdominal trauma, 2nd edition. New York: Thieme Medical. pp. 160-189.

Ricci, L. (1980) NCSS statistics: passenger cars, Report No. DOT HS 805 531. National Highway Traffic Safety Administration, Washington, DC, and University of Michigan, Highway Safety Research Institute, Ann Arbor, MI.

Rietsch, F., Bouette, B. (1990) The compression yield behavior of polycarbonate over a wide range of strain rates and temperatures. European Polymer Journal 10: 1071-1075.

Roetling, J. (1965) Yield stress behavior of polymethylmethacrylate. Polymer 6: 311-317.

Rouhana SW. (2002) Biomechanics of abdominal trauma. In: Nahum AM and Melvin JW, eds. Accidental injury: biomechanics and prevention, 2nd edition. New York: Springer-Verlag. pp. 405-453.

Rouhana, S.W., Foster, M.E. (1985) Lateral impact – an analysis of the statistics in the NCSS. Proc. 29th Stapp Car Crash Conference, pp. 79-98. Society of Automotive Engineers, Warrendale, PA.

Rouhana, S.W., Lau, I.V., Ridella, S.A. (1985) Influence of velocity and forced compression on the severity of abdominal injury in blunt, nonpenetrating lateral impact. Journal of Trauma 25(5): 490-500.

Rouhana, S.W., Ridella, S.A., Viano, D.C. (1986) The effect of limiting impact force on abdominal injury: a preliminary study. Proc. 30th Stapp Car Crash Conference, pp. 65-79. Society of Automotive Engineers, Warrendale, PA.

Rupp, J.D., Klinich, K.D., Moss, S., Zhou, J., Pearlman, M.D., Schneider, L.W. (2001) Development and testing of a prototype pregnant abdomen for the small-female Hybrid III ATD. Stapp Car Crash Journal 45: 375-392.

Satmarel, C., von Ferber, C., Blumen, A. (2005) Dynamics of end-linked star polymers. Journal of Chemical Physics 123(3): 034907-1 – 034907-13.

Stein, P.D., Sabbah, H.N., Hawkins, E.T., White, H.J., Viano, D.C., Vostal, J.J. (1983) Hepatic and splenic injury in dogs caused by direct impact to the heart. Journal of Trauma 23(5): 395-404.

Tamura, A., Omori, K., Miki, K., Lee, J.B., Yang, K.H., King, A.I. (2002) Mechanical characterization of porcine abdominal organs. Stapp Car Crash Journal 46: 55-69.

Trollope, M.L., Stalnaker, R.L., McElhaney, J.H., Frey, C.H. (1973) The mechanism of injury in blunt abdominal trauma. Journal of Trauma 13(11): 962-970.

Viano, D.C., Lau, I.V. (1985) Thoracic impact: a viscous tolerance criterion. 10th International ESV Conference Proceedings, pp. 104-114. NHTSA, Washington, DC.

Viano, D.C., Lau, I.V., Asbury, C., King, A.I., Begeman, P.C. (1989) Biomechanics of the human chest, abdomen, and pelvis in lateral impact. Proc. 33rd Annual Meeting of the Association for the Advancement of Automotive Medicine, pp. 367-382. AAAM, Des Plaines, IL.

Walfisch G, Fayon A, et al. (1980) Designing of a dummy's abdomen for detecting injuries in side impact collisions. In: 5th International IRCOBI Conference Proceedings, pp. 149-164.

Yoganandan N, Pintar FA, Maltese MR. (2001) Biomechanics of abdominal injuries. Critical Reviews in Biomedical Engineering 9(2): 173-246.

Zoli, M., Magalotti, D., Bianchi, G., et al. (1999) Total and functional hepatic blood flow decrease in parallel with ageing. Age and Ageing 28: 29-33.

APPENDIX A

LIVER FORCE CALCULATION

Free Body Diagram of Aluminum Plate:

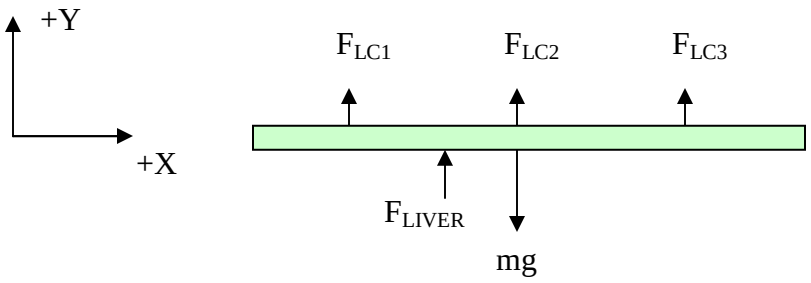

- Mass of aluminum plate = 4.03 kg
- Total mass of load cells = 1.42 kg
- Effective mass = 4.03 + ½ * 1.42 = 4.74 kg

Force balance:

$$\sum F_y = m * a_y = F_{LC1} + F_{LC2} + F_{LC3} - mg + F_{LIVER}$$

where:

$m * a_y$ = effective mass * resultant acceleration measured by accelerometer

$F_{LC1} + F_{LC2} + F_{LC3}$ = sum of load cells

mg = effective mass * gravitational constant = 4.74 kg * (-9.81 m/s^2)

F_{LIVER} = force of the liver acting on the aluminum plate

Note: Only three load cells are shown in diagram for simplicity

APPENDIX B

EQUIVALENT SPHERE CALCLUATION:

APPROXIMATING CHANGE IN CROSS-SECTION AREA WITH DEPTH

x_b = radius of a circle with area equal to liver base area (A_b)

x_h = radius of a circle with area equal to liver loaded surface area (A_h)

y_h - y_b = liver height at maximum compression (70% of pre-test liver height)

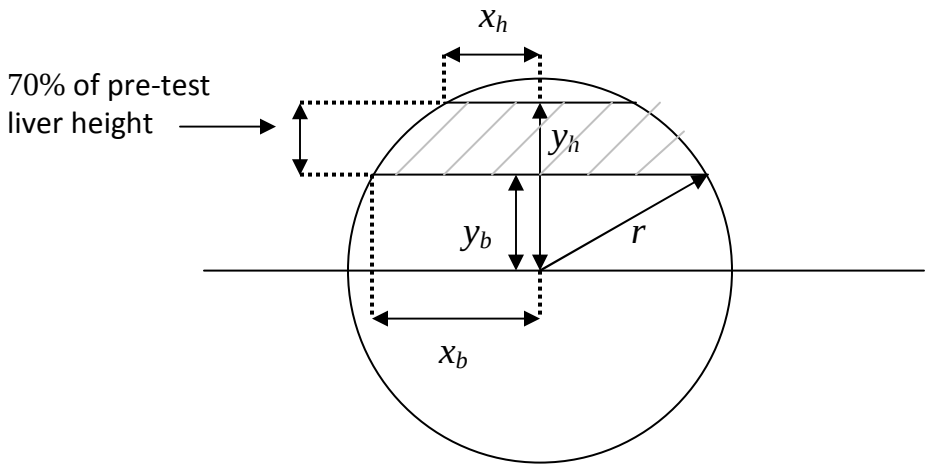

The gray hashed region is analogous to the compressed liver.

The radius r of an equivalent sphere was calculated for each liver specimen using values of x_b, x_h, and (y_h - y_b) determined from experimental data.

The cross-sectional area at any depth (A_i) may be calculated using:

$$A_i = \pi (x_i)^2 = \pi (r^2 - y_i^2)$$

where $y_b \leq y_i \leq y_h$

APPENDIX C

INTERNAL PRESSURE-TIME HISTORIES

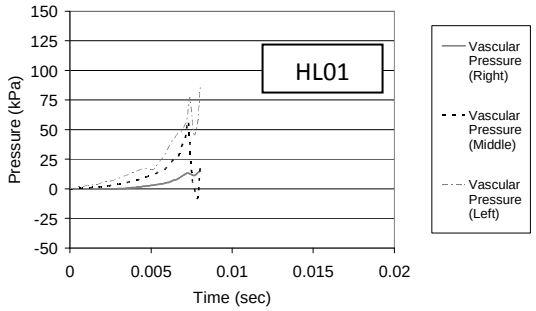
HL01
Pressure (kPa)
Time (sec)
Vascular Pressure (Right)
Vascular Pressure (Middle)
Vascular Pressure (Left)

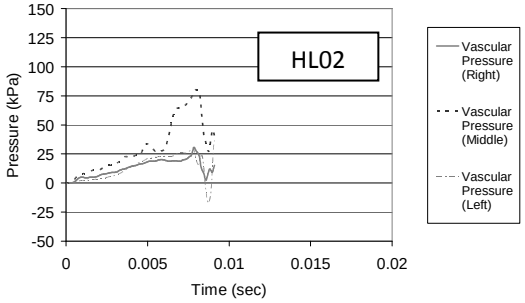
HL02
Pressure (kPa)
Time (sec)
Vascular Pressure (Right)
Vascular Pressure (Middle)
Vascular Pressure (Left)

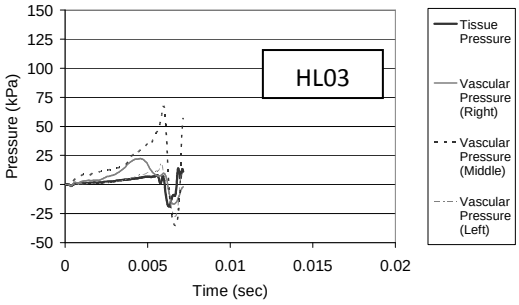
HL03
Pressure (kPa)
Time (sec)
Tissue Pressure
Vascular Pressure (Right)
Vascular Pressure (Middle)
Vascular Pressure (Left)

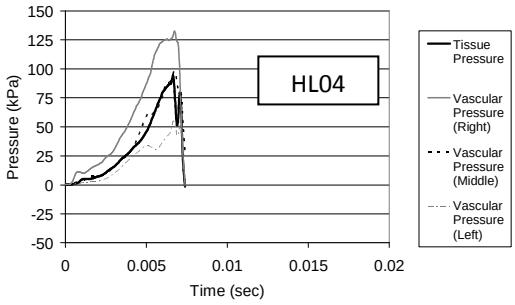
HL04
Pressure (kPa)
Time (sec)
Tissue Pressure
Vascular Pressure (Right)
Vascular Pressure (Middle)
Vascular Pressure (Left)

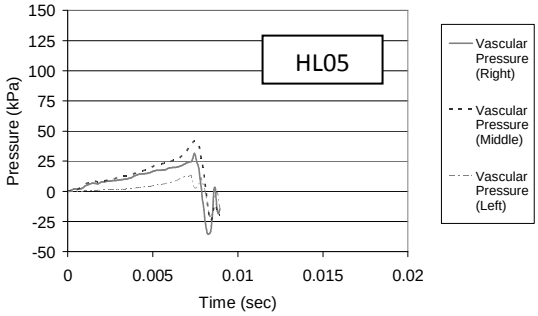
HL05
Pressure (kPa)
Time (sec)
Vascular Pressure (Right)
Vascular Pressure (Middle)
Vascular Pressure (Left)

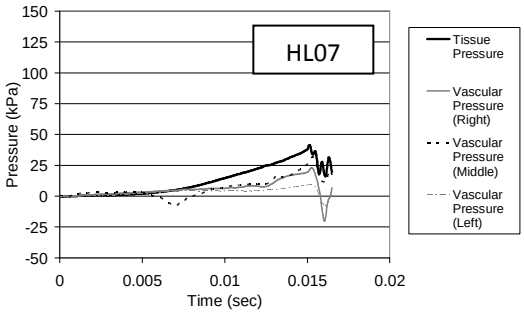
HL07
Pressure (kPa)
Time (sec)
Tissue Pressure
Vascular Pressure (Right)
Vascular Pressure (Middle)
Vascular Pressure (Left)

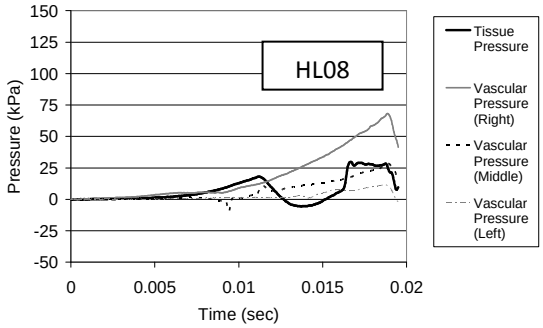
HL08
Pressure (kPa)
Time (sec)
Tissue Pressure
Vascular Pressure (Right)
Vascular Pressure (Middle)
Vascular Pressure (Left)

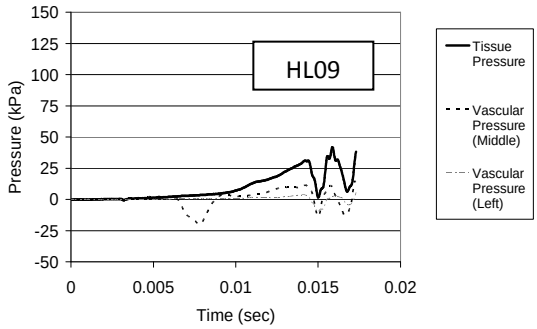
HL09
Pressure (kPa)
Time (sec)
Tissue Pressure
Vascular Pressure (Middle)
Vascular Pressure (Left)

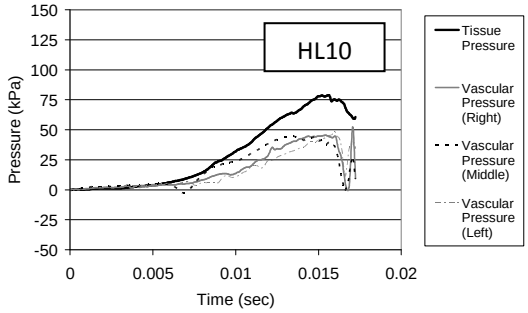
HL10
Pressure (kPa)
Time (sec)
Tissue Pressure
Vascular Pressure (Right)
Vascular Pressure (Middle)
Vascular Pressure (Left)

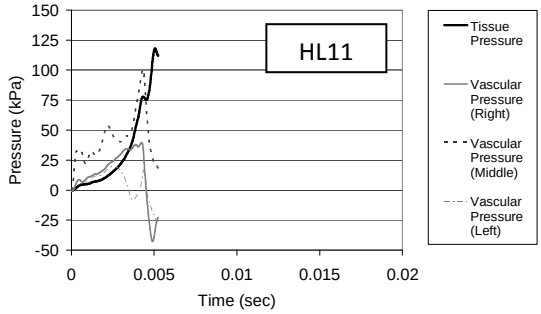
HL11
Pressure (kPa)
Time (sec)
Tissue Pressure
Vascular Pressure (Right)
Vascular Pressure (Middle)
Vascular Pressure (Left)

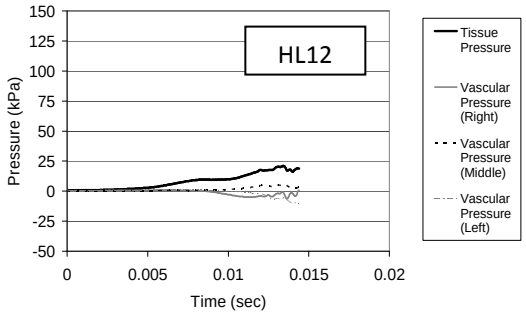
HL12
Pressure (kPa)
Time (sec)
Tissue Pressure
Vascular Pressure (Right)
Vascular Pressure (Middle)
Vascular Pressure (Left)

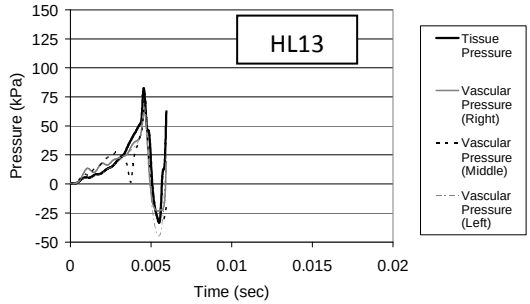
HL13
Pressure (kPa)
Time (sec)
Tissue Pressure
Vascular Pressure (Right)
Vascular Pressure (Middle)
Vascular Pressure (Left)

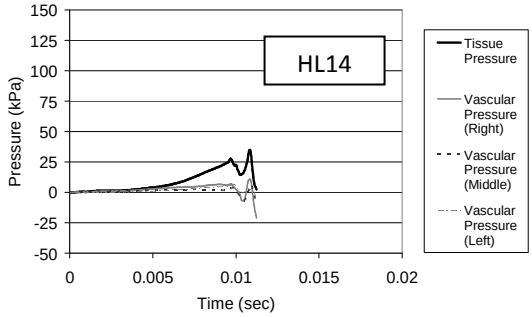
HL14
Pressure (kPa)
Time (sec)
Tissue Pressure
Vascular Pressure (Right)
Vascular Pressure (Middle)
Vascular Pressure (Left)

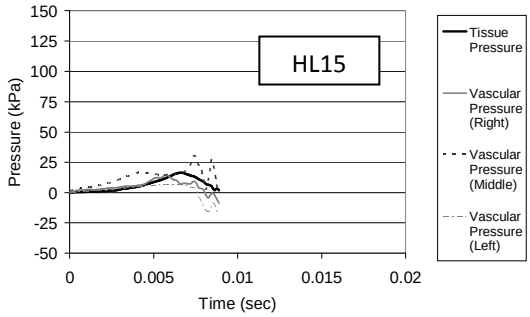
HL15
Pressure (kPa)
Time (sec)
Tissue Pressure
Vascular Pressure (Right)
Vascular Pressure (Middle)
Vascular Pressure (Left)

APPENDIX D

APPLIED STRESS VERSUS NOMINAL STRAIN CURVES

HL02

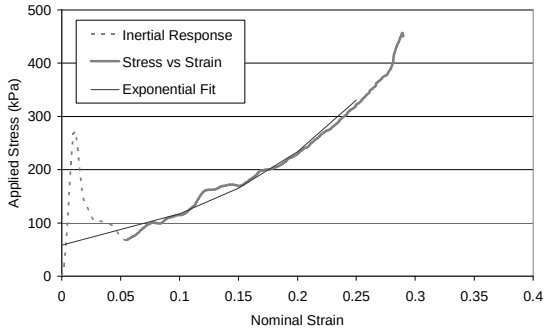

HL03

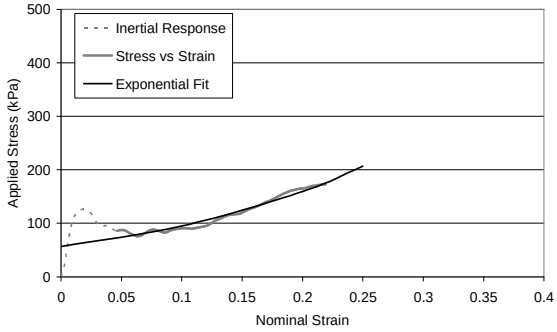

HL04

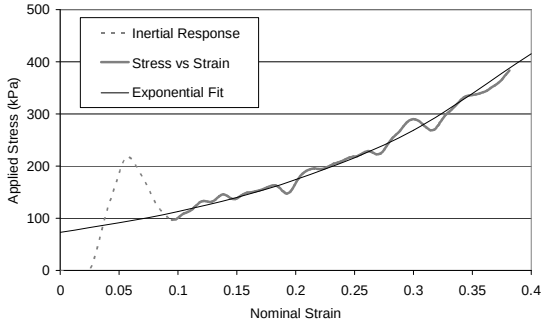

HL05

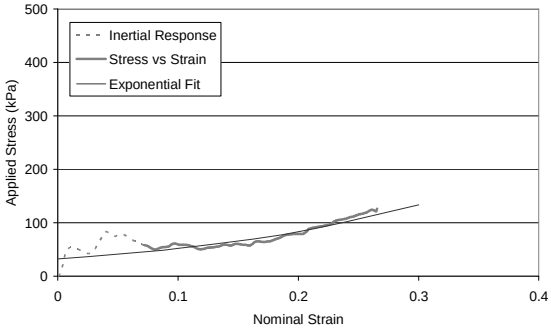

HL07

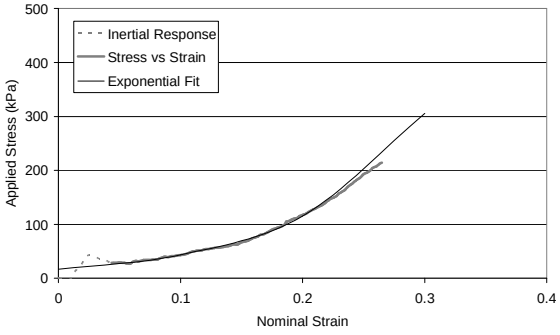

HL08

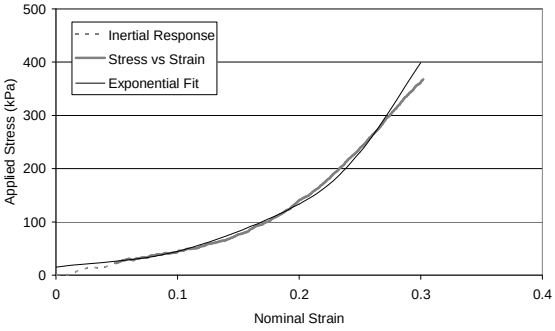

HL09

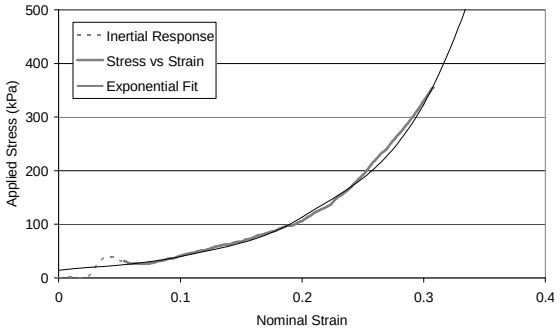

HL10

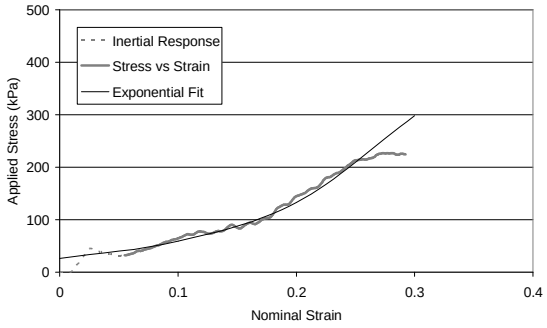

HL11

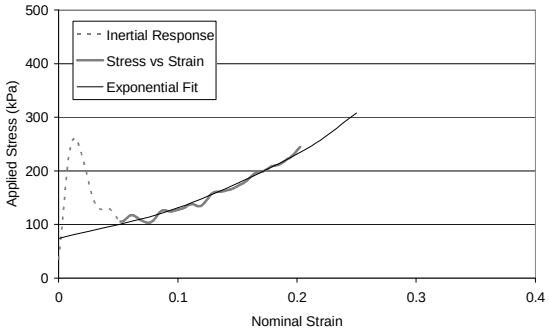

HL12

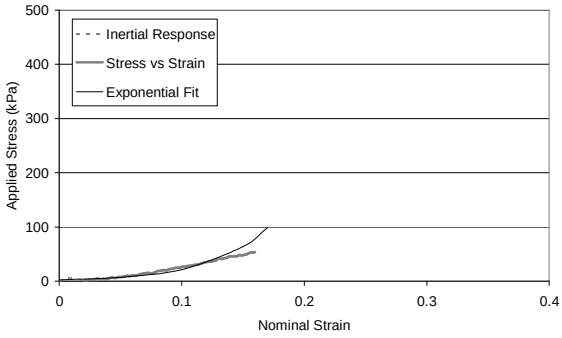

HL13

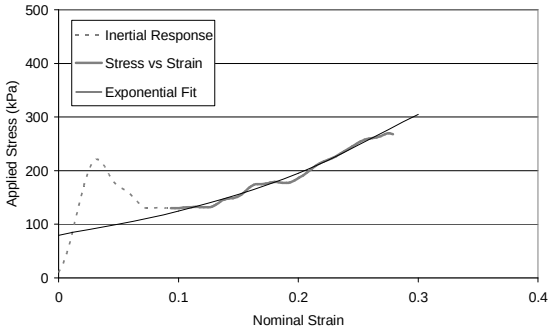

HL14

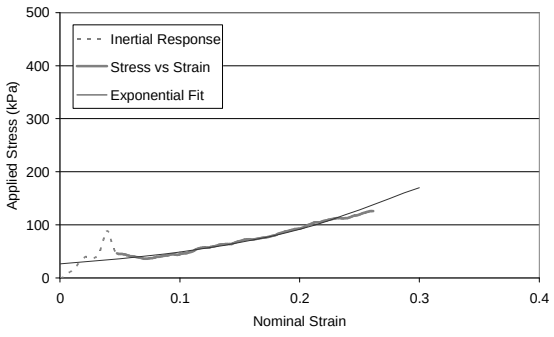

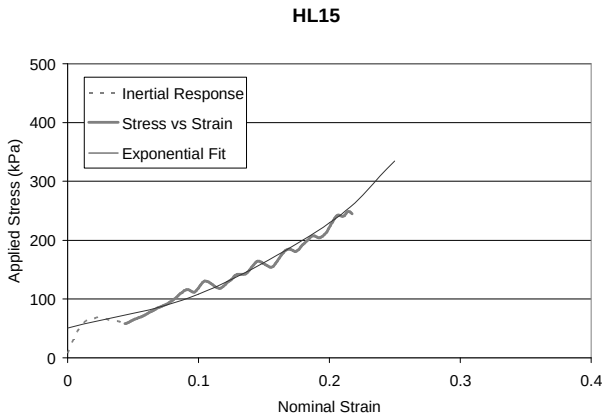

* Stress and strain data not recorded in HL01
* HL06 excluded from all analysis due to abnormally high pressure in liver bile duct system
* HL12 excluded from Chapter 5 analysis

APPENDIX E

INJURY RISK FUNCTIONS

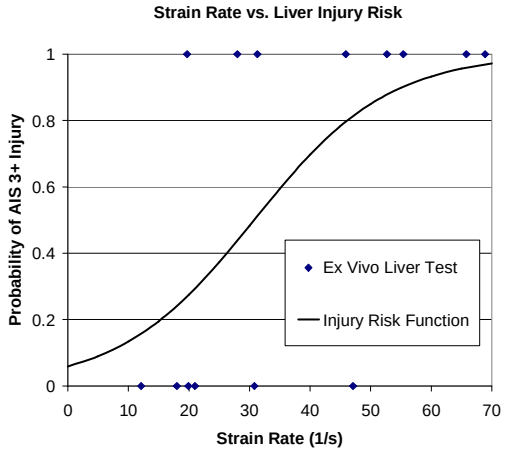
Strain Rate vs. Liver Injury Risk
Probability of AIS 3+ Injury
Strain Rate (1/s)
Ex Vivo Liver Test
Injury Risk Function

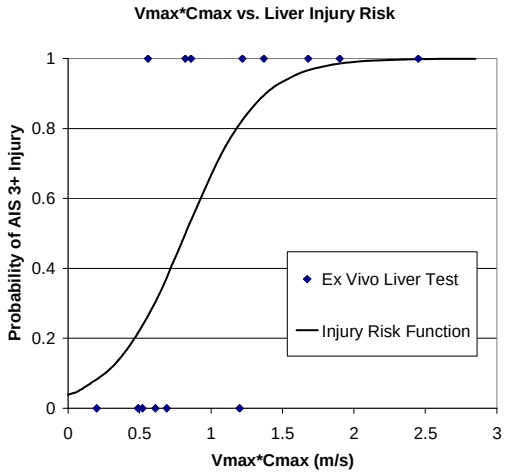
Vmax*Cmax vs. Liver Injury Risk
Probability of AIS 3+ Injury
Vmax*Cmax (m/s)
Ex Vivo Liver Test
Injury Risk Function

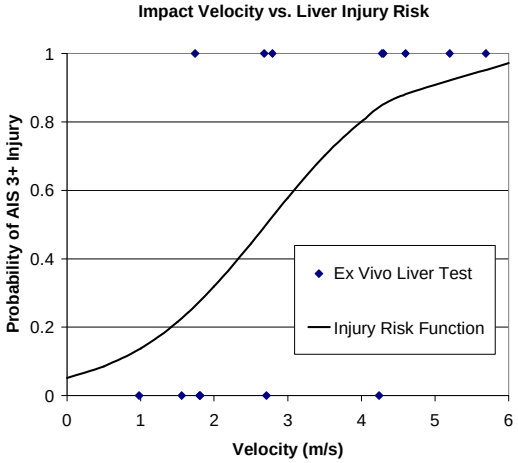
Impact Velocity vs. Liver Injury Risk
Probability of AIS 3+ Injury
Velocity (m/s)
Ex Vivo Liver Test
Injury Risk Function

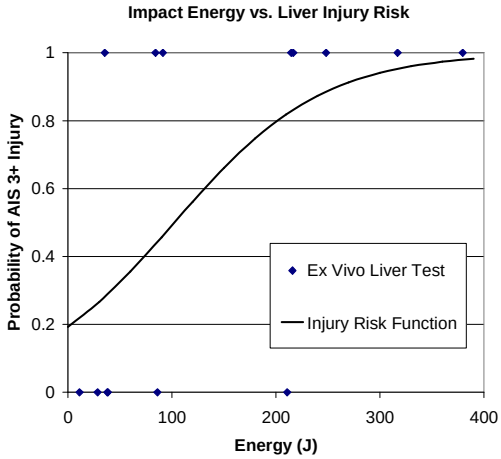
Impact Energy vs. Liver Injury Risk
Probability of AIS 3+ Injury
Energy (J)
Ex Vivo Liver Test
Injury Risk Function

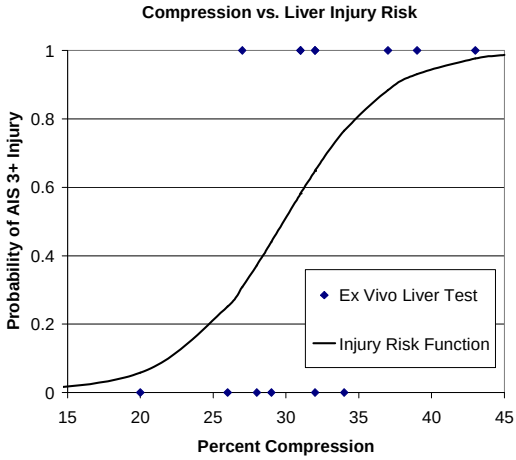
Compression vs. Liver Injury Risk
Probability of AIS 3+ Injury
Percent Compression
Ex Vivo Liver Test
Injury Risk Function

APPENDIX F

CALCULATION OF LIMITING VALUE OF JUNCTION POINT DENSITY (*N*)

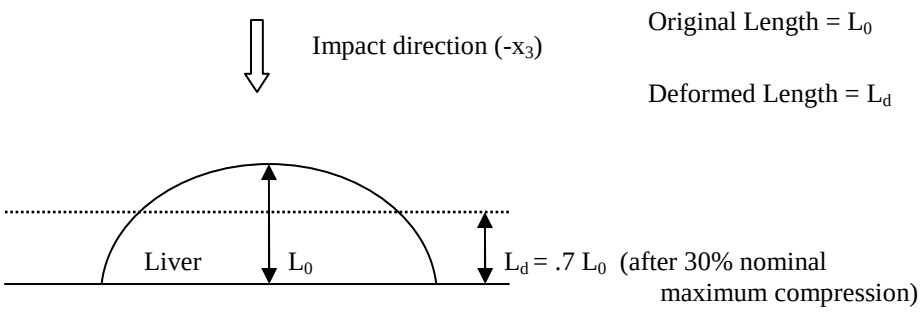

Maximum stretch in loading direction:

$$\lambda_3 = \frac{L_d}{L_0} = .70$$

Assume incompressibility:

$$\lambda_1 \lambda_2 \lambda_3 = 1$$

$$\lambda_1 = \lambda_2 = 1.195$$

Calculate effective chain stretch $\overline{\lambda}_{ch}$:

$$\overline{\lambda}_{ch} = \sqrt{\frac{1}{3}\left(\lambda_1^2 + \lambda_2^2 + \lambda_3^2\right)} = 1.056$$

Calculate limiting value of *N*:

$$\overline{\lambda}_{ch} = \sqrt{N_{\lim}}$$

$$N_{\lim} = 1.115$$

The model parameter *N* must be greater than 1.115.

(The parameter *N* fit to experimental data was *N* = 1.23.)